AN EXPERIMENTAL AND THEORETICAL STUDY OF RADIATIVE AND CONDUCTIVE HEAT TRANSFER IN NON-GRAY SEMI-TRANSPARENT MEDIA

Norman D. Eryou

Leon R. Glicksman

Report No. DSR 76194-66

Contract No. NSA-496

Department of Mechanical Engineering
Engineering Projects Laboratory
Massachusetts Institute of Technology

October 1969

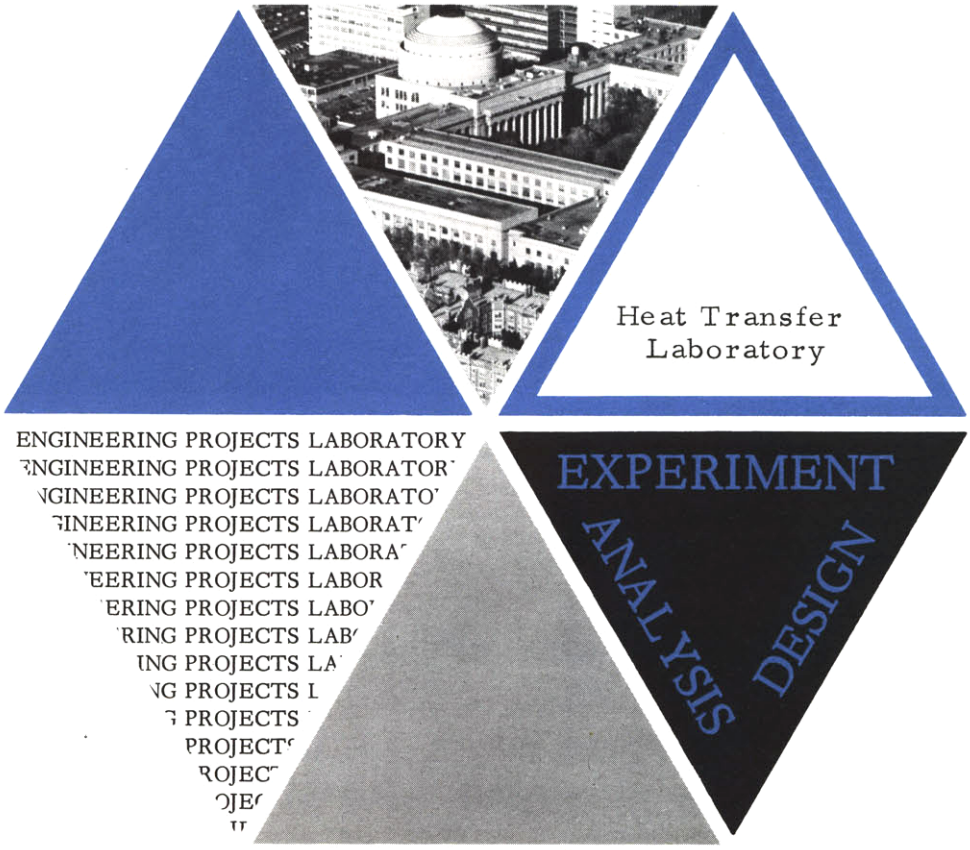

Technical Report No. 76194-66

AN EXPERIMENTAL AND THEORETICAL STUDY OF RADIATIVE AND CONDUCTIVE HEAT TRANSFER IN NONGRAY SEMITRANSPARENT MEDIA

by

N. Dennis Eryou

Leon R. Glicksman

Sponsored by the

National Aeronautics and
Space Administration
Grant No. NSA - 496

DSR Project No. 76194

October 1969

Engineering Projects Laboratory
Department of Mechanical Engineering
Massachusetts Institute of Technology
Cambridge, Massachusetts 02139

ABSTRACT

One dimensional temperature profiles and heat fluxes within a slab of molten glass were measured experimentally. The glass slab was contained in a platinum foil lined ceramic tray inside a high temperature furnace. An optical method of temperature measurement was developed in which a helium-neon laser beam was directed along an isothermal path through the glass. The attenuation of the beam was a strong function of temperature and was used to evaluate the local temperatures within the glass slab.

In order to perform a theoretical analysis the spectral absorption coefficient of the glass was measured between .6328 microns and 2.75 microns from 2000^{o}F to 2300^{o}F. Two analyses were performed; one for a diffuse platinum-glass boundary and the other for a specular boundary. The experimentally measured temperature profiles and heat fluxes agreed with the predicted profiles within 5^{o}F and the heat fluxes to within ten percent.

ACKNOWLEDGEMENTS

For their guidance and advice during this research project, the authors would like to thank Professors E. Cravalho, B. Mikic, P. Griffith, and A Sarofim. Mr. F. Johnson assisted in the construction of the experimental apparatus.

The research was supported by the National Aeronautics and Space Administration sustaining university grant number NSA - 496. The computations were performed at the M.I.T. Information Processing Center.

TABLE OF CONTENTS

LIST OF FIGURES

NOMENCLATURE

B	-	surface radiosity
E_n	-	exponential integral - $E_n(\tau) = \int_0^1 x^{n-2} e^{-\frac{\tau}{x}} dx$
EB	-	black body emission in a wavelength band
e	-	emissive power
G	-	incident intensity at lower boundary
g	-	incident intensity at upper boundary
I	-	intensity of radiation
j	-	volumetric emission coefficient
K_T	-	thermal conductivity
K	-	absorption coefficient
k	-	extinction coefficient
L	-	plate separation
N	-	radiation-conduction number
n	-	real part of complex refractive index
P	-	specular reflection coefficient
q	-	heat flux
R	-	Fresnel reflection coefficient
S	-	path length
T	-	temperature
t	-	dummy variable of integration
V	-	volume
y	-	distance from boundary
$\bar{y}$	-	dimensionless distance (Y/L)
i	-	$\sqrt{-1}$

GREEK LETTERS

β - dimensionless wall radiosity

δ - increment

ϵ - emissivity

θ - angle from surface normal

λ - monochromatic

μ - $\cos \theta$

σ - Stefan-Boltzman constant

ρ - reflectivity

τ - optical length

ϕ - azimuthal angle

ω - solid angle

Φ - dimensionless temperature = T/T_1

SUBSCRIPTS

b - black body

c - cold wall

eff - effective

d - dielectric

h - hot wall

L - denoted Y = L

m - metal

n - order of exponential integral

r - radiative

t	-	total
o	-	denotes y = 0
1	-	lower wall
2	-	upper wall
//	-	parallel polarization
$\perp$	-	perpendicular polarization

I INTRODUCTION

1.1 Outline of Problem

The accurate prediction of heat fluxes and temperature profiles within a nongray radiating-conducting medium is of concern to the designers of rocket engines, ablation heat shields and glass-melting furnaces. The basic theory of radiating media has been sufficiently developed that accurate solutions of various simplified forms of the governing equations have been calculated by numerical techniques. Due to the difficulties inherent in performing high-temperature controlled experiments and measuring temperature levels accurately, extensive experimental data is not available to check on the validity of the analytical models. Therefore, progress in the development of an adequate theory and understanding of heat transfer in radiating media has come about mainly by analysis.

Two different types of experimental data are presently available. The first type consists of spectral radiosity measurements of isothermal and non-isothermal gas and vapor mixtures [1, 2, 3]*. In the non-isothermal case the temperature gradient was imposed upon the mixture in a one-dimensional tube furnace, and the spectral radiant flux was measured and compared with predictions. The second type of data is temperature maps of rocket exhausts calculated from spectral radiosity measurements of the combustion products [4]. This type of data is difficult to check analytically due to the complexity of the heat transfer processes in rocket exhaust. The reader is referred to the literature review in Appendix A for a more complete coverage of previous analytical and experimental investigations of heat transfer in radiating-conducting media.

No experimental data are available for a nongray medium of intermediate optical thickness in which radiative and conductive heat transfer are strongly coupled. It was felt that useful data would be obtained from a controlled one-dimensional experiment in which only the boundary temperatures and not the temperature profile within the medium were

---

*Numbers in brackets refer to references on page 70.

imposed.

1.2 SCOPE AND OBJECTIVES

The objective of this investigation was to evaluate the agreement between experimental data and recent theoretical developments in coupled radiative and conductive heat transfer in nongray media. A one-dimensional medium was chosen in order to reduce the number of parameters studied.

An experimental program was set up to produce temperature profile and heat flux data for a radiating-conducting medium in which only the boundary temperatures are imposed and the temperature profile in the medium is due to radiative and conductive transfer with the walls. Water-white plate glass* was chosen as the experimental medium due to its convenient thermophysical properties. Its spectral absorption coefficient changes gradually with temperature and almost stepwise with wavelength and it does not exhibit line radiation. The spectral absorption coefficient can be modified by doping the glass with small amounts of metallic oxides. Optical thicknesses near unity can be achieved with apparatus of reasonable size.

Due to uncertainities of the exact nature of the reflections at the glass boundaries, two extensive analytical models were developed and solved numerically. The first analysis (see Section 2.5) modelled a nonisothermal glass slab with a diffusely reflecting boundary while the second (see Section 2.6) modelled a specularly reflecting boundary. The experimental data (see Section 4) were checked against the two analytical predictions to evaluate the validity of the models.

---

*Trademark of the Pittsburg Plate Glass Co. Ltd.

II ANALYSIS OF COMBINED RADIATION AND CONDUCTION

2.1 Introduction

The basic principle governing the temperature field within an absorbing, emitting and conducting medium is the conservation of energy within the medium. Local thermodynamic equilibrium is assumed to exist within the medium. The population of the atomic and molecular states that contribute to absorption and emission are given by their equilibrium distribution. The energy equation for a stationary radiating-conducting medium is:

$$\nabla \cdot \left(K_T \nabla T \right) = \nabla \cdot q_R \qquad 2.1$$

q_R = radiative flux. $= \int_0^\infty \int_{4\pi} I_\lambda \bar{s} \cdot \bar{n} \, d\omega \, d\lambda$

The radiant energy flux vector is defined as the net flow of radiant energy in a given direction per unit of area and time due to radiation from all directions. The radiative flux term in the energy equation requires a knowledge of the radiation intensity field within the medium. The following equation of transfer governs the intensity distribution in a stationary non-scattering medium.

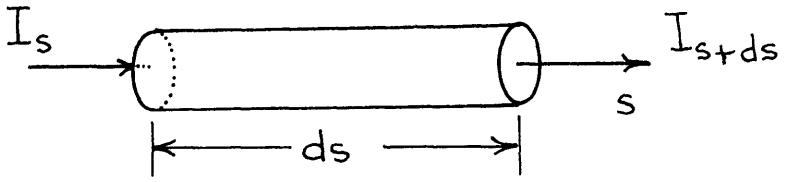

$$\left(s \cdot \nabla \right) I_\lambda = - K_\lambda I_\lambda + \frac{n^2 e_{b\lambda}}{\pi} \qquad 2.2$$

The first term on the right hand side of equation 2.2 represents absorption of radiation by the medium and the second term represents emission from the medium.

In the general case the transfer equation (2.2) is coupled with the energy equation (2.1) and they must be solved simultaneously. The solutions are difficult to achieve due to the nonlinearity of the coupled

equations, the large number of parameters involved, and the dependence of the radiation flux on the geometrical configuration of the system. Most methods involving complex geometries use a "zone method" such as the one developed by Hottel [5].

2.1.1 THE MODEL

In the remainder of this analysis combined radiative and conductive steady-state heat transfer is considered in a one-dimensional nongray stationary medium which conducts, absorbs and emits energy. Figure 1 indicates the coordinate system used in the analysis. In order to make the problem more tractable, several simplifications were used in constructing the model.

The medium between the boundaries is homogeneous on a continuum scale and therefore does not scatter radiant energy significantly. The molten glass used in the experiments became homogeneous after all the entrained air bubbles were removed by continued heating above $2000^{o}F$. Scattering effects were not observed when a collimated beam of light was passed through the glass.

The thermal conductivity of the medium is not a function of temperature at the temperature level of the experiments. The data shown on Figure B13 indicates that the thermal conductivity increases with temperature up to $1800^{o}F$ and then remains constant at higher temperatures. Since the experiments were run at temperatures above $1800^{o}F$ the thermal conductivity was assumed to be constant.

Although the refractive index of many absorbing materials is a complex quantity, it was assumed to be real for glass. Radiant transfer occurs in the glass at wavelengths below 4.75 microns (measured in air) where the glass does not absorb strongly. At these wavelengths the imaginary portion of the refractive index is negligible compared to the real portion, due to the weak absorption properties.

The refractive index of the glass is assumed to be a constant as the limited data shown on Figure B12 indicates that the fractional changes with temperature in the infrared region would be less than ten per cent.

The applicable energy equation follows from equation 2.1 simplified for infinite parallel plates and constant thermal conductivity.

$$K_T \frac{d^2T}{dY^2} = - \frac{dq_R}{dy} \qquad 2.3$$

Boundary Conditions :

$$Y = 0 \qquad T = T_1$$

$$Y = L \qquad T = T_2$$

In order to solve equation (2.3) the radiative flux must be expressed in terms of the temperature of the medium. The radiative transport equation is used to yield the required expression.

2.2 RADIATIVE TRANSPORT EQUATION

The radiative transport equation can be derived from the equation of transfer. For mathematical convenience, the monochromatic intensity will be divided into two components as shown in Figure 1. The intensity in the positive y-direction is $I_\lambda^+(Y,\theta)$ and the intensity in the negative y-direction is $I_\lambda^-(Y,\theta)$. For the present case equation (2.2) can be written as:

$$\mu \frac{dI_\lambda^+}{d\tau_\lambda} + I_\lambda^+ = n^2 e_{b\lambda}(\tau_\lambda) \qquad 2.4$$

$$\mu \frac{dI_\lambda^-}{d\tau_\lambda} + I_\lambda^- = n^2 e_{b\lambda}(\tau_\lambda) \qquad 2.5$$

$$\tau_\lambda = \int_0^Y K_\lambda dy \qquad \mu = \cos\theta$$

$$\tau_{o\lambda} = \tau_\lambda \text{ at } Y = L \qquad 2.6$$

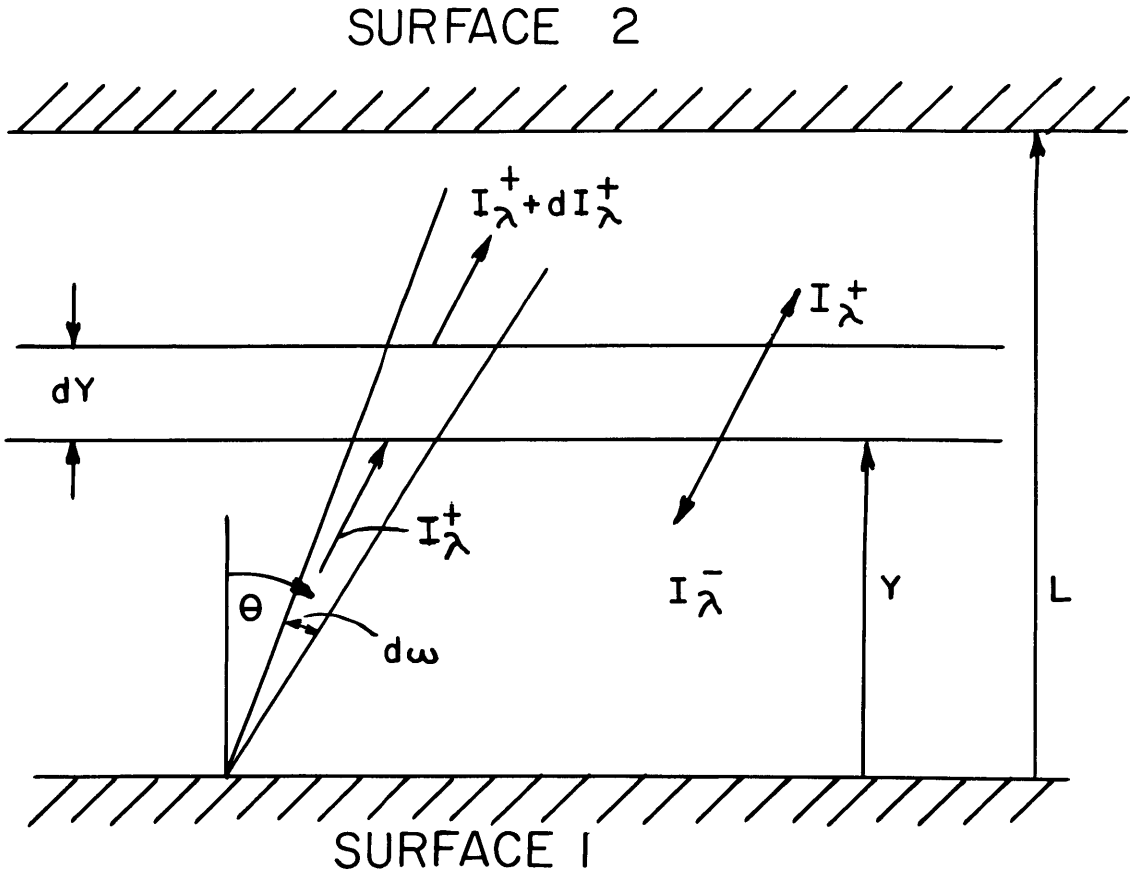

FIGURE 1 PHYSICAL MODEL FOR DIFFUSE WALLS

The boundary conditions on the intensities are:

$$I_\lambda^+(\tau_\lambda,\mu) = I_\lambda^+(0,\mu) \qquad \tau_\lambda = 0 \qquad 2.7$$

$$I_\lambda^-(\tau_\lambda,\mu) = I_\lambda^-(\tau_{o\lambda},\mu) \qquad \tau_\lambda = \tau_{o\lambda} \qquad 2.8$$

The evaluation of $I_\lambda^+(0,\mu)$ and $I_\lambda^-(\tau_\lambda,\mu)$ requires a knowledge of the directional emission and reflection properties of the surfaces, and the surface temperatures.

A solution to the radiative transport equations can be found by using an integrating factor [6]:

$$I_\lambda^+(\tau_\lambda,\mu) = I_\lambda^+(0,\mu)e^{-\frac{\tau_\lambda}{\mu}} + \frac{1}{\pi}\int_0^{\tau_\lambda} e_{b\lambda}(t)\, e^{-\left(\frac{\tau_\lambda - t}{\mu}\right)} \frac{dt}{\mu} \qquad 2.9$$

$$I_\lambda^-(\tau_\lambda,\mu) = I_\lambda^-(\tau_{o\lambda},\mu)e^{-\left(\frac{\tau - \tau_\lambda}{\mu}\right)} - \frac{1}{\pi}\int_{\tau_\lambda}^{\tau_{o\lambda}} e_{b\lambda}(t)e^{-\left(\frac{\tau_\lambda - t}{\mu}\right)}\frac{dt}{\mu} \qquad 2.10$$

The first term on the right side indicates the attenuation of energy from the boundary by absorption within the medium while the integral term represents the augmentation of energy due to emission from the medium over a finite path length. In general the emissive power distribution is initially unknown and the intensity relations are coupled to the energy equation through the radiative flux term.

2.3 RADIATIVE FLUX EQUATION

The local monochromatic radiative flux in the medium at the optical coordinate τ_λ is given by:

$$q_{R\lambda} = 2\pi\int_0^1 I_\lambda^+ \mu\, d\mu - 2\pi\int_0^{-1} I_\lambda^- \mu\, d\mu \qquad 2.11$$

Substituting equations (2.9) and (2.10) into the above equations, simplifying and taking the gradient;

$$-\frac{dq_{R\lambda}}{d\tau} = 2\pi\int_0^1 I_\lambda^+(0,\mu)\, e^{-\frac{\tau_\lambda}{\mu}} d\mu + 2\pi\int_0^1 I_\lambda^-(\tau_{o\lambda},-\mu)\, e^{-\frac{(\tau_{o\lambda}-\tau_\lambda)}{\mu}} d\mu$$

$$+ 2\int_0^{\tau_{o\lambda}} n^2 e_{b\lambda}(t) E_1(|\tau_\lambda - t|)\, dt - 4n^2 e_{b\lambda}(\tau_\lambda) \qquad 2.12$$

where

$E_n(t)$ - exponential integral

The above equation must be integrated over wavelength in order to calculate the derivative of the total heat flux.

2.4 ENERGY EQUATION AND LIMITING CASES

The derivative of the total radiative heat flux can be substituted into the energy equation (2.3) to arrive at the following equation for the local temperature:

$$K_T \frac{d^2T}{dY^2} = -\int_0^\infty \left(K_\lambda \left[2\pi\int_0^1 I_\lambda^+(0,\mu)\, e^{-\frac{\tau_\lambda}{\mu}} d\mu + 2\pi\int_0^1 I_\lambda^-(\tau_{o\lambda},-\mu)\, e^{-\frac{(\tau_{o\lambda}-\tau_\lambda)}{\mu}} d\mu + 2\int_0^{\tau_{o\lambda}} n^2 e_{b\lambda}(t) E_1(|\tau_\lambda - t|)\, dt - 4n^2 e_{b\lambda}(\tau_\lambda) \right] \right) d\lambda \qquad 2.13$$

The above integro-differential equation is nonlinear in temperature due to the nonlinear dependence of the emissive power upon the temperature.

The essential boundary conditions are derived from the required continuity of temperature at the boundaries implied by the conductive heat

transfer.

$$T = T_1 \qquad \text{at} \qquad \tau_\lambda = 0 \qquad 2.14$$

$$T = T_2 \qquad \text{at} \qquad \tau_\lambda = \tau_{o\lambda} \qquad 2.15$$

In addition $I_\lambda^+(0, \mu)$ and $I_\lambda^-(\tau_{o\lambda}, \mu)$ must be specified at both boundaries.

Many investigators [7, 8, 9, 10, 11, 12] apply the gray medium approximation, in which the absorption coefficient is independent of wavelength. Although this usually is not a physical realistic approximation, it is useful for comparison with the literature and as a first step towards nongray analysis.

The energy equation (2.13) can be nondimensionalized for a gray medium:

$$N \frac{d^2\Phi}{d\tau^2} = n^2 \Phi^4 - \frac{1}{2}\left[\beta(0) E_2(\tau) + \beta(\tau_o) E_3(\tau_o - \tau) + \int_0^{\tau_o} n^2 E_1(|\tau - \tau'|) \Phi^4 d\tau'\right] \qquad 2.16$$

where

$N = \dfrac{K_T K}{4\sigma T_H^3}$ - conduction-radiation number

$\Phi = T/T_H$ - dimensional temperature

$T_H =$ hot wall temperature

$\tau =$ optical thickness

$\tau' =$ dummy variable of integration

$\beta = B/\sigma T_H^4$ - dimensionless wall radiosity

The magnitude of the conduction-radiation number N for optically

thick media and N/τ^2 for optically thin media show the significance of conductive heat transfer compared to radiative heat transfer. When N is very large conduction is the dominant mode of heat transfer. This can occur if the thermal conductivity is high, if the material is opaque, or if the temperature level is very low. Low values of N, which occur at high temperatures and/or low thermal conductivity, indicate that radiation is the dominant mode of heat transfer.

The optical thickness, τ, defined by equation (2.6) is a very important parameter associated with radiating media. If the absorption coefficient is independent of temperature the optical thickness is simply the ratio of the characteristic length to the photon mean free path. Therefore the optical length is used to classify the various regimes of radiation.

When the optical length is much greater than unity the photon mean free path is much smaller than the characteristic length and a photon continuum exists which is analagous to continuum molecular conduction. The radiative transfer can be modelled as a diffusion process by the Rosseland equation for the optically thick limit:

$$q_{R\lambda} = -\frac{4}{3K_\lambda} \nabla e_{b\lambda} \qquad 2.17$$

The optically thin limit occurs when the optical length is much less than unity and the photon mean free path is much larger than the characteristic length. Every element of the medium can exchange radiation directly with the boundaries and there is no radiative interaction between various elements of the medium. The limit of zero optical thickness denotes a nonparticipating medium.

The regime involving intermediate values of the optical thickness occurs most often in engineering applications. Radiative transfer occurs between the medium and its boundaries and also between different elements of the medium. Consequently the energy equation (2.13) is an integro-differential equation.

For a transparent or nonparticipating medium the absorption coefficient and the divergence of the radiative flux are equal to zero. When the medium is completely opaque to thermal radiation the radiative flux is zero. Thus the radiation term in the energy equation (2.1) vanishes for the limiting cases of a transparent or an opaque medium.

Radiative equilibrium occurs away from the boundaries when radiation is the dominant mode of heat transfer. At the boundaries the thermal conductivity of the medium must be zero for radiative equilibrium. The following form of the energy equation is valid for radiative equilibrium:

$$\nabla \cdot q_R = 0 \qquad 2.18$$

The conservation of energy equation combined with the equation of transfer becomes an integral equation which is linear in the emissive power.

2.5 DIFFUSE BOUNDARIES, NONGRAY MEDIUM

In order to solve the energy equation (2.13), the intensity of the radiation leaving the surfaces must be specified. The radiation properties of the surface must be known in order to find the intensity at the surface. In this section a solution will be presented for bounding surfaces which emit and reflect radiation diffusely. In section 2.6 specularly reflecting boundaries are considered. Both solutions are for a nongray medium and nongray walls. The actual situation probably falls between specular reflection and diffuse reflection.

For a surface which emits and reflects radiation diffusely, the radiation intensities at the boundaries are independent of direction and may be expressed in terms of the surface radiosities.

$$I_\lambda^+(0,\mu) = B_{1\lambda}/\pi \qquad 2.19$$

$$I_\lambda^-(\tau_{0\lambda},\mu) = B_{2\lambda}/\pi \qquad 2.20$$

The wall radiosities are given by the following pair of simultaneous equations:

$$B_{1\lambda}=\epsilon_{1\lambda}n^2e_{b1\lambda}+2(1-\epsilon_{1\lambda})\left[B_{2\lambda}E_3(\tau_{o\lambda})+\int_0^{\tau_{o\lambda}}n^2e_{b\lambda}(t)E_3(t)\,dt\right] \qquad 2.21$$

$$B_{2\lambda}=\epsilon_{2\lambda}n^2e_{b2\lambda}+2(1-\epsilon_{2\lambda})\left[B_{1\lambda}E_3(\tau_{o\lambda})+\int_0^{\tau_{o\lambda}}n^2e_{b\lambda}(t)E_3(\tau_o-t)\,dt\right] \qquad 2.22$$

The energy equation (2.13) can be simplified when the expressions for wall radiosity are applied:

$$K_T\frac{d^2T}{dY^2}=-\int_0^{\infty}\Big(K_\lambda\left[2B_{1\lambda}E_3(\tau_\lambda)+2B_{2\lambda}E_3(\tau_{o\lambda}-\tau_\lambda)\right.$$
$$\left.+2\int_0^{\tau_{o\lambda}}n^2e_{b\lambda}(t)E_1(|\tau_\lambda-t|)\,dt-4n^2e_{b\lambda}(\tau_\lambda)\right]\Big)\,d\lambda \qquad 2.23$$

The above equation cannot be solved in closed form and a numerical technique similar to that of R.Viskanta and R.J. Grosh [8] was applied.

2.5.1 A NUMERICAL SOLUTION OF THE ENERGY EQUATION FOR DIFFUSE WALLS

The energy equation (2.23) must be integrated over wavelength accounting for the nongray glass and boundary properties, before it can be solved for temperature.

Figure 2 shows the model which is used to perform the integration over wavelength. The emissivity of platinum and the absorption coefficient were modelled as step functions of wavelength by applying averages weighted over wavelength. The absorption coefficient were measured (Appendix B) and the platinum emissivity data was taken from earlier reports [13, 14, 15]. The spread in the platinum data is due to different surface finishes and test procedures. The glass was assumed to be opaque at wavelengths beyond 3.0 microns. The wavelength scale on

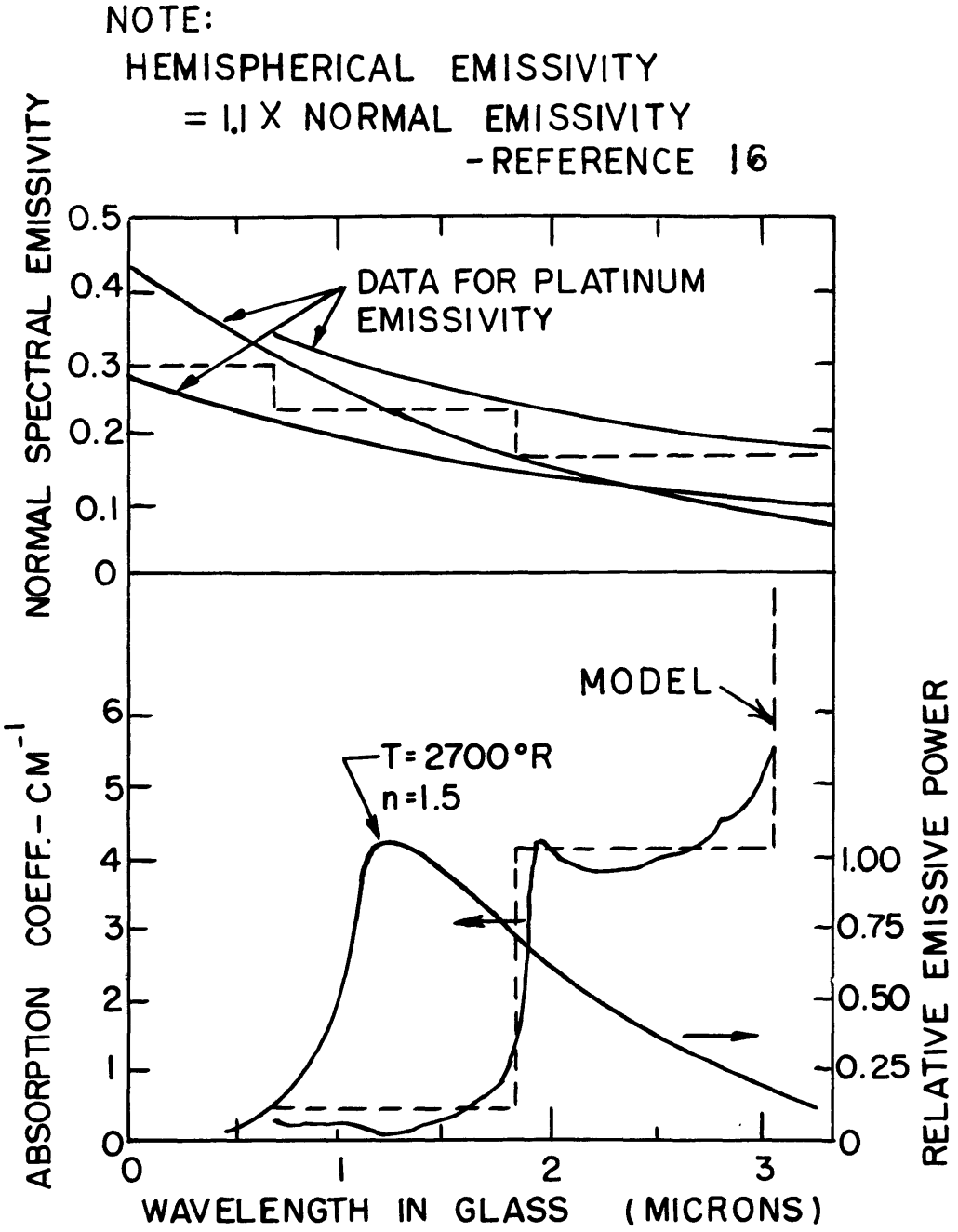

FIGURE 2 BAND MODEL FOR NONGRAY MEDIA

Figure 2 corresponds to the actual wavelengths within the glass. The absorption coefficient of the glass was measured by a monochrometer which was calibrated for wavelength in air. The actual wavelength in glass was calculated by dividing the wavelengths in air by the refractive index of the glass, taken as 1.5.

The integration over wavelength was replaced by a summation over a finite number of wavelength bands. The following tabulated function (6) was used in the summation:

$$EB(n, T_i, \lambda_j) = \frac{e_b(n\lambda_j T_i - n\lambda_{j+1} T_i)}{n^2 \sigma T_i^4} \qquad 2.24$$

This function gives the percentage of black body energy emitted by a body at T_i, in the "j" wavelength band.

Thus, the energy equation can be written as:

$$\frac{K_T}{4\sigma T_1^3 L^2} \frac{d^2 \Phi_i}{d\bar{\tau}^2} = \sum_{j=1}^{m} K_j \Big[n^2 \Phi^4 EB(n, T_i, \lambda_j) - \tfrac{1}{2}\big(\beta_{1j} E_3(\tau_j) + \beta_{2j} E_3(\tau_{oj} - \tau_j) \big) + \frac{n^2}{2} \int_0^{\tau_{oj}} E_1(|\tau_j - t|) \Phi^4 EB(n, T_i, \lambda_j)\, dt \Big] \qquad 2.25$$

and:

$$\beta_{1j} = n^2 \epsilon_1 \Phi_1^4 EB(n, T_1, \lambda_j) + 2(1-\epsilon_1)\Big[\beta_{2j} E_3(\tau_{oj}) + n^2 \int_0^{\tau_{oj}} E_2(\tau') \Phi^4 EB(n, T, \lambda_j)\, d\tau' \Big] \qquad 2.26$$

$$\beta_{2j} = n^2 \epsilon_2 \Phi_2^4 EB(n, T_2, \lambda_j) + 2(1-\epsilon_1)\Big[\beta_{1j} E_3(\tau_{oj}) + n^2 \int_0^{\tau_{oj}} E_2(\tau_{oj} - \tau') \Phi^4 EB(n, T, \lambda_j)\, d\tau' \Big] \qquad 2.27$$

where: j - denotes the wavelength under consideration

m - max. no. of wavelength band.

BOUNDARY CONDITIONS :

$$\Phi(\tau) = \Phi(0) \quad \text{at} \quad \tau = 0 \quad \text{or} \quad \bar{Y} = 0 \qquad 2.28$$

$$\Phi(\tau) = \Phi(\tau_0) \quad \text{at} \quad \tau = \tau_0 \quad \text{or} \quad \bar{Y} = 1 \qquad 2.29$$

The energy equation (2.25) is a second order nonlinear integro-differential equation in which the unknown temperature function occurs in the fourth power under the integral sign. R. Viskanta and R.J. Grosh [8] have shown that the energy equation for a gray medium can be integrated to get an integral equation which can be solved by an iterative method. In a similar manner equation (2.25) can be integrated twice with respect to τ from 0 to τ to give a nonlinear Fredholm integral equation of the second kind:

$$\Phi(\bar{Y}) = \frac{2\sigma T_1^3 L^2}{K_T} \sum_{j=1}^{m} \frac{1}{K_j} \left[G(\tau_j) - n^2 \int_0^{\tau_{oj}} \left(-E_3(\|\tau_j - \tau'\|) + E_3(\tau') + \frac{\tau_j}{\tau_{oj}} \left[E_3(\tau_0 - \tau') - E_3(\tau') \right] \right) \Phi \, EB(n, T, \lambda_j) \, d\tau \right] \qquad 2.30$$

where:

$$G(\tau_j) = \frac{1}{n^2} \left[\beta_{ij} E_4(\tau_j) - \frac{\tau_j}{\tau_{oj}} E_4(\tau_{oj}) - \frac{1}{3}\left(1 - \frac{\tau_j}{\tau_{oj}}\right) \right]$$

$$+ \beta_{2j} \left[\left(1 - \frac{\tau_j}{\tau_{oj}}\right) E_4(\tau_{oj}) - E_4(\tau_{oj} - \tau_j) - \frac{1}{3}\left(\frac{\tau_j}{\tau_{oj}}\right) \right]$$

$$+ \frac{K_T}{2n^2 \sigma T_1^3} \left[\Phi_1 - \frac{\tau_j}{\tau_{oj}} \left(\Phi_2 - \Phi_1 \right) \right] \Bigg] \qquad 2.31$$

j - denotes wavelength bands.

The method of successive approximations was used to solve equation (2.30). The medium between the boundaries was divided by a number of equispaced planes and equation (2.30) was applied at each plane. Thus, a discrete temperature function was used and the integrals were approximated by Simpson's rule across the inteval. A temperature function $\Phi_i(\bar{Y})$ was assumed and inserted on the right side of equation (2.30). This produced a new temperature function which converged toward a solution. The process was repeated until the following convergence criterion was met:

$$\frac{\Phi_{i+1}(\bar{Y}) - \Phi_i(\bar{Y})}{\Phi_i(\bar{Y})} < |.0001| \qquad 2.32$$

i = interation number

The solution usually converged in six iterations. The solution tended to oscillate when the ratio of conductive heat transfer to radiative heat transfer was less than .1. It was found that if $.5(\Phi_{i+1} + \Phi_i)$ was substituted for Φ_{i+1} to obtain Φ_{i+2}, the oscillation was reduced in the first few iterations and convergence took place. The number of spatial divisions was increased until the solution was no longer changed by a change in the number of divisions. For the glass slab calculations fifty spatial divisions were necessary.

The calculations were performed on an I.B.M. - 360 digital computer. The black body emissive power functions were interpolated from a table while the exponential integrals were approximated by polynomials. Further details of the computer solution are contained in Appendix E1.

Figures 3 and 4 show temperature profiles and heat fluxes calculated by the numerical method described above. Figure 3 shows temperature profiles in glass slabs of varying thickness with fixed boundary temperatures. The diffuse boundaries and nongray medium were modelled as shown in Figure 2. The departure from a linear temperature profile increases for larger slab thicknesses. Figure 4 shows the variation in local conductive and radiative fluxes within a .6 inch thick slab of glass. The sum of the local conductive and radiative fluxes is constant throughout the medium.

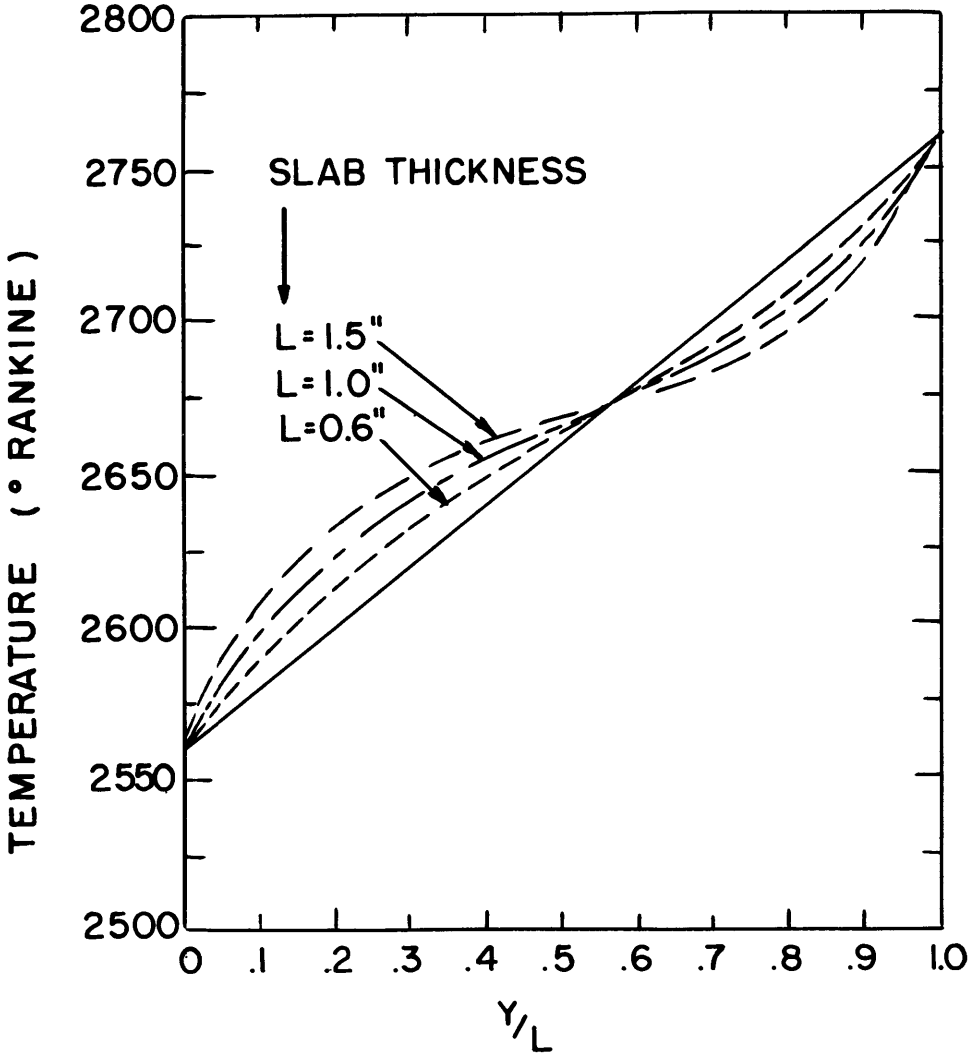

FIGURE 3 TEMPERATURE PROFILES IN GLASS WITH DIFFUSE WALLS

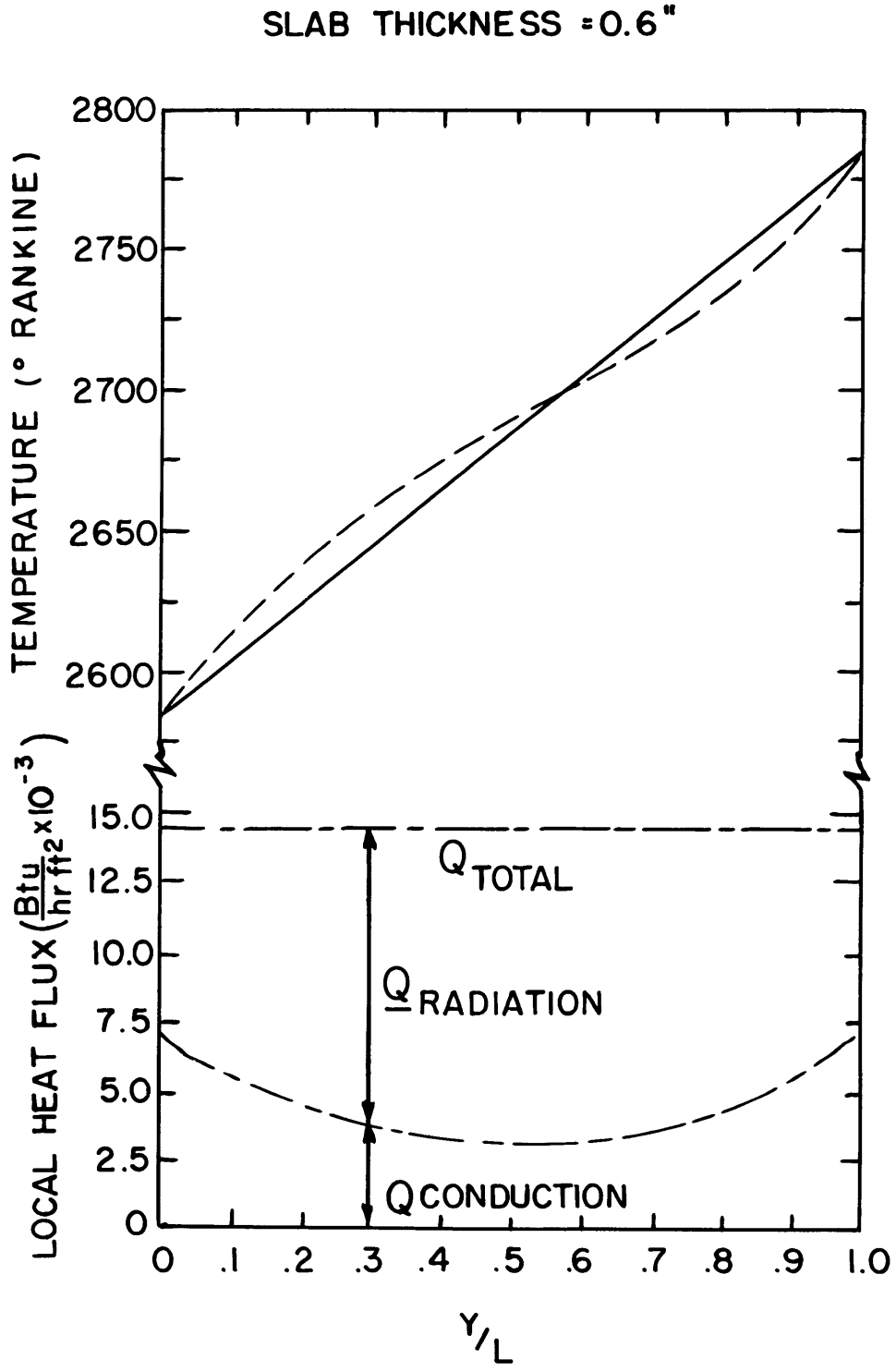

FIGURE 4 TEMPERATURE PROFILE AND HEAT FLUX IN GLASS WITH DIFFUSE WALLS

2.6 SPECULAR BOUNDARIES, NONGRAY MEDIUM

For specular or mirrorlike reflection the incident beam and reflected beam are contained within a solid angle $d\omega_i = d\omega_r$ inclined at the same angle with respect to the surface normal as shown below:

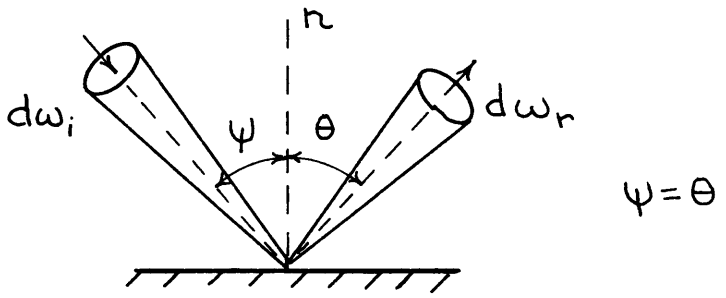

$d\omega_i$ - solid angle of incident radiation

$d\omega_r$ - solid angle of reflected radiation

The biangular monochromatic reflectivity of most materials is a function of wavelength and the angle of incidence. In measuring the biangular reflectivity the incident radiation is a beam oriented at a specific angle to the surface normal and the reflected radiation is collected in a specific angular direction. The interface used in the experiments involved glass and pure platinum foil which had a surface roughness of approximately .2 microns (rms). The angular hemispherical reflectivity of the platinum-glass interface was modelled by the Fresnel equations for specular reflection on an optically smooth interface. Appendix C contains the calculated results for the Fresnel reflectivity of platinum glass and platinum-air interfaces, as a function of angle and wavelength.

A previous investigation [16] involving platinum-air interface has shown that the Fresnel relations produce excellent agreement with experimental data from platinum foil surfaces. Figure (5) shows the agreement of the experimental data [16] with the Fresnel theory at a wavelength of two microns. Similar agreement between the data [16] and Fresnel

theory exists at wavelengths of one and five microns, as shown in Figures 6 and 7.

Earlier investigators' data [15] agrees qualitatively with the angular variations shown on Figure 5, but the absolute magnitudes are high due to surface preparation differences. The Fresnel theory accounts for the nongray reflectivity of platinum as the optical constants are wavelength dependent. The optical constants used were from room temperature data [17]. The emissivities calculated from these optical constants agree with the values measured by Rolling [16] as shown by Figures 5, 6, and 7. A representative emissivity of a platinum glass interface is shown in Figure 8 and the reader is referred to Appendix C1 for more detailed results. The agreement between the measured platinum emissivities and those calculated from the Fresnel equations for a platinum-air interface does not prove that the platinum-glass interface is a pure specular reflector.

2.6.1 NUMERICAL SOLUTION OF THE ENERGY EQUATION FOR SPECULAR WALLS

Figure 9 shows the configuration under consideration. A semi-transparent stationary medium of infinite extent in the horizontal plane has upper and lower specularly reflecting boundaries which are at different temperatures. The temperature distribution within the medium and the heat flux across it are initially unknown. Heat transfer within the medium occurs by conduction and radiation. A solution is required for the steady-state temperature profile and heat flux.

An implicit solution [5] for the temperature profile was derived by dividing the medium up into layers of thickness "ΔY" and writing a heat balance equation for each layer in terms of the temperature of all of the layers. This equation can be written for each layer and a system of "n" equations in "n" unknown temperatures is derived. (n is the number of layers). The specular boundaries are modelled by the Fresnel equations introduced in Section 2.6. The nongray absorption coefficient of the glass was modelled as a step-function of wavelength, as mentioned

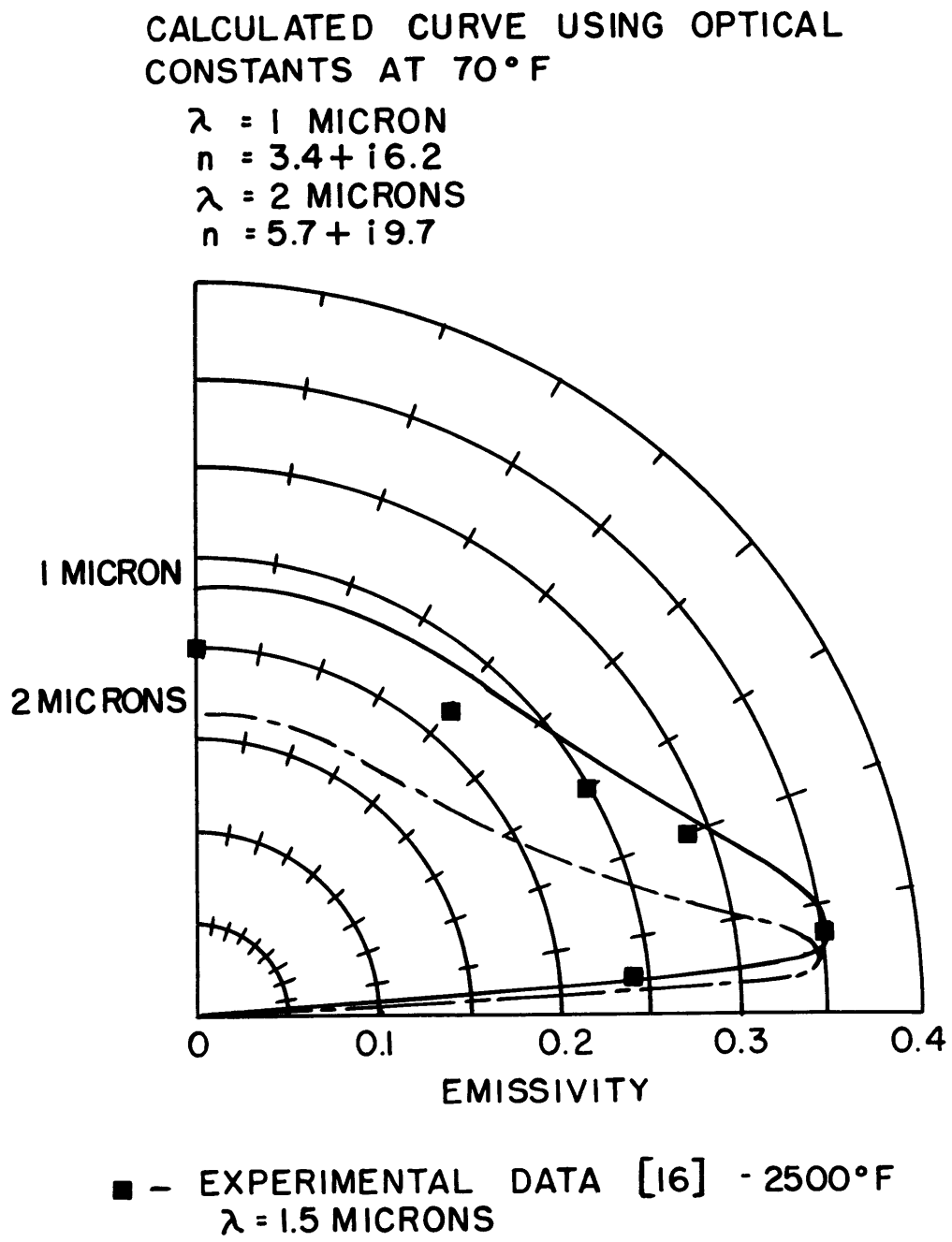

FIGURE 5 SPECTRAL DIRECTIONAL EMISSIVITY OF PLATINUM IN AIR -EXPERIMENTAL + THEORETICAL

CALCULATED CURVE USING OPTICAL CONSTANTS AT 70° F

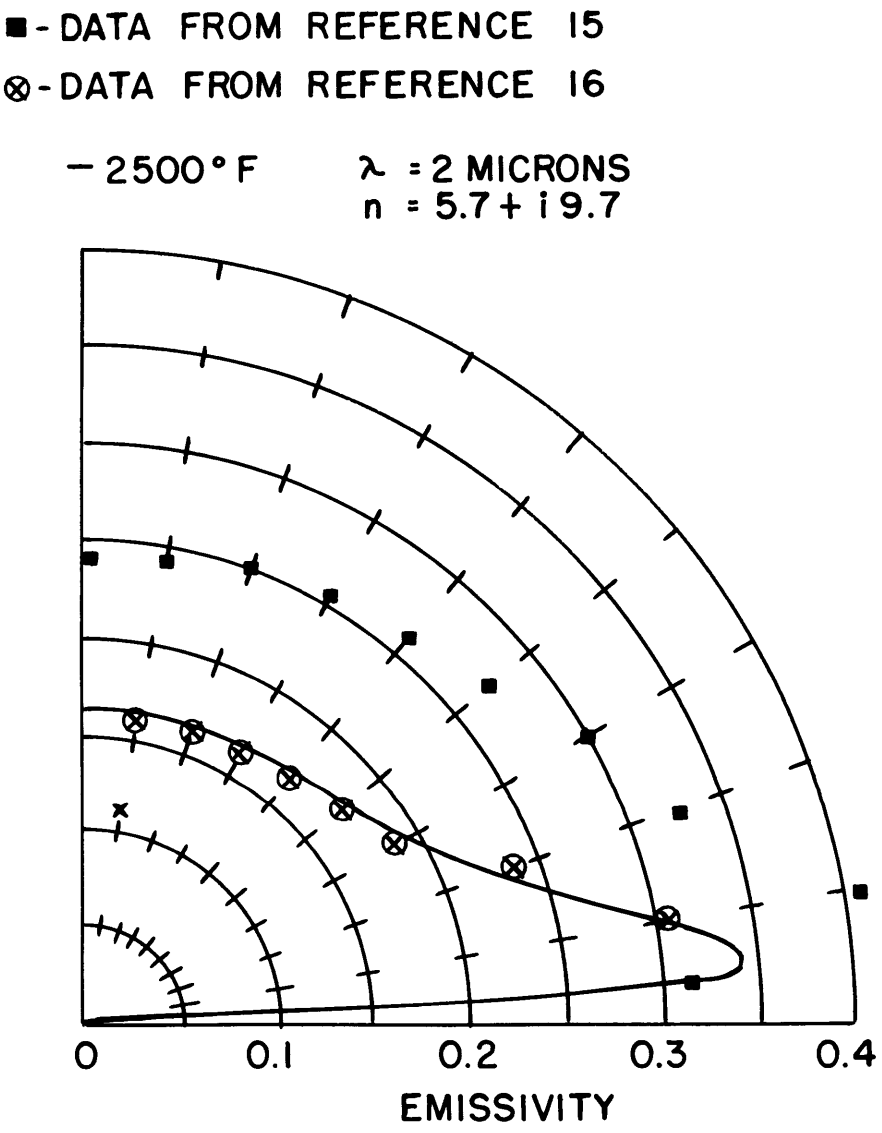

FIGURE 6 SPECTRAL DIRECTIONAL EMISSIVITY OF PLATINUM IN AIR - EXPERIMENTAL + THEORETICAL

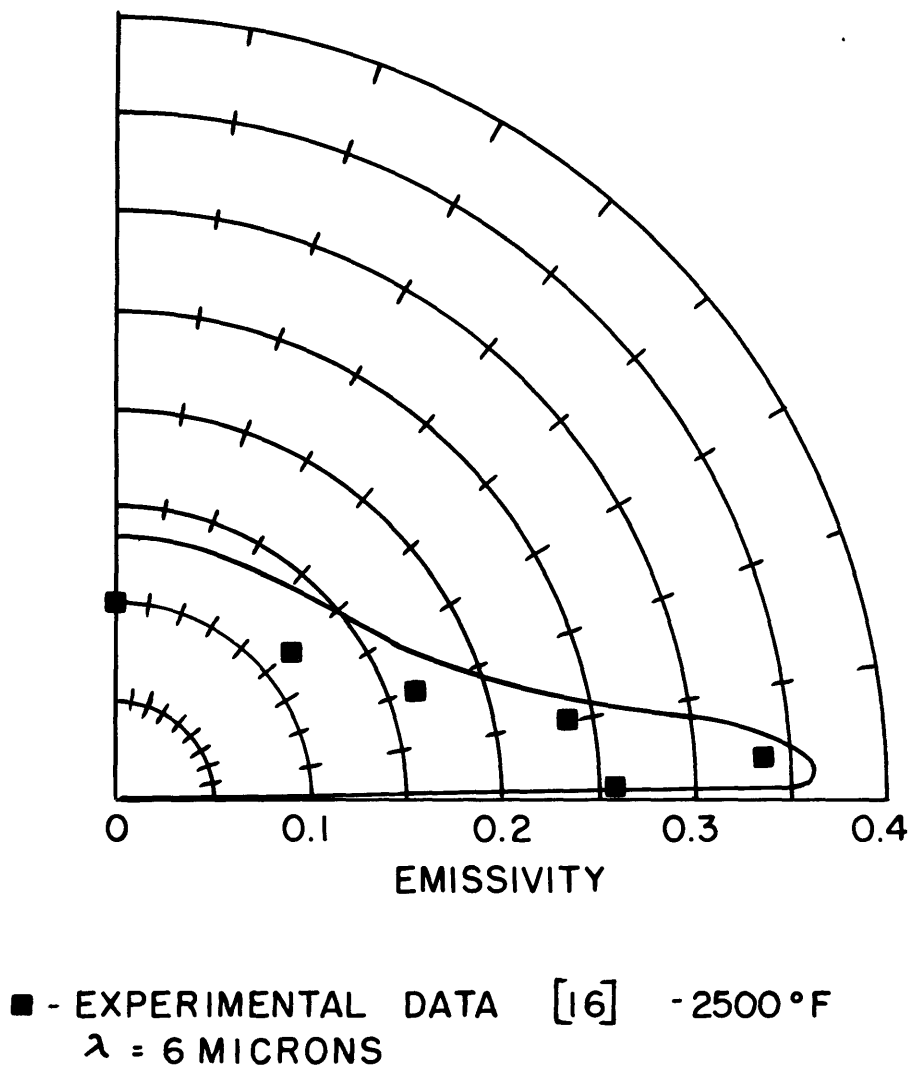

FIGURE 7 SPECTRAL DIRECTIONAL EMISSIVITY OF PLATINUM IN AIR - EXPERIMENTAL + THEORETICAL

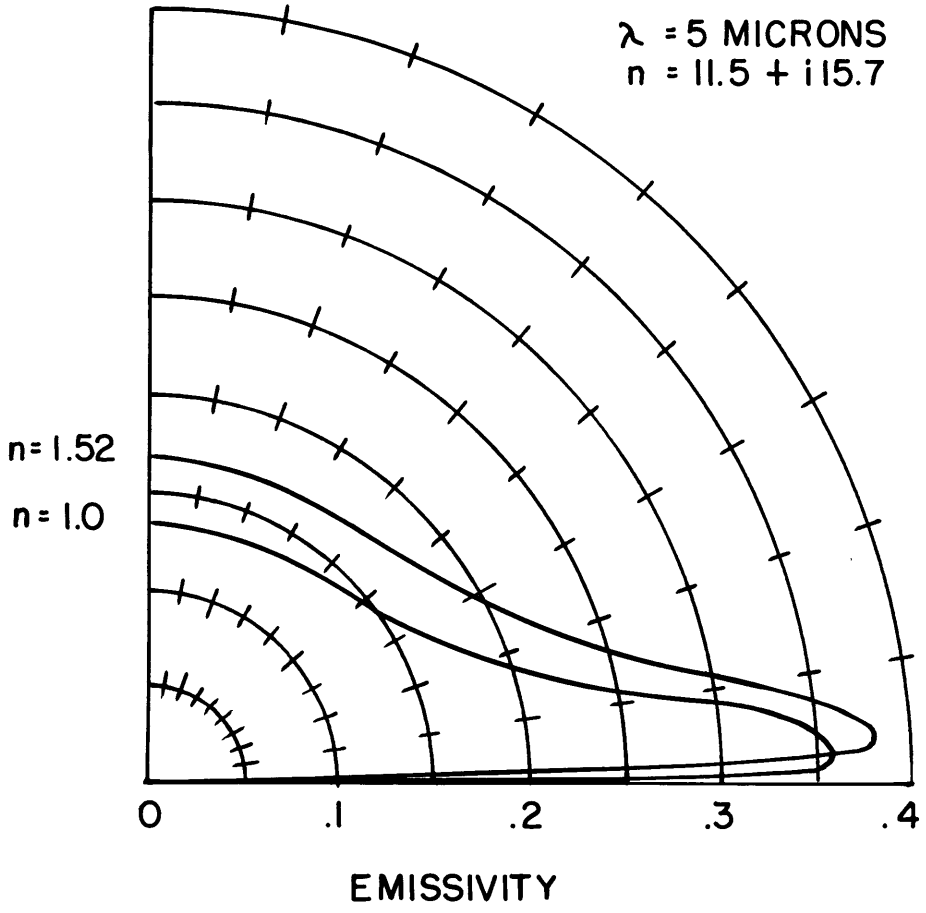

FIGURE 8 SPECTRAL DIRECTIONAL EMISSIVITY OF PLATINUM

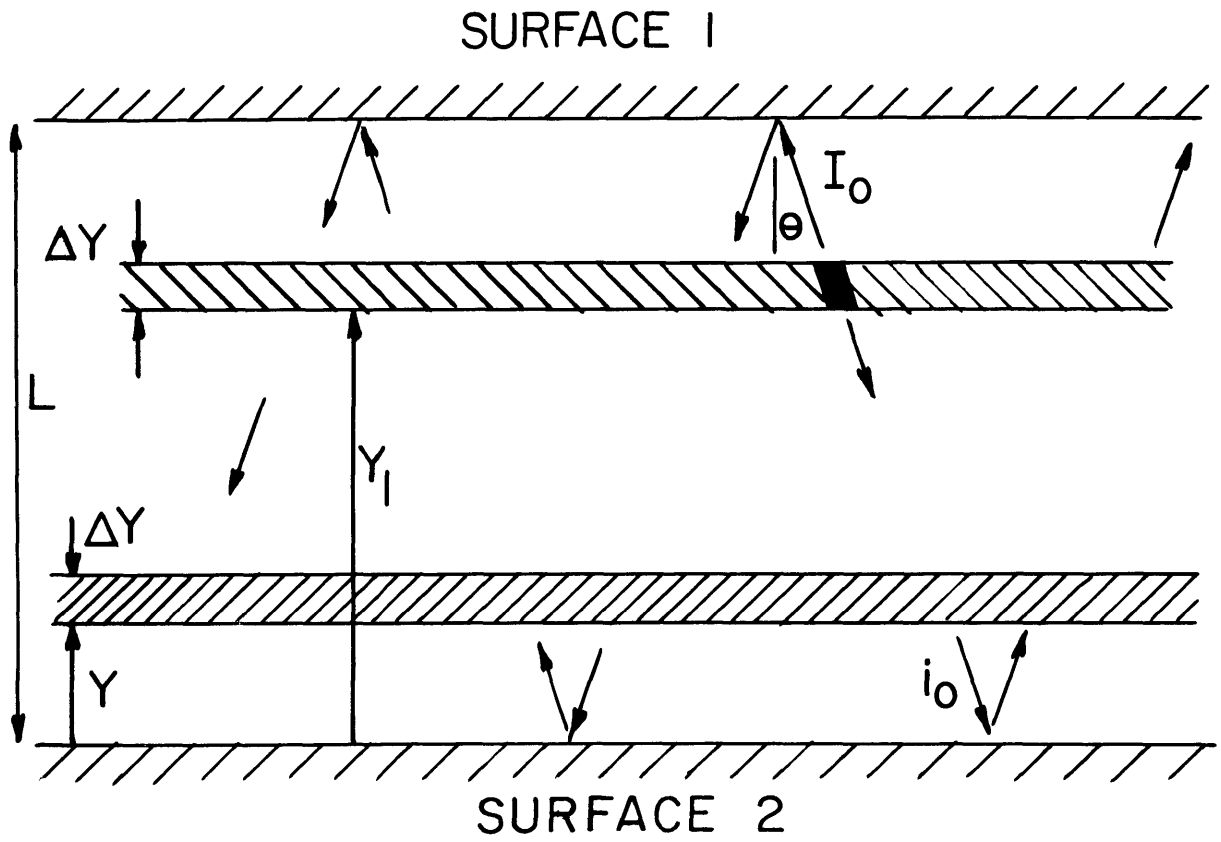

FIGURE 9 PHYSICAL MODEL FOR SPECULAR BOUNDARIES

in Section 2.5.1

The heat balance is complicated because energy can arrive at a given layer by several different methods. Radiative heat transfer between an emitting layer and an absorbing layer can occur by direct exchange or by multiple internal reflections (heatafter referred to as M.I.R.) from the specularly reflecting boundaries. In M.I.R. exchange a beam of radiation emitted by a layer at "Y_1" is reflected by the upper wall, travels to "Y", is partially absorbed there, and the transmitted portion is reflected by the lower surface, and reaches the level "Y" several times, until the beam has been completely absorbed. The M.I.R. terms were written as an infinite series, which could be expressed as a closed form analytical expression. Energy can be radiated from the boundaries to a layer by direct or M.I.R. exchange. Heat can be conducted into a given layer from the adjacent layers.

The following equation results from a steady-state qualitative heat balance on a layer at distance "Y" from the boundary.

ENERGY ABSORBED BY DIRECT EXCHANGE WITH SURROUNDING MEDIUM

\+ ENERGY ABSORBED BY M.I.R. EXCHANGE WITH SURROUNDING MEDIUM

\+ ENERGY ABSORBED BY DIRECT EXCHANGE WITH LOWER BOUNDARY

\+ ENERGY ABSORBED BY M.I.R. EXCHANGE WITH LOWER BOUNDARY

\+ ENERGY ABSORBED BY DIRECT EXCHANGE WITH UPPER BOUNDARY

\+ ENERGY ABSORBED BY M.I.R. EXCHANGE WITH UPPER BOUNDARY

\+ NET HEAT CONDUCTED IN

\- ENERGY EMITTED BY LAYER

\+ ENERGY EMITTED BY LAYER WHICH DOES RETURN TO SAME LAYER BY M.I.R. AND IS REABSORBED

= 0

Appendix D gives the complete algebraic derivations for each individual term in the heat balance expression. The calculation of the radiative flux terms is complicated by the fact that they must be integrated over angle due to the Fresnel boundary conditions, and summed over wavelength according to the nongray band model given in section 2.5.1. The integration over angle was approximated by Gaussian quadrature. The number of points used was varied in order to ensure that the integration increments were so small, that the solution did not change when they were made smaller.

A system of "n" nonlinear algebraic equations in the unknown temperature of each layer can be formulated by writing out the heat balance for each of the "n" slabs located between the boundaries. It is convenient to express the equations in matrix notation as follows:

Aij coefficients in heat balance due to conduction heat flux into a layer given by equations D45, D44

Bij coefficients in heat balance due to radiative exchange between individual layers given by equations D17, D33, D43

Cij coefficients in heat balance due to radiative exchange from the boundaries (known temperature) to a layer given by equation D28

$$[A](T) + [B](T^4) + (C) = 0 \qquad 2.33$$

The Newton-Raphson iterative method was used to solve the system of nonlinear algebraic equations. A brief description of the method

follows and the reader is referred to a text on numerical analysis for more details.

The matrix equation was solved in terms of the emissive power as the terms in "T^4" predominate over those in "T". A trial temperature vector was substituted into the heat balance equation and a non-zero residual vector resulted if the trial vector was not the correct solution.

The Newton-Raphson method permits the calculation of a correction to be added to the previous emissive power to yield a new emissive power which is closer to the correct solution. This process converges on the correct solution as the residual vector becomes very small. The correction vector is calculated by taking the gradient of the matrix equation and equating it to the negative of the residual vector.

As the equation for the correction vector is linear in the change in emissive power, it was solved, by a standard subroutine for linear simultaneous equations.

The numerical results of this analysis are shown in figures 10 and 11. Figure 10 compares the temperature profiles for specular, diffuse and black boundaries. The effect of specular boundaries seems to be a larger distortion from a linear profile then in the diffuse or black case. Figure 11 shows the temperature profiles for specular, diffuse and black boundaries for radiative equilibrium. Specular reflection causes a smaller temperature gradient in the medium than diffuse reflection or black walls.

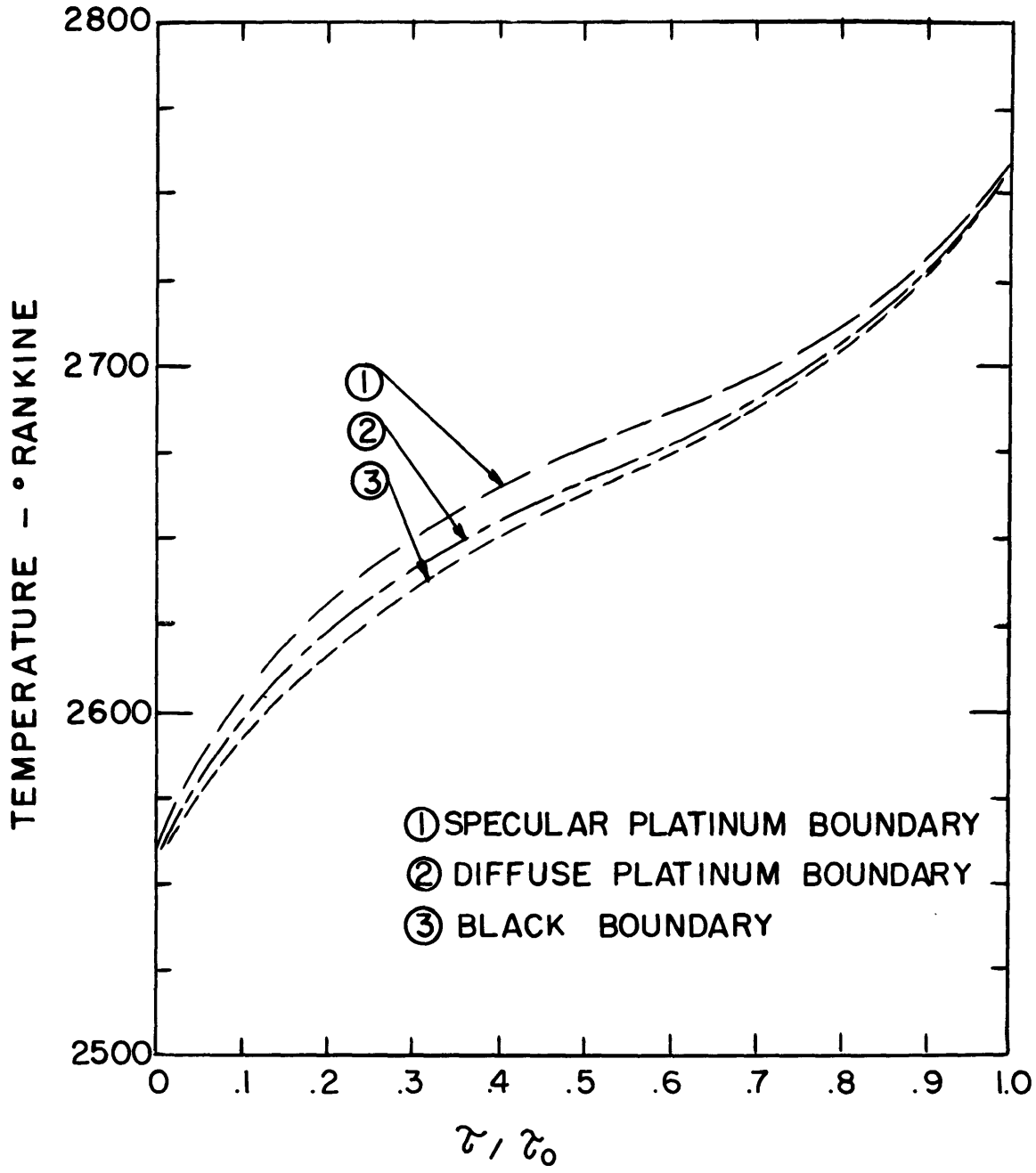

$\tau_0 = 0.283$, GRAY MEDIUM

$N/\tau^2 = 0.295$

FIGURE 10 TEMPERATURE PROFILES FOR DIFFERENT BOUNDARIES

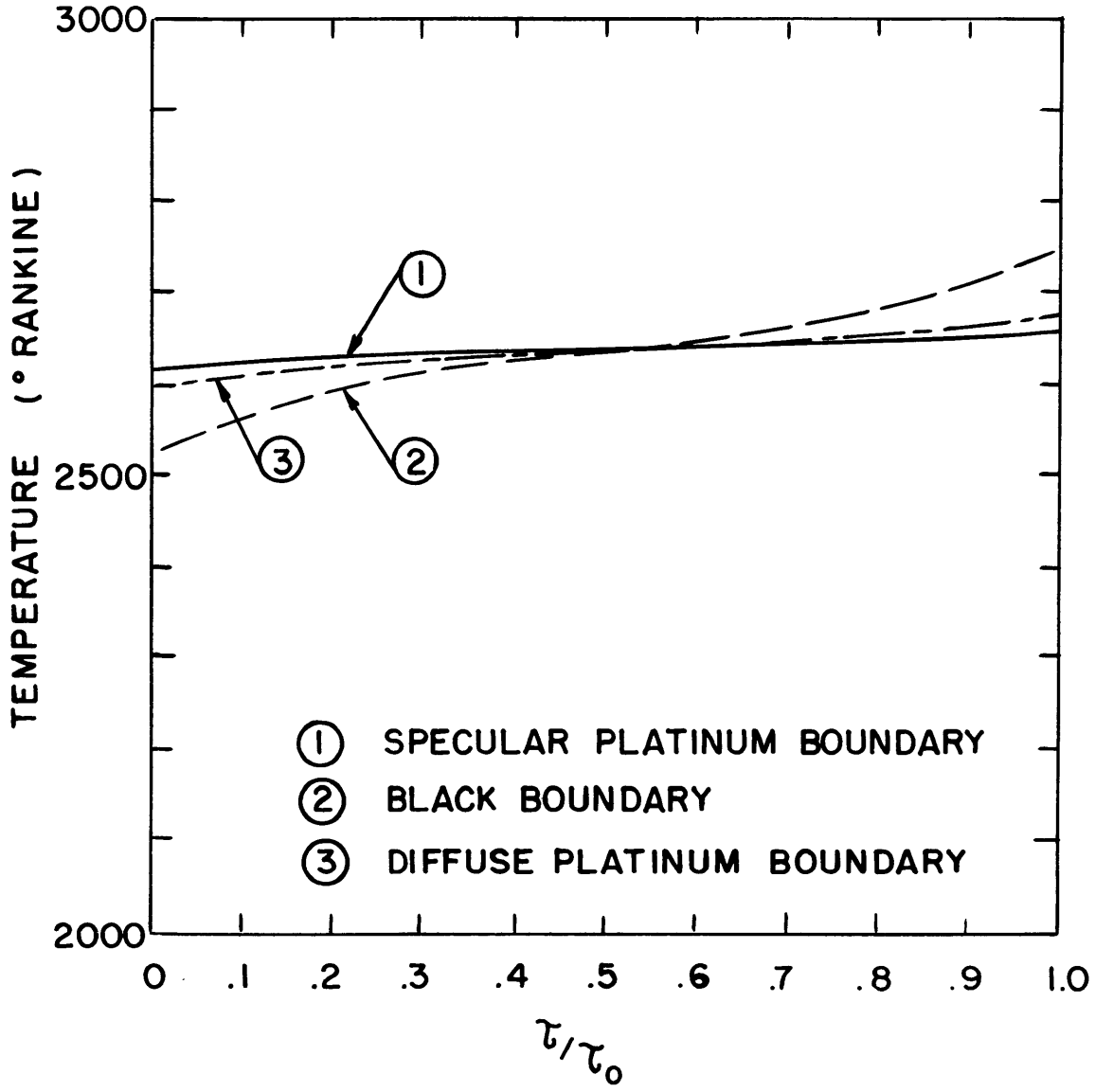

FIGURE 11 TEMPERATURE PROFILES FOR RADIATIVE EQUILIBRIUM

III. EXPERIMENTAL PROGRAM

3.1 Experimental Objectives

The purpose of the experimental investigation was to obtain measurements of the temperature profile within and the heat flux across a slab of glass in a one-dimensional temperature field. The data obtained were used to evaluate the accuracy of the proposed analytical models. The thickness of the glass slab was kept constant but the temperatures of its boundaries were varied.

3.2 Design Considerations

In order to fulfill the experimental objectives the apparatus had to perform the following functions:

1.) A one-dimensional heat flux was to be simulated. The upper boundary of a 8.25" x 8.25" x 1.5" horizontal glass slab was cooled and the lower boundary was heated. Heat losses from the edge of the glass slab were minimized in order to attain a one-dimensional temperature profile.

2.) The temperature level of the glass slab was to be varied in order to operate from the regime where conductive and radiative fluxes are equal to the regime where radiation dominates. In order to achieve this the isothermal boundary temperatures were independently variable between 1900^{o}F and 2300^{o}F with the lower boundary being the hotter one.

3.) The boundaries were to be made of materials with known optical properties. Therefore the upper and lower boundaries were lined with .0005 inch platinum foil.

4.) The heat flux across the slab and the temperatures at the glass slab boundaries were to be measured as described in Section 3.3.1.

5.) Local temperatures within the glass were to be measured so that the temperature profile could be determined. The laser method in Section 3.3.3 was developed to measure the temperatures.

3.3 Description of Apparatus

Many problems were encountered in the design of the experimental apparatus due to the high temperature level and the corrosiveness of the molten glass. The apparatus design is considered in three parts; the tray to contain the glass, the furnace to heat the tray and the optical system to measure local temperatures within the glass.

3.3.1 Tray to Contain Glass

The material used to construct the tray could not contaminate the glass and change its optical properties, and it had to have sufficient strength. A fusion cast high purity alumina ceramic (MONOFRAX A*) was tested and found to possess the required properties. Figure 14 shows a cross-section of the ceramic tray used to contain the 8.25" x 8.25" x 1.5" slab of glass. The bottom and top of the tray were made of 1.5" slabs of MONOFRAX A and lined with .0005" of platinum foil on the inside. Platinum lining was used because its optical properties have been established with greater accuracy than those of MONOFRAX A. The windows which the laser beam passed through were made of synthetic sapphire which is transparent in the visible portion of the spectrum and resistant to molten glass up to 2700°F.

The temperatures at twenty positions on the upper and lower boundaries of the glass were measured by Pt-Pt/10% Rh thermocouples located at the platinum-MONOFRAX interface as shown in Figure 13. The heat flux through the bottom of the tray was calculated by measuring the temperature drop across it and applying the Fourier equation. The thermal conductivity of Monofrax A at 2000°F is 41.7 Btu/hr ft^{2}°F/in.+

3.3.2 Furnace

Figures 15 and 16 show the furnace used to heat the tray of glass. Eight Globar** heating elements capable of producing seven kilowatts at

---

*Trademark of Carborundum Co.

**Silicon Carbide, trademark of Carborundum Co.

+ Measured by Dynatech Corporation

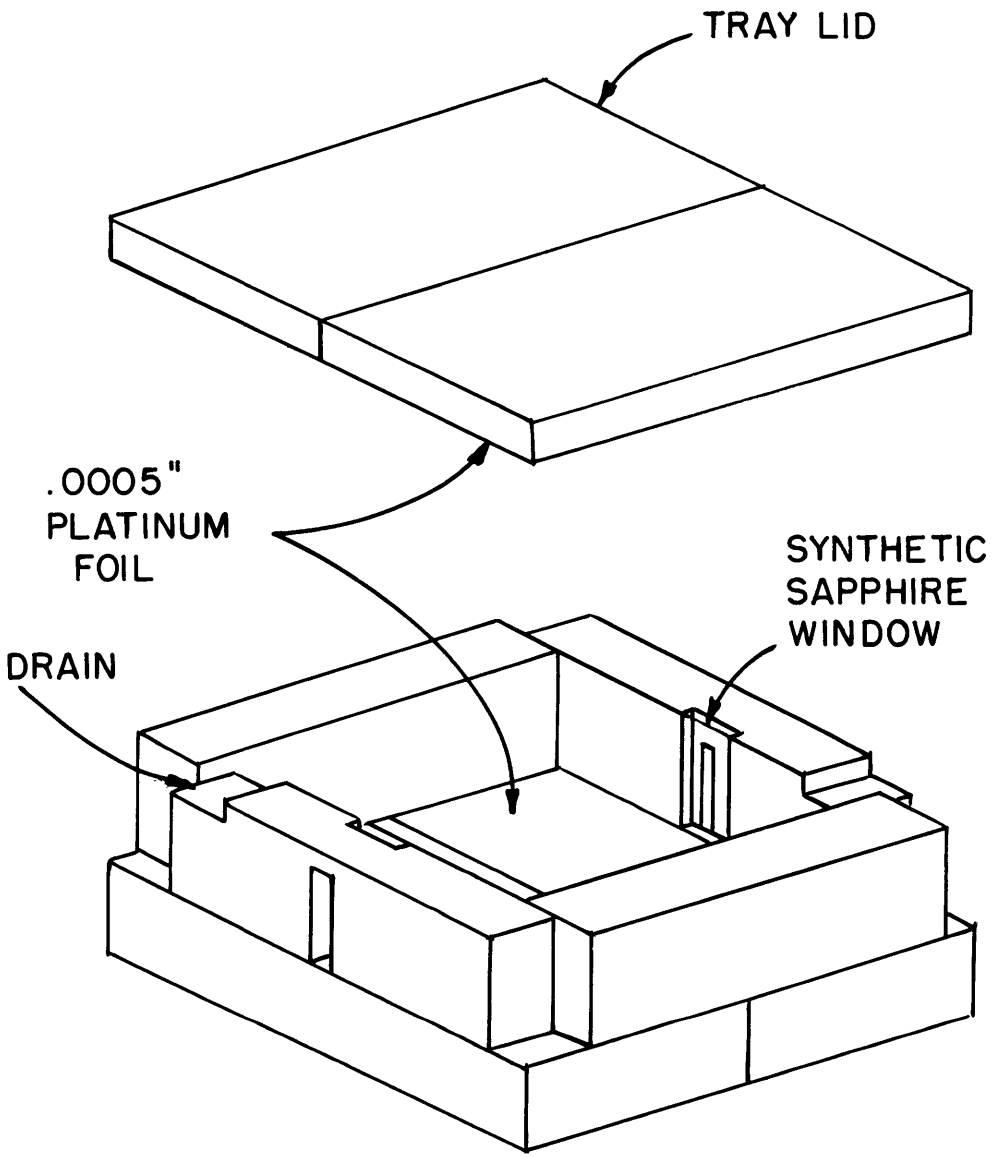

FIGURE 12 ASSEMBLY DRAWING OF TRAY

TOP VIEW OF CERAMIC TRAY

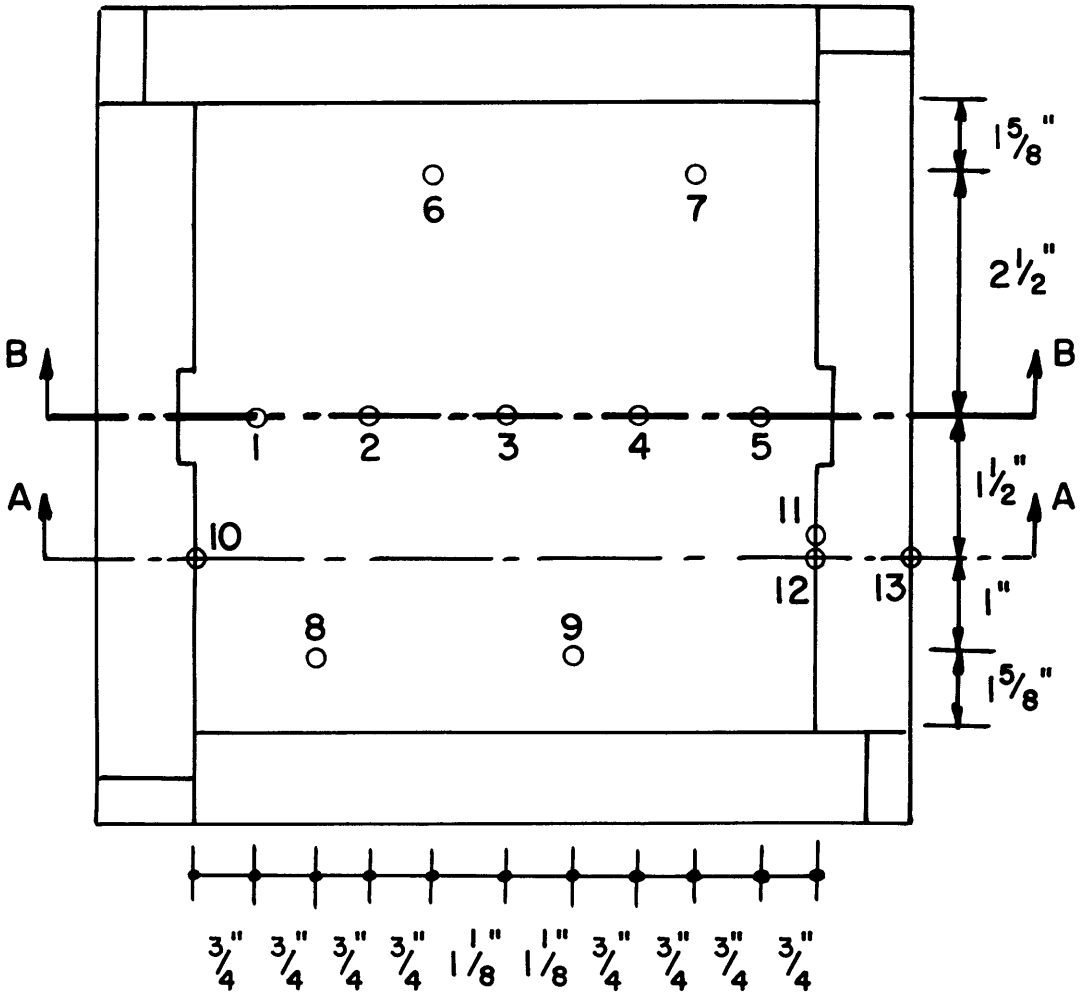

NOTE: SECTIONS A-A AND B-B ARE ON THE FOLLOWING DRAWING

FIGURE 13 THERMOCOUPLE POSITIONS ON CERAMIC TRAY

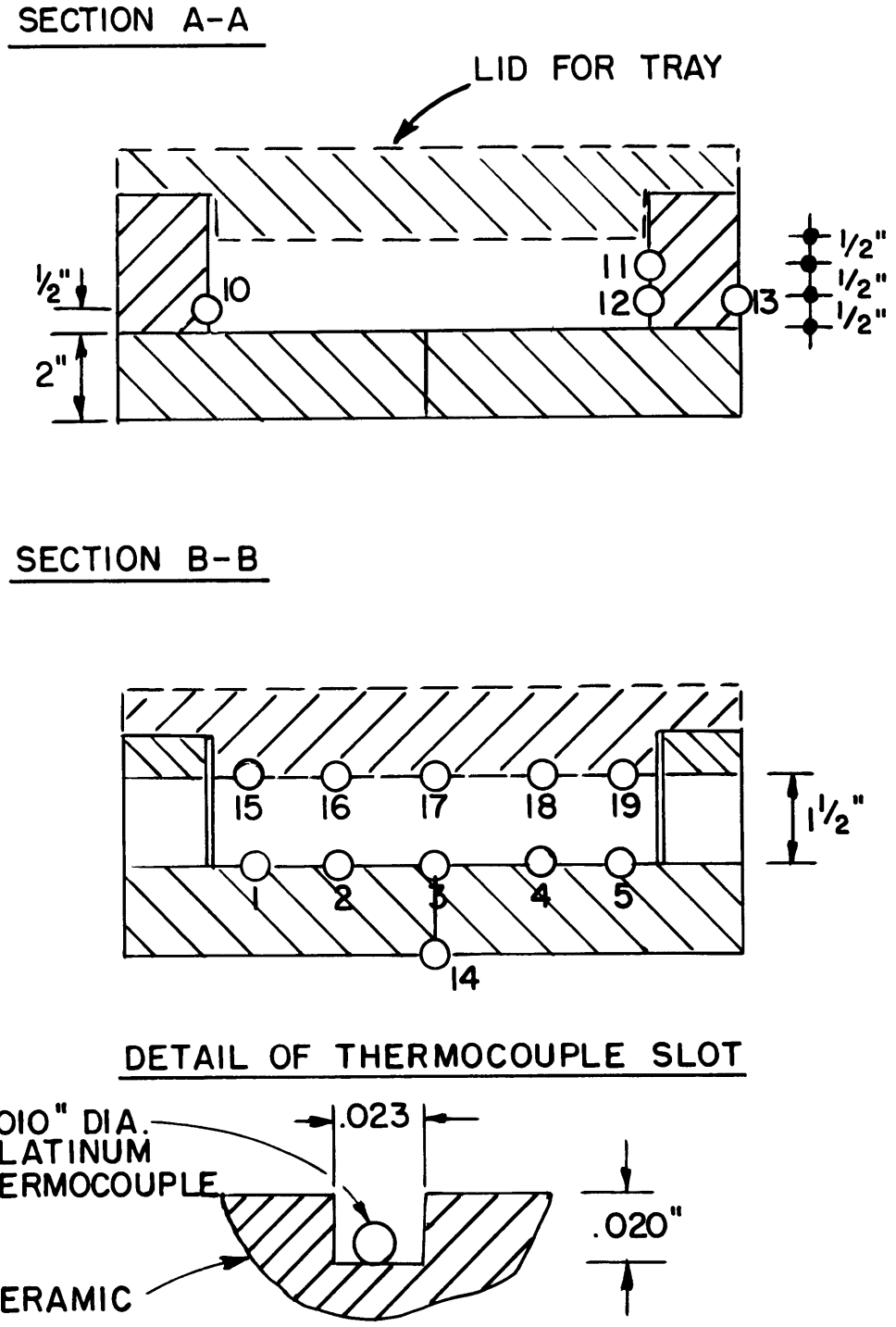

FIGURE 14 THERMOCOUPLE POSITIONS ON CERAMIC TRAY

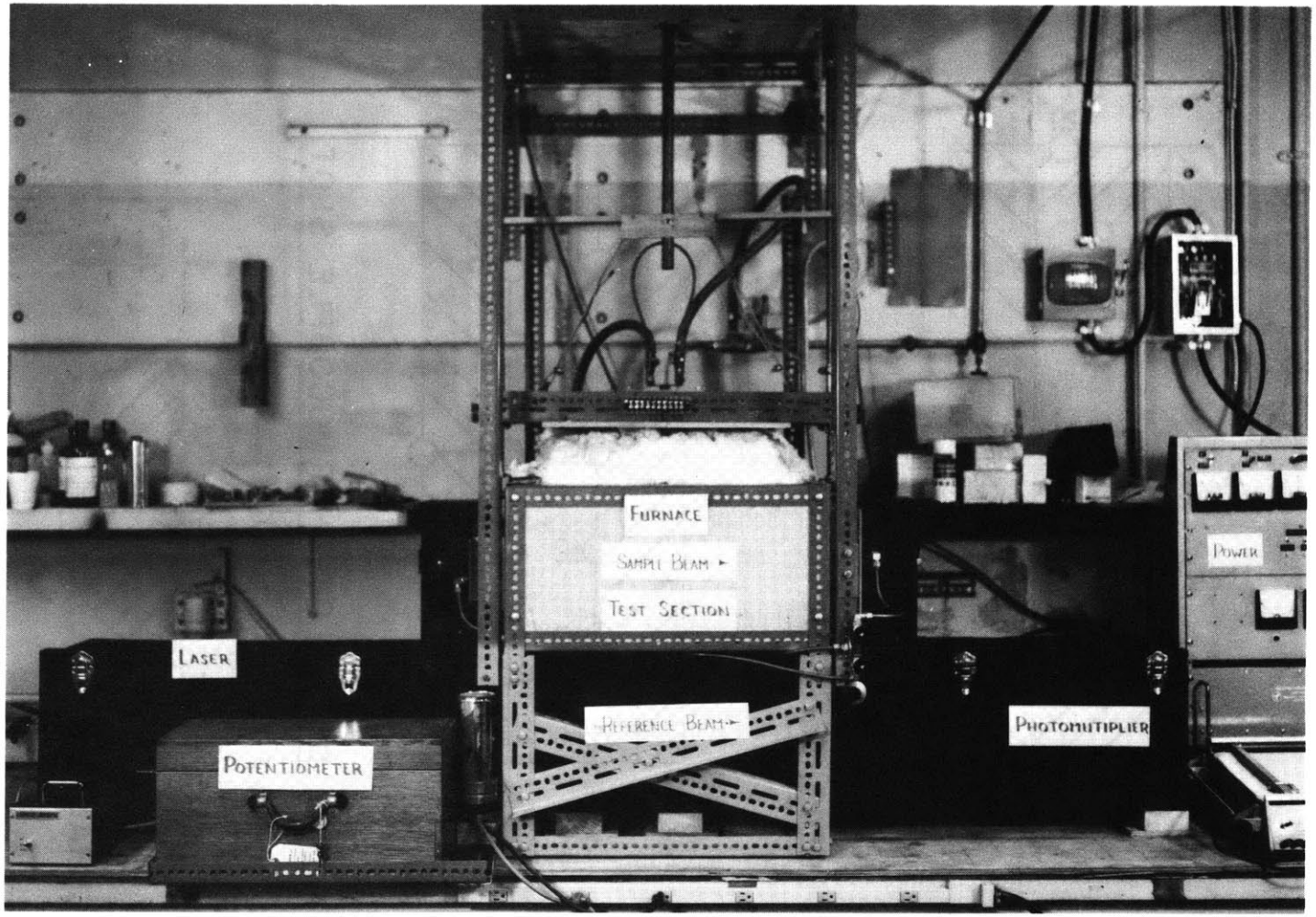

FIGURE 15 PHOTOGRAPH OF APPARATUS

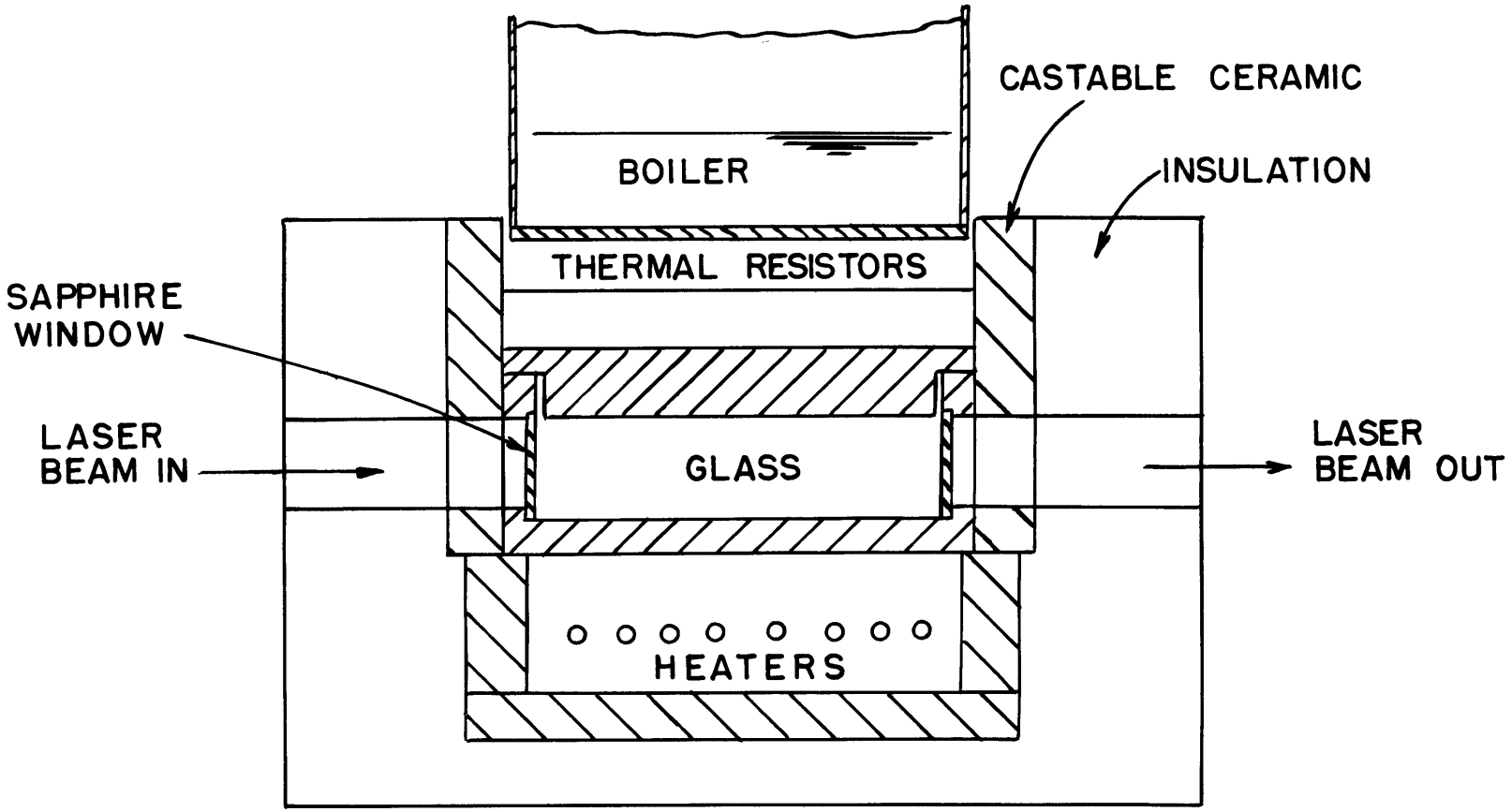

FIGURE 16 FURNACE CROSS SECTION

2800°F were placed below the tray. The heating elements were built in three independent sections, each controlled separately so that the heat flux could be adjusted to make the bottom of the tray isothermal.

The inner portion of the furnace was made of castable ceramic and the sides were insulated with a low-conductivity ceramic fiber. This configuration was used to produce a one-dimensional heat flux through the slab of glass. The heat flux out the ends of the slab was determined by measuring the temperature drop across the walls of the ceramic tray. This heat flux provided a measure of the departure from a one-dimensional heat flux. The values of the end flux are given in Section 4.

3.3.3 Optical System

Experimental measurements of temperature profiles within semi-transparent media are difficult to obtain because the temperature sensor distorts the radiation environment. One method [18] is to immerse a series of thermocouples of decreasing size, and extrapolate the results to zero thermocouple size. This method has several drawbacks. The physical presence of the thermocouple in the medium disturbs the temperature profile by interfering with the heat transfer processes. Due to their low strength fine thermocouples must be mechanically supported in the medium, interfering further with the heat transfer.

An optical method of temperature measurement has been developed. The variation of the monochromatic absorptivity of glass with temperature was used to measure the local temperature within the molten glass. Figure 17 is a schematic of the optical system used to measure the one-dimensional temperature profiles within the glass slab.

A brief description of the apparatus follows and the reader is referred to an earlier report [19] for details on the design and construction of the apparatus. A Helium-Neon continuous wave gas laser (.6328 micron wavelength) having a power level of two milliwatts and a beam diameter of 1.4 mm was used a source of monochromatic light. A reflecting beam splitter and a 700 Hertz chopper wheel were used to pro-

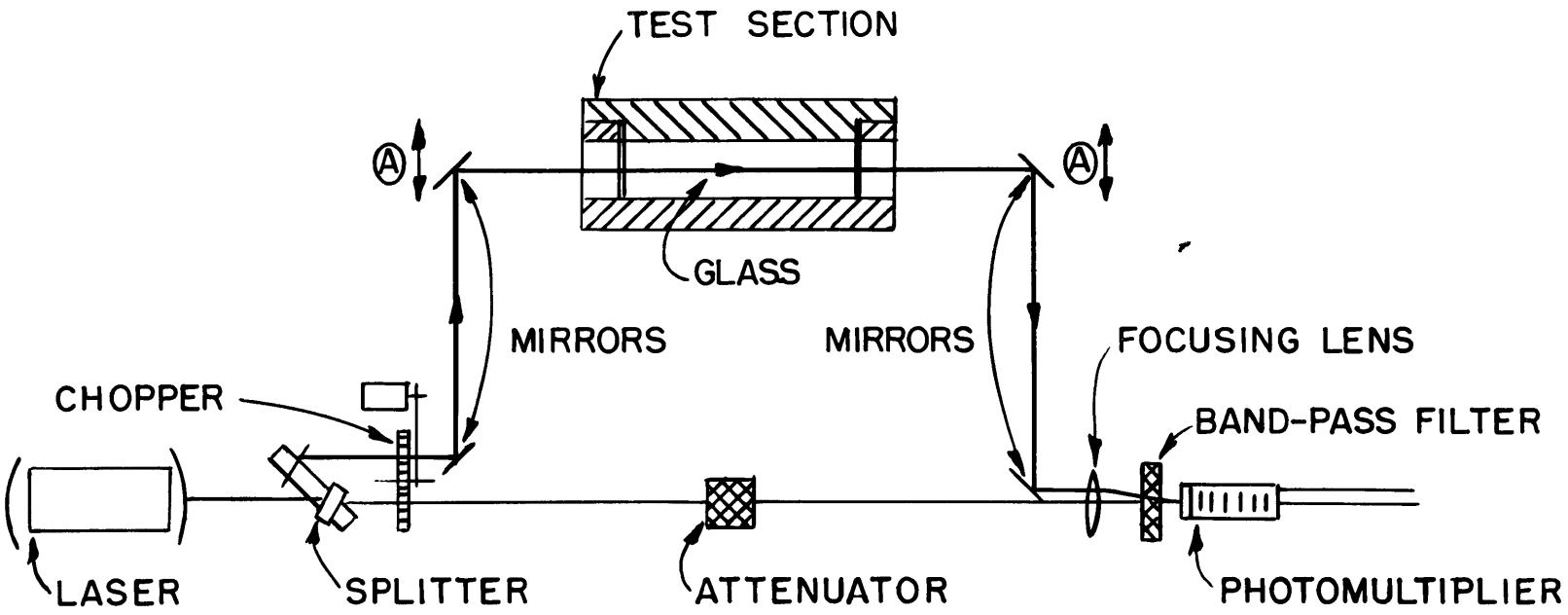

FIGURE 17 OPTICAL SYSTEM, SCHEMATIC

duce two out-of-phase beams which could be measured on a single detector. The reference beam passed through a variable attenuator (polarizing prism), a focusing lens and an optical bandpass filter on to a photomultiplier tube. The test beam was directed through the test section by means of plane mirrors. The mirror system was capable of traversing the beam across the glass slab and the beam position could be read to within .001" by means of a set of dial micrometer gauges mounted on the mirrors. The test beam, after leaving the test section, passed through the focusing lens, bandpass filter and onto the photomultiplier tube. The signals from the photomultiplier were observed on an oscilloscope. If the test beam and the reference beam were not of equal magnitude, a 700 Hertz square wave was observed on the oscilloscope. The amplitude of the waveform was proportional to the difference of intensity of the test and reference beams. By adjusting the variable attenuator, the square waveform could be nulled, balancing the intensity of the two beams at the detector.

Jeryan [19] showed that the monochromatic absorption coefficient of Waterwhite glass increased monotonically with increasing temperature. The optical system described herein was used to measure one-dimensional temperature profiles within the glass by measuring the attenuation of a given laser beam path through the glass and relating it to the local temperature.

3.4 EXPERIMENTAL PROCEDURE

The method of operation is described next. The ceramic tray in the furnace was loaded with pieces of glass and the lid was supported above the tray by ceramic wedges. The tray was slowly heated to 1800^{o}F until all the glass had melted. The temperature was then raised to 2100^{o}F and held there until all the entrained bubbles rose to the surface. Then the tray lid was lowered by removing the ceramic wedges and the calibration tests were started. The glass slab was kept isothermal by adjusting the furnace power and insulation. The temperature of the slab was read by the Pt-Pt/10% Rh thermocouples on the test sec-

tion walls. The laser beam was then switched on and the intensities of the test and reference beams were balanced by adjusting the attenuator to produce a null of the waveforms. This calibration procedure was repeated at a number of different temperature levels and the variable attenuator was calibrated in terms of temperature. Then a one-dimensional temperature gradient was imposed on the glass slab by cooling the top of the furnace and the laser beam was traversed to a given position, nulled by adjusting the attenuator and the temperature was read from the attenuator calibration curve. The beam was then moved to a new position and the procedure was repeated. In this way, a temperature profile was measured in the glass, between the upper and lower boundaries of the test section.

3.5 DISCUSSION OF EXPERIMENT

Five calibration tests and four data tests were performed according to the procedure outlined in Section 3.4. Figure 18 shows the calibration curve for the variable attenuator. The calibration data of this work is in agreement with that of Jeryan [19] at temperatures above 1950°F. Below this temperature the glass transmissivity measured by Jeryan [19] was lower than that of the present work. Temperature profiles and heat fluxes from the four data sets are presented in Section IV. The heat flux was calculated by measuring the temperature gradient across the bottom of the tray and applying Fourier's law. In each test radiation was more significant than conduction. It was not possible to operate the apparatus in a conduction dominated regime because the low temperature levels required would make the glass crystallize and become opaque.

The temperature of the glass near the upper and lower boundaries was not measured due to clouding of the edges of the synthetic sapphire windows. The clouding was caused by glass leaking onto the outside of the windows and crystallizing.

The exact nature of the reflection at the platinum-glass interface was not determined by the experiments. Figures 19 and 20 are photomicrographs of the platinum foil from the test section before and after

testing. The platinum foil was smooth, except for random scratches before the tests. The samples examined after the tests show a marked increase in surface roughness and waviness. The increase in roughness would tend to cause reflections from the platinum foil to be more diffuse. However, it is not known whether the increase in roughness occurred during the tests, or as a result of contraction during cooling.

The average temperature of the lower surface was calculated by averaging the temperatures of thermocouples 1, 2, 3, 4 and 5. Similarly, the average temperature of the upper plate was calculated from thermocouples 15, 16, 17, 18 and 19.

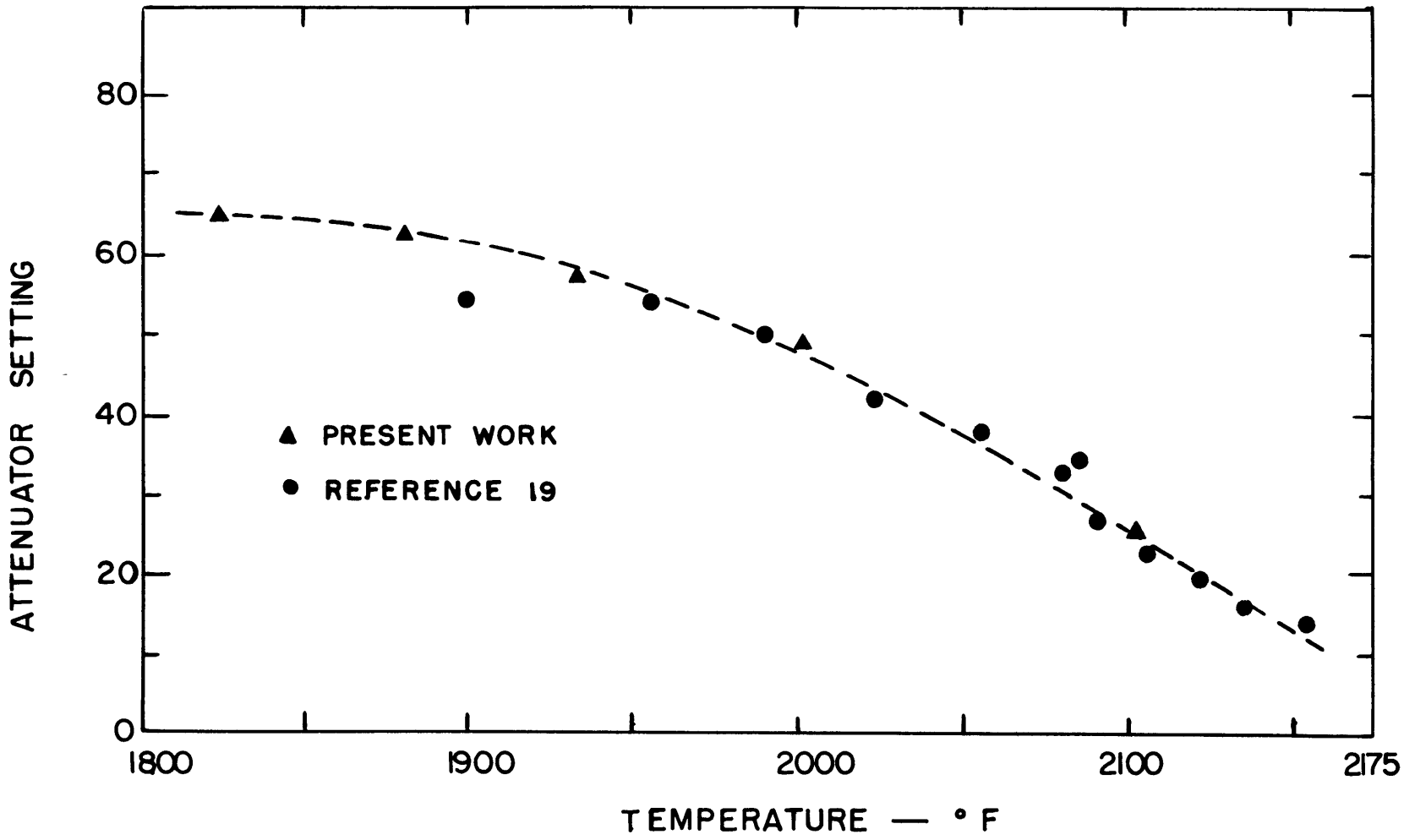

FIGURE 18 ATTENUATOR CALIBRATION

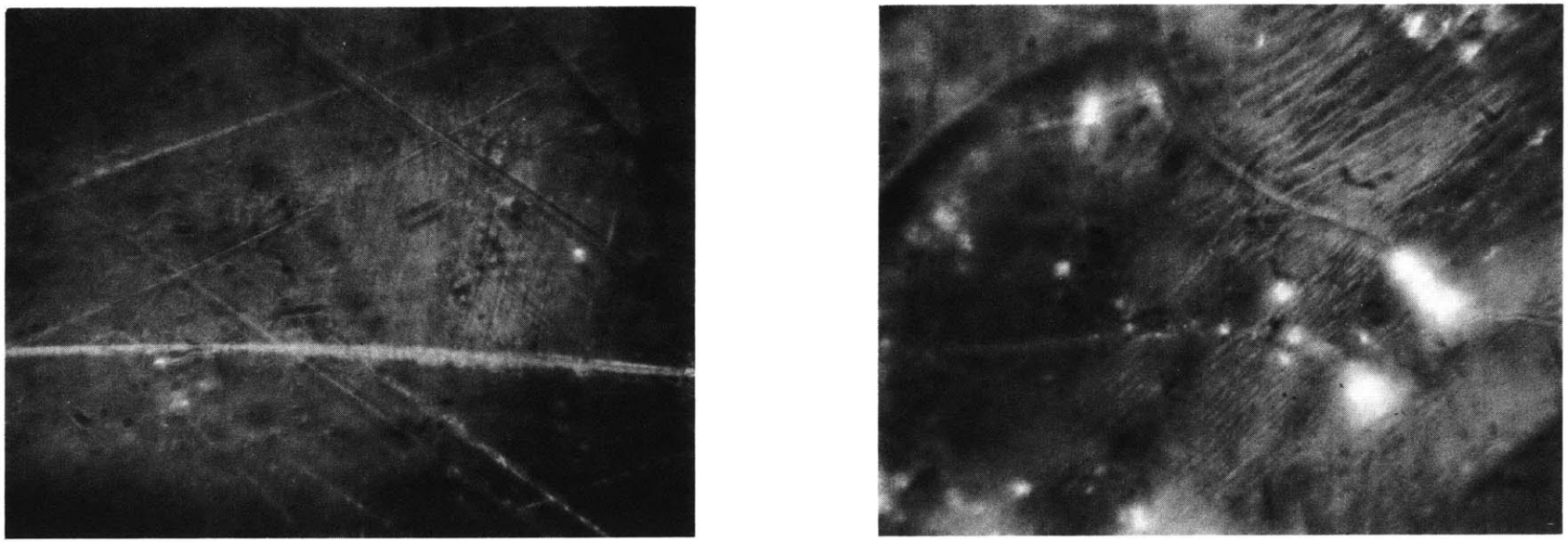

FIGURE 19 PHOTOMICROGRAPH OF PLATINUM FOIL

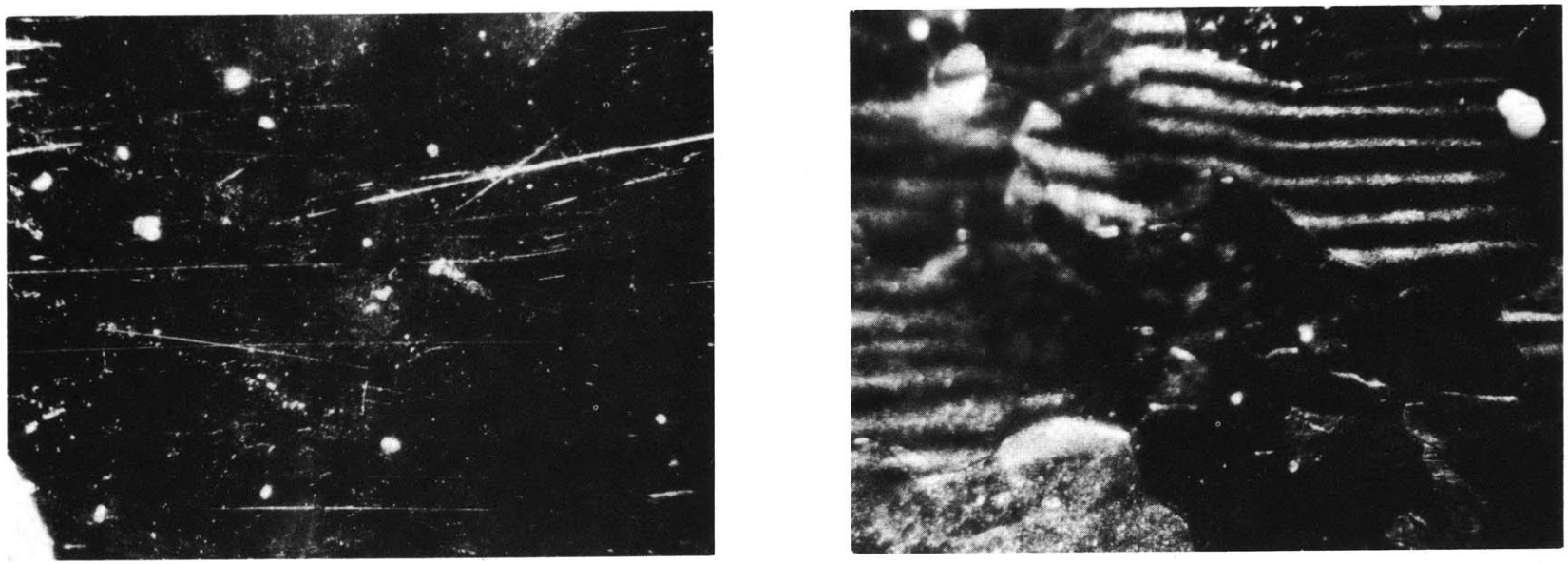

FIGURE 20 PHOTOMICROGRAPH OF PLATINUM FOIL

IV COMPARISON OF ANALYTICAL AND EXPERIMENTAL RESULTS

Figures 21, 22, 23 and 24 show the temperature profiles predicted by the two analytical models of the bounding surfaces and the measured temperature profiles. The predicted profiles are discussed first, and then the experimental data are compared with the predictions.

The temperature profiles predicted by the specular model tend to a more uniform distribution in the center of the medium than the diffuse model predictions. The average path length for radiation emitted diffusely from one wall and reflected specularly from the opposite wall is less than the average path length for radiation reflected diffusely. Consider a ray of energy incident on the boundary at an angle near the normal to the surface. If the boundary reflects diffusely, the incident ray is reflected over a hemisphere and only a fraction of the energy reflected at angles far from the surface normal reaches the other boundary. Less than one percent of the energy reflected at angles greater than eighty degrees from the surface normal reaches the opposite boundary. For the glass slab used in this analysis, specular boundaries caused a decrease in the average path length for energy emitted diffusely from the opposite boundary, and returned to the original boundary.

The shorter path length for specular reflections results in more reflections before a given ray is attenuated by absorption. Therefore the net effect of multiple internal reflections is to average the radiative flux within the medium. For specular reflections the radiative flux from the boundaries will be closer to the mean emissive power of the boundaries than for diffuse reflection. Such is the case for radiative equilibrium (See Figure 11). The specular heat flux is higher than the diffuse as less attenuation of energy radiated between the boundaries occurs.

For radiation and conduction, as shown in Figures 21, 22, 23, and 24, the effect of specularly reflecting walls is to increase the temperature level on the cool side of the glass slab and decrease the temperature level on the hot side. This effect is a result of averaging the radiative flux due to reflections from the walls. Conduction tends to

mask the effect of multiple internal reflections, as it requires continuity of temperature at the boundaries and causes steep gradients due to the correspondingly high conductive heat fluxes.

Due to uncertainities in the values of the thermophysical properties the diffuse model was tested for a representative case to evaluate its sensitivity to changes in the thermal conductivity, the index of refraction, and the absorption coefficient. A twenty-five percent change in the thermal conductivity produces a change of five degrees Fahrenheit in the temperature profile and an eight percent change in the heat flux. (See Figure 25). The sensitivity of the solution to a change in the index of refraction is shown in Figure 26. A fourteen percent change in the refractive index causes a maximum change of four degrees Fahrenheit in the temperature profile and a twenty percent change in the heat flux. Similarly a twenty percent change in the absorption coefficient produces a four degree Fahrenheit change in temperature and a one percent change in the heat flux (See Figure 27.)

The measured temperature profiles are shown in Figures 21, 22, 23 and 24, along with those predicted by the diffuse and specular models. Figure 21 contains the data for the greatest temperature difference between the upper and lower boundaries. The experimental data on this figure fall between the predictions of the specular and diffuse models. The conductive heat flux is proportional to the temperature gradient and therefore is greatest near the walls. Figures 22, 23 and 24 show the temperature profiles for smaller wall temperature differences, and the data falls between the specular and diffuse predictions.

Due to the similarity of the diffuse and specular predictions, no conclusions can be drawn regarding the exact nature of reflections at the boundaries. The errors in the glass and wall temperatures were estimated to be $\pm 3^{o}F$. (See Appendix H). The effect of a temperature drop at the end of the isotherms, caused by heat losses from the sapphire windows, is discussed in Appendix E. The magnitude of the temperature drop is evaluated for two extreme cases, an optically thin medium and an optically thick medium. The results indicate that tem-

perature perturbations caused by the windows would decay within .75 inches of the window. The heat fluxes measured through the side wall give an estimate of the temperature gradient at the inside of the side wall. The data indicate that the temperature gradient at the wall is less than ten degrees Fahrenheit per inch, assuming that the glass is optically thick.

Table 1 shows the calculated and measured heat fluxes. The measured heat fluxes tend to agree with the diffuse model predictions. The value of the thermal conductivity of the ceramic used to evaluate the measured heat fluxes was extrapolated from measured values at 1600^{o}F and 2000^{o}F.

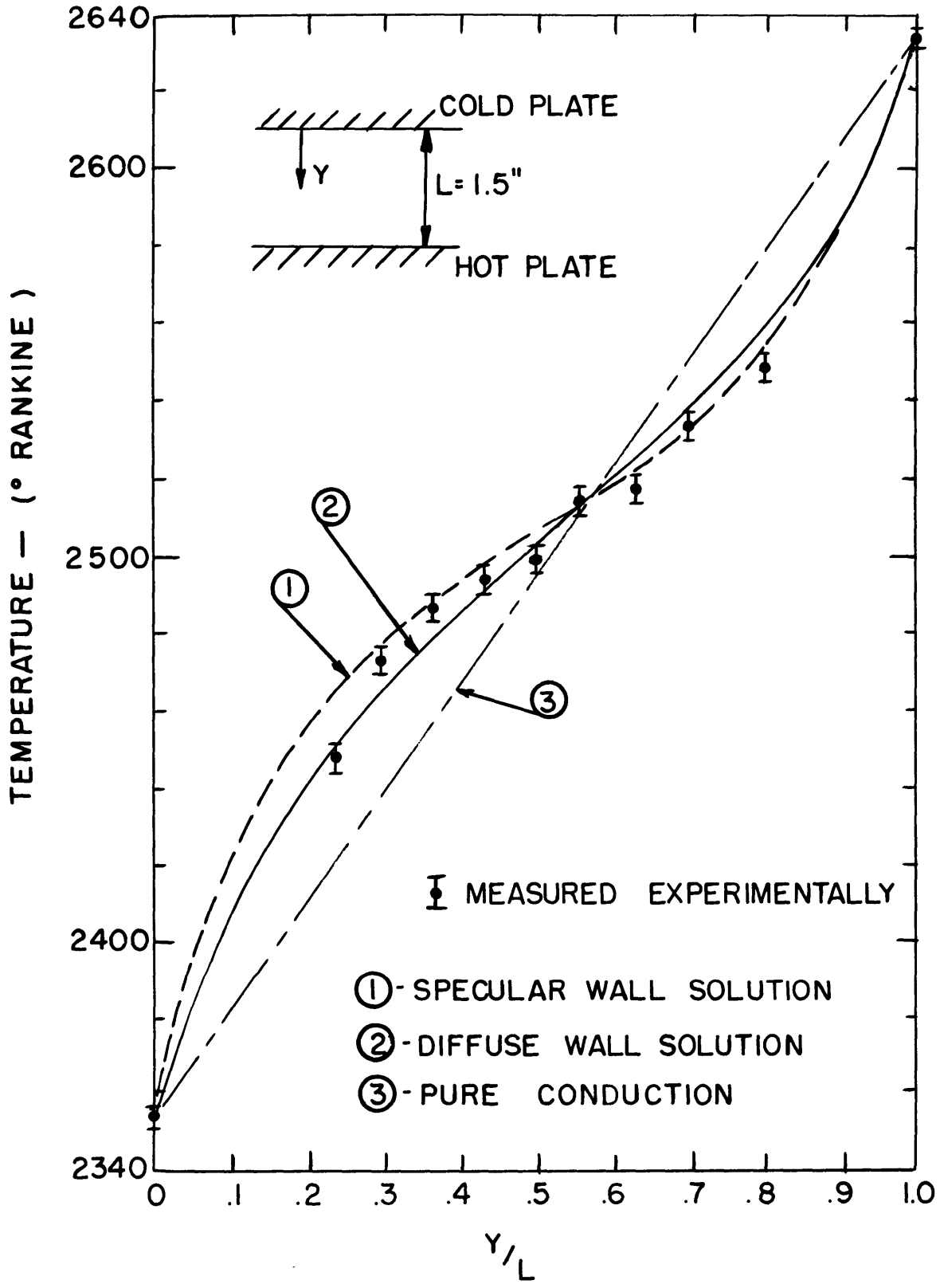

FIGURE 21 TEMPERATURE PROFILES IN GLASS

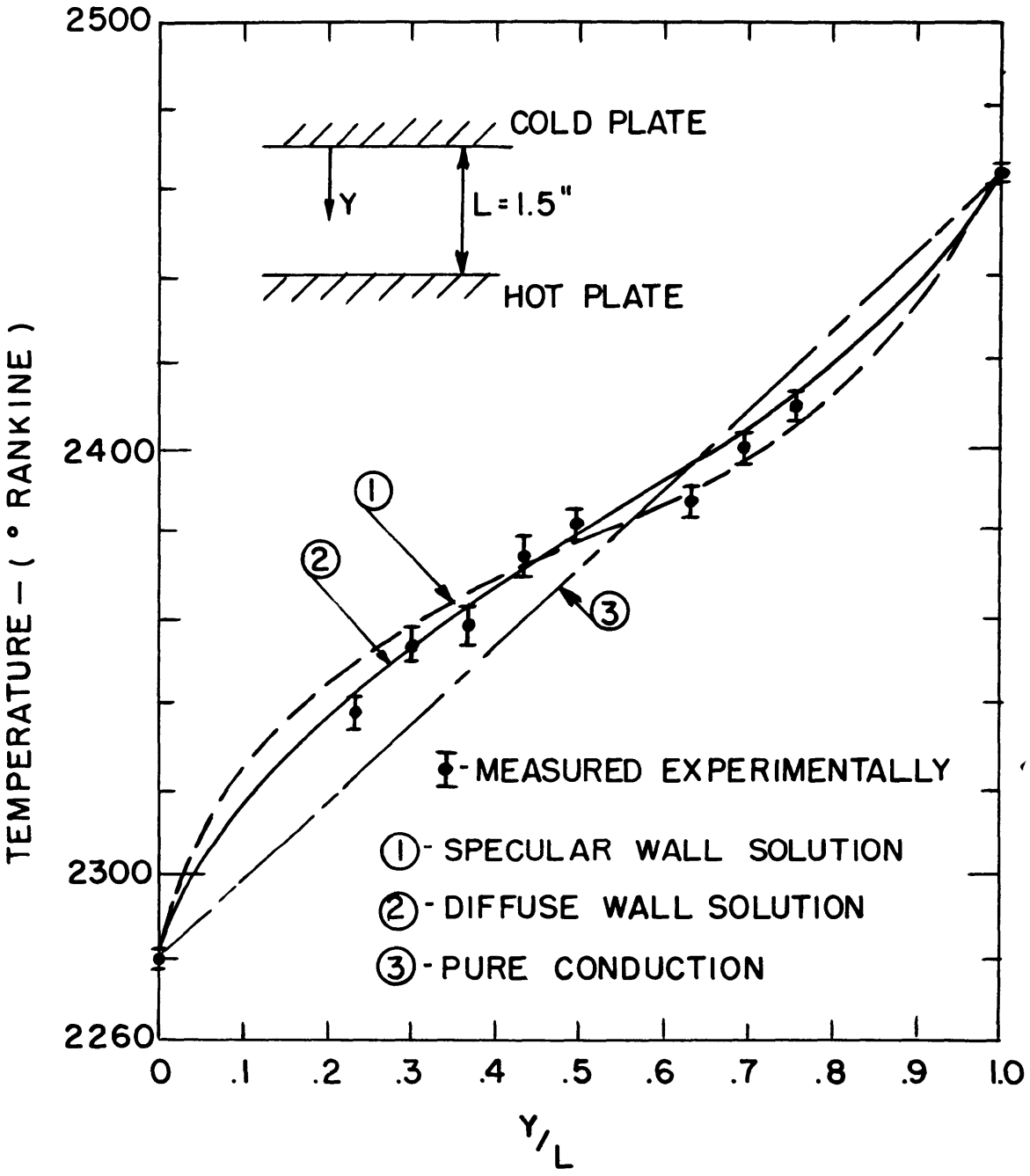

FIGURE 22 TEMPERATURE PROFILES IN GLASS

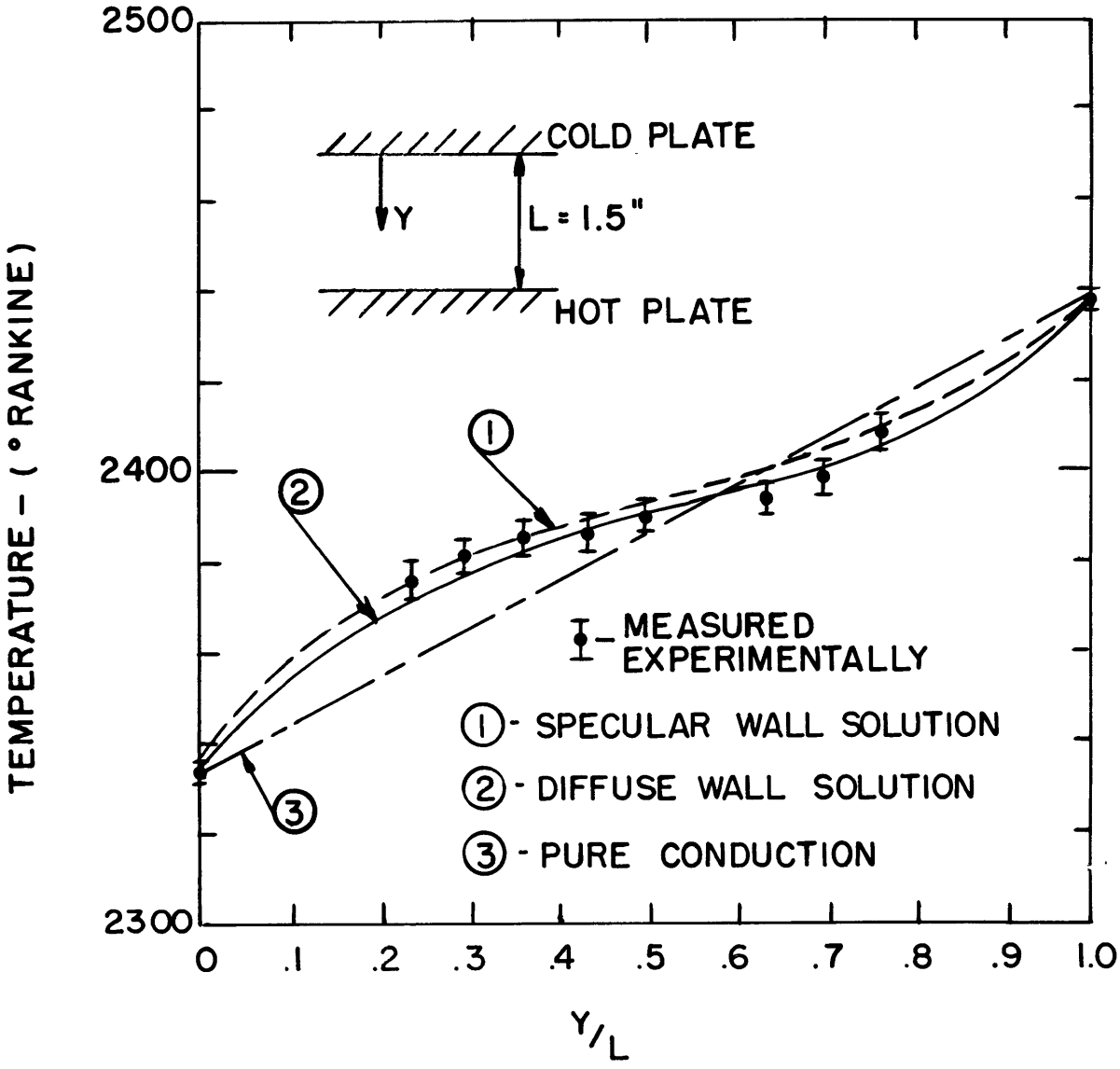

FIGURE 23 TEMPERATURE PROFILES IN GLASS

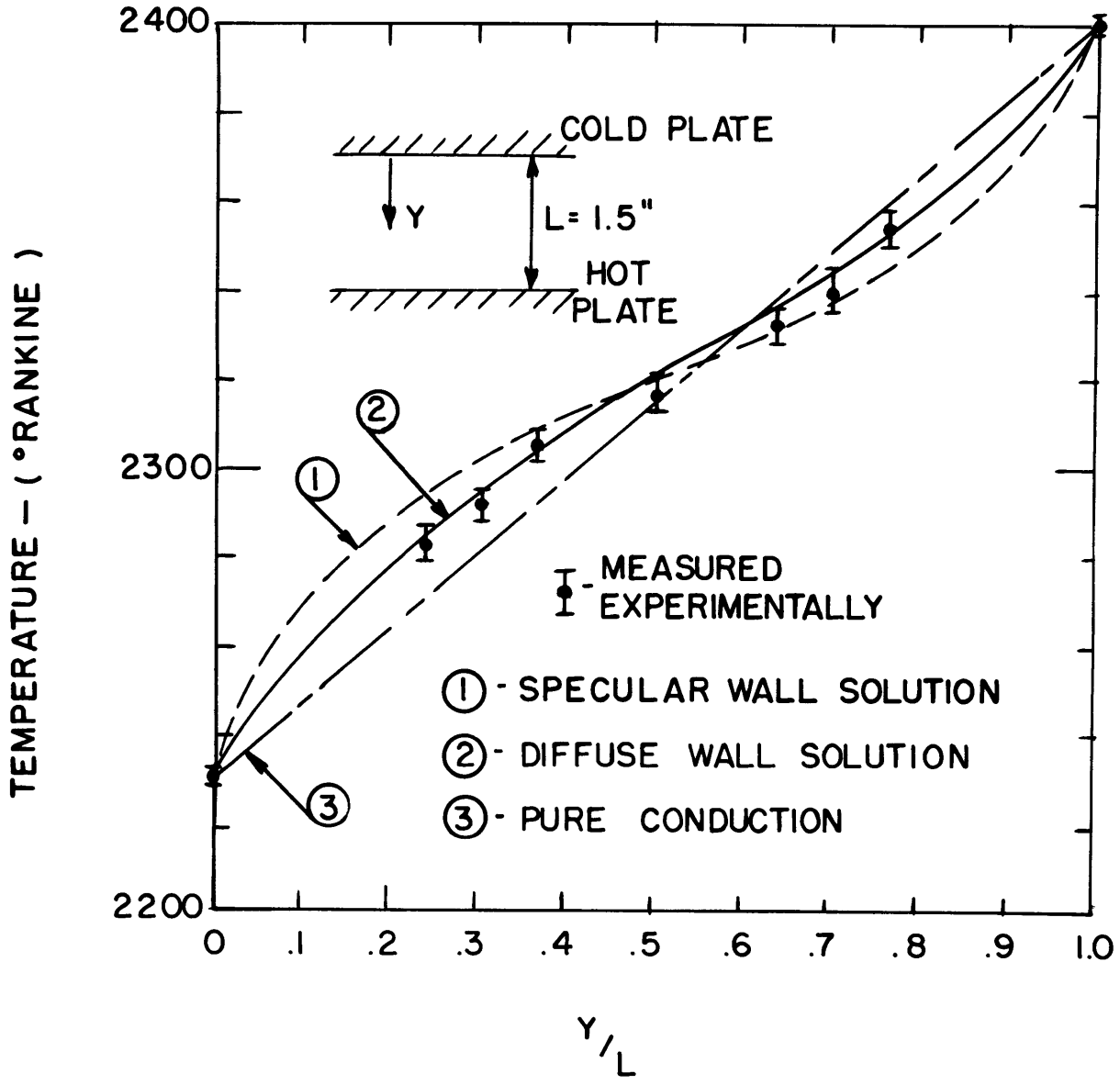

FIGURE 24 TEMPERATURE PROFILES IN GLASS

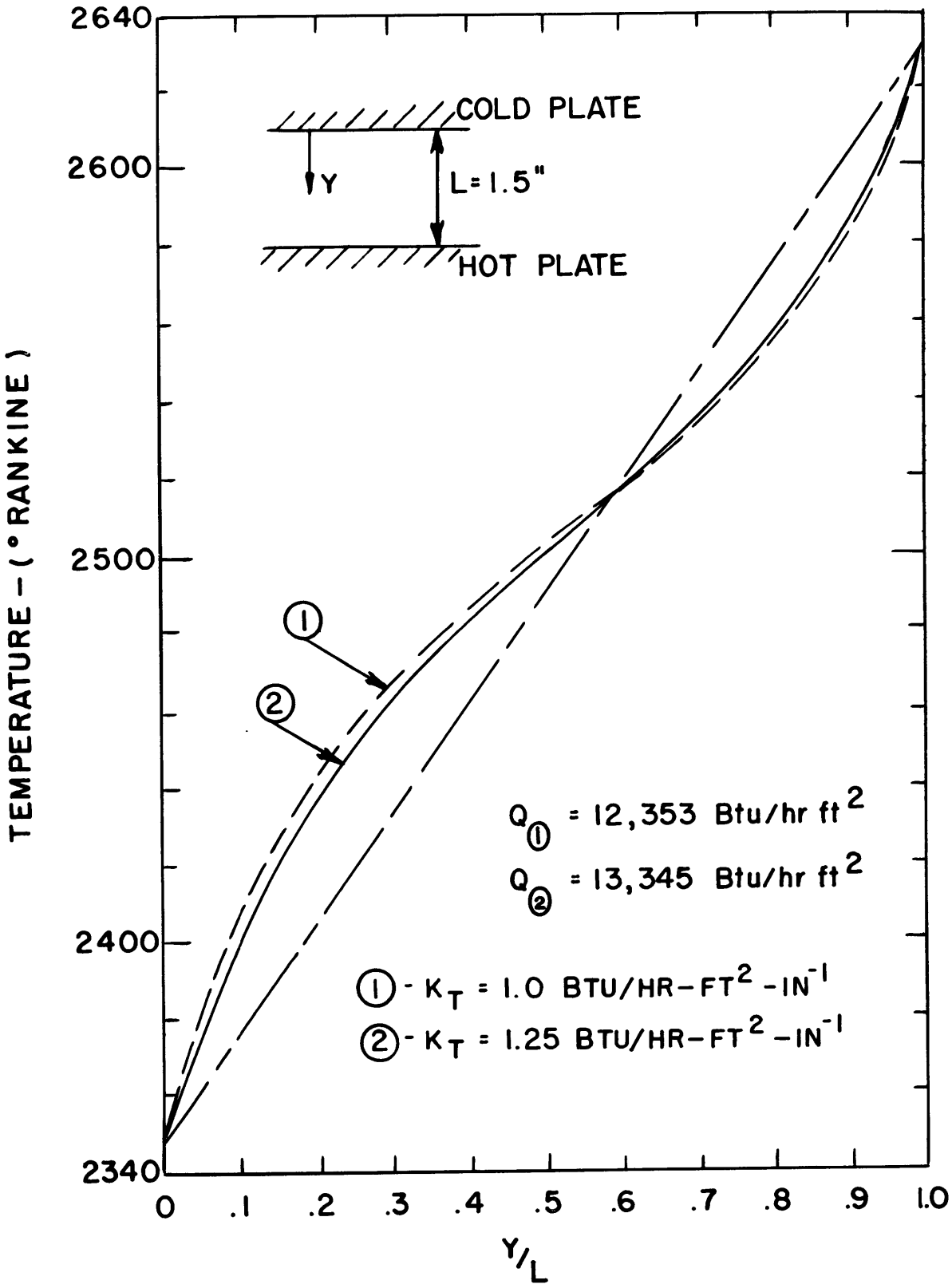

FIGURE 25 TEMPERATURE PROFILE IN GLASS WITH DIFFUSE BOUNDARIES

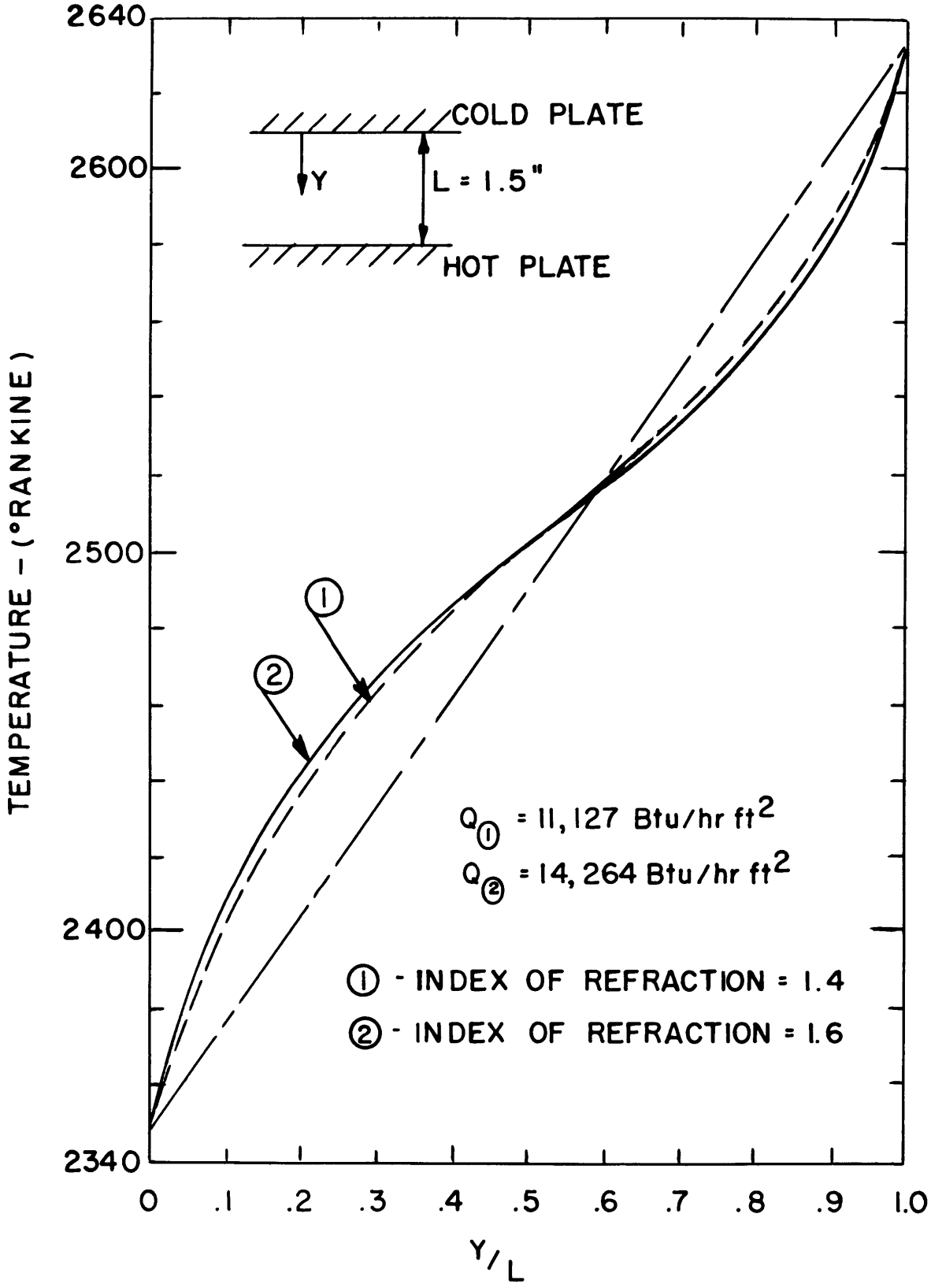

FIGURE 26 TEMPERATURE PROFILES IN GLASS WITH DIFFUSE BOUNDARIES

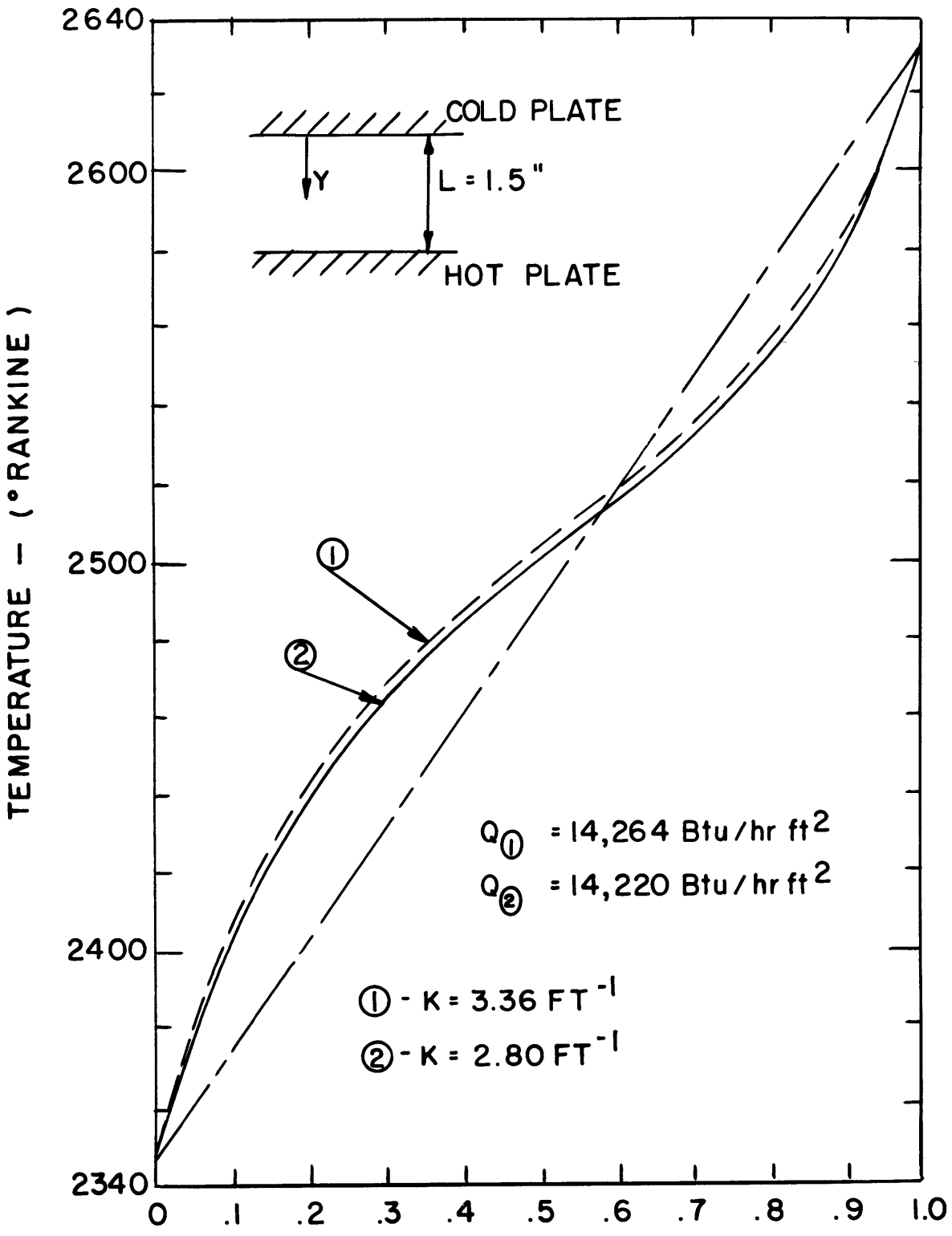

FIGURE 27 TEMPERATURE PROFILES IN GLASS WITH DIFFUSE BOUNDARIES

	CALCULATED		EXPERIMENTAL
FIGURE	SPECULAR	DIFFUSE	MEASURED
21	13,326	12,804	12,400
22	7,000	6,612	6,700
23	4,270	3,656	3,800
24	5,987	5,672	5,100

TABLE 1 - NET HEAT FLUXES (Btu/hr ft^2)

V CONCLUSIONS

The following conclusions were made as a result of this study.

1) The laser method of temperature measurement, as outlined in Section 3.3.3, is useful for measuring temperature profiles in semi-transparent media with linear isotherms. The absorption properties at the laser wavelength must vary monotonically with temperature.

2) The analytical models indicate that for the conditions of this study the mode of reflection at the boundaries does not strongly influence the temperature profiles and heat fluxes. The difference between the diffuse and specular temperature profiles was less than ten degrees Fahrenheit, and the heat fluxes differed by less than ten percent.

3) The experimental results fall between the specular and diffuse predictions, indicating that the platinum-glass interface reflectivity had both specular and diffuse components.

4) Glass is a useful medium for controlled radiation-conduction experiments, due to its convenient thermophysical properties and absorption characteristics. The spectral absorption coefficient can be modelled accurately as a step-function of wavelength, thus simplifying analysis.

REFERENCES

1. D.K. Edwards, "Radiation Interchange in a Nongray Enclosure Containing a Carbon Dioxide-Nitrogen Gas Mixture", Journal of Heat Transfer, p. 1, 1962.

2. F. Simmons, "Band Models for Nonisothermal Radiating Gases", Applied Optics, Vol. 5, 1966, p. 1801; Vol. 6, 1967, p. 1423.

3. B. Krakow and H. Babrov, "Review of Experimental Vertification of the Curtis-Godson Approximation for Infrared Spectral Radiation from High Temperature Gases", "Specialist Conference on Molecular Radiation", edited by R. Goulard, NASA TMX-53711.

4. W. Herget, "Temperature and Concentration Measurements in Model Exhaust Plumes Using Inversion Techniques", "Specialist Conference on Molecular Radiation", edited by R. Goulard, NASA TMX-53711.

5. H.C. Hottel and A.F. Sarofim, Radiative Transfer, McGraw-Hill Book Company, New York, 1967.

6. E.M. Sparrow and R.D. Cess, Radiation Heat Transfer, Brooks/Cole Publishing, Belmont, Calif., 1966.

7. R. and M. Goulard, "One-Dimensional Energy Transfer in Radiant Media", International Journal of Heat and Mass Transfer, p. 81, 1960.

8. R. Viskanta and R.J. Grosh, "Heat Transfer by Simultaneous Conducting and Radiation in an Absorbing Medium," ASME Journal of Heat Transfer Feb., 1962, pp. 63-72.

9. R. Viskanta and R.J. Grosh, "Effect of Surface Emissivity on Heat Transfer by Simultaneous Conduction and Radiation," Int. J. Heat Mass Transfer, Vol. 5, pp. 729-734.

10. T.H. Einstein, "Radiant Heat Transfer to Absorbing Glasses Enclosed Between Parallel Flat Plates with Flow and Conduction," NASA Tech. Report R-154.

11. R. Viskanta, "Heat Transfer by Conduction and Radiation in Absorbing and Scattering Materials," ASME Journal of Heat Transfer, Feb., 1965, pp. 143-150.

12. R.F. Probstein, "Radiation Slip," AIAA Journal, Vol. 1, No. 5, pp. 1202-1204.

13. Y.S. Touloukian, ed., Thermophysical Properties of High Temperature Solid Materials, Volume 1, Macmillan Press, New York.

14. Seban, R.A., Thermal Radiation Properties of Materials, Part III (WADD TR-60-370 Pt III) Univ. Calif. (Berk.) Aug. 1963.

15. R. Sievel and J.R. Howell, Thermal Radiation Heat Transfer, NASA SP-164, Vol. 1.

16. R. Rolling, "Effect of Surface Roughness on the Spectral and Total Emittance of Platinum", Progress in Aeronautics and Astronautics, Vol. 20, 1967, pp. 91-114.

17. Weast, R.C. ed., Handbook of Chemistry and Physics, 44th ed., Chemical Rubber Co., 1962.

18. Calderbank, J.C., "Thermocouple Miniaturization and Testing to Reduce Errors due to Radiation," S.M. Thesis, September 1969.

19. Jeryan, R.A., "An Optical Temperature Measuring Technique for Semi-Transparent Media," S.M. Thesis, June 1969.

20. S. Chandrasekhar, "Radiative Transfer", Dover, 1960.

21. V. Kourganoff, Basic Methods in Transfer Problems, Dover Publications, New York, 1963.

22. J.A. Wiebelt, Engineering Radiation Heat Transfer, Holt, Rinehart, Winston, New York, 1966.

23. T.J. Love, Radiative Heat Transfer, C.E. Merrill Publishing Co., Columbus, Ohio, 1968.

24. C.M. Usiskin and E.M. Sparrow, "Thermal Radiation Between Parallel Plates Separated by an Absorbing-Emitting Nonisothermal Gas," International Journal of Heat and Mass Transfer, Vol. 1, pp. 28-36, 1960.

25. M.A. Heaslet and R.F. Warming, "Radiative Transport and Wall Temperature Slip in an Absorbing Planar Medium", International Journal of Heat and Mass Transfer, p. 979, 1965.

26. R. Viskanta and R.J. Grosh, "Heat Transfer in a Thermal Radiation Absorbing and Scattering Medium," International Heat Transfer Conference, Boulder, Colorado, 1961, p. 820.

27. W. Lick, "Energy Transfer by Radiation and Conduction," Proceedings of the 1963 Heat Transfer and Fluid Mechanics Institute, Stanford University Press, Palo Alto, Calif., 1963, pp. 14-26.

28. R.G. Deisler, "Diffusion Approximation for Thermal Radiation in Gases with Jump Boundary Conditions", Journal of Heat Transfer, p. 240, 1964.

29. R.V. Meghreblian, "An Approximate Analytic Solution for Radiation Exchange Between Two Flat Surfaces Separated by an Absorbing Gas", International Journal of Heat and Mass Transfer, p. 1051, 1962.

30. R.D. Cess and A.E. Sotak, "Radiation Heat Transfer in an Absorbing Medium Bounded by a Specular Reflector"ZAMP," 15, pp. 642-647, 1964.

31. D.B. Olfe, "A Modification of the Differential Approximation for Radiative Transfer," AIAA Journal, Vol. 5, No. 4, 1967.

32. C.S. Landram and R. Greif, "Semi-Isotropic Model for Radiation Heat Transfer," AIAA Journal, Vol. 5, No. 11, 1967, pp. 1971-1975.

33. Y. Taitel and J.P. Hartnett, "Application of Rosseland Approximation and Solution Based on Series Expansion of the Emission Power to Radiation Problems," AIAA Journal, Vol. 6, No. 1, p. 80, 1968.

34. L.R. Glicksman, "An Approximate Method for Multidimensional Problems of Radiating Energy Transfer in an Absorbing and Emitting Media", To be published in the Journal of Heat Transfer.

35. H.C. Hottel and E.C. Cohen, "Radiant Heat Exchange in a Gas-Filled Enclosure", American Institute of Chemical Engineers Journal, 4, p. 3, 1958.

36. J.R. Howell and M. Perlmutter, "Monte Carlo Solution of Radiant Heat Transfer in a Nongray, Nonisothermal Gas with Temperature Dependent Properties", American Institute of Chemical Engineers Journal, P. 562, 1964.

37. D.K. Edwards and K.E. Nelson, "Rapid Calculation of Radiant Energy Transfer Between Nongray Walls and Isothermal H_2O or CO_2 Gas", Journal of Heat Transfer, p. 273, 1962.

38. J.A.L. Thomson, "Radiation Model for Nonscattering Rocket Exhaust Gases", "Specialist Conference on Molecular Radiation", edited by R. Goulard, NASA TMS-53711.

39. R. Cess, P. Mighdoll, S. Tiwari, "Infrared Radiative Heat Transfer in Nongray Gases," International Journal of Heat and Mass Transfer, 1967, Vol. 10, p. 1521.

40. A.L. Crosbie and R. Viskanta, "The Exact Solution to a Simple Nongray Radiative Transfer Problem", Journal of Quantitative Spectroscopy and Radiative Transfer, p. 553, May, 1963.

41. D.K. Edwards, L.K. Glassen, W.C. Hauser, J.S. Tuchscher, "Radiation Heat Transfer in Nonisothermal Nongray Gases", Journal of Heat Transfer, p. 219, Aug., 1967.

42. J. Gille and R. Goody, "Convection in a Radiating Gas", Journal of Fluid Mechanics, Vol. 20, p. 47, 1964.

43. R.D. Cess, "The Interaction of Thermal Radiation with Conduction and Convection Heat Transfer," Advances in Heat Transfer, Vol. 1, Academic Press, New York, 1964.

44. R. Viskanta, "Radiation Transfer and Interaction of Convection with Radiation Heat Transfer", Advances in Heat Transfer, Vol. 3, 1966, Academic Press.

45. R. Greif, "Energy Transfer by Radiation and Conduction with Variable Gas Properties", International Journal of Heat and Mass Transfer, p. 891, 1964.

46. A.A. Fowle et al., "Prediction of Heat Transfer in Multiple Glaze Transparencies," A.D. Little, NAS 9-4204.

47. R. Gardon, "The Emissivity of Transparent Materials," Journal of the American Ceramic Society, Vol. 39, No. 8, p. 278.

48. R. Gardon, "Calculation of Temperature Distributions in Glass Plates Undergoing Heat Treatment," Journal of the American Ceramic Society, Vol. 41, No. 6, p.200, 1958.

49. R. Van Laethem, L. Leger, M. Boffe, and E. Plumat, "Temperature Measurement of Glass by Radiation Analysis," Journal of the American Ceramic Society, Vol. 44, No. 7, 1960.

50. W.D. Kingery, "Heat Conductivity Processes in Glass," Journal of the American Ceramic Society, 44, pp. 302-304, 1961.

51. A.F. Van Zee and C.L. Babcock, "Method for Measurement of Thermal Diffusivity of Molten Glass," J. Am. Ceramic Soc., 34, (8), 224-250, 1951.

52. K.L. Wray and T.J. Connolly, "Thermal Conductivity of Clear Fused Silica at High Temperatures," J. Applied Phys., 30, 1702-1705, 1959.

53. C. Kittel, "Interpretation of the Thermal Conductivity of Glasses," Physical Review, Vol. 75, No. 6, 1949.

54. F.J. Grove and P.E. Jellyman, "Infrared Transmission of Glass in the Range Room Temperature to 1400°," Journal of the Society of Glass Technology, 39 (186) 3-15 T, 1955.

55. Norbert Neuroth, "Der Einfluss der Temperatur auf die Spektrale Absorption von Glasern im Ultraroten I. (Effect of Temperature on Spectral Absorption of Glasses in the Infrared, I) Glastech. Ber. 2 (8), 242-49 (1952).

56. Norbert Neuroth, "Der Einfluss der Temperatur auf die Spektrale Absorption von Glasern im Ultraroten, II" (Effect of Temperature on Spectral Absorption of Glasses in the Infrared, II) Glastech. Ber. 26 (3), 66-69., 1953.

57. C.J. Phillips, Glass - Its Industrial Applications, Reinhold Publishing Corp., New York.

58. Norbert Neuroth, "Der Temperature influss auf die Optischen Konstanten von Glas im Gebiet Starker Absorption", (The Temperature Effects on Optical Constants of Glass in the Range of Strong Absorption) Glastech. Ber. 28 (11), 411-22 (1955).

59. K.H. Chen, "Measurement of Thermal Conductivity of Glass at High Temperature," S.M. Thesis in Mech. Eng., M.I.T., June 1968.

60. F.J. Grove, "Spectral Transmission of Glass at High Temperatures and its Application to Heat-Transfer Problems," Journal of the American Ceramic Society, Vol. 44, No. 7, pp. 317-320, 1961.

61. M. Born and E. Wolf, Principles of Optics, Pergamon Press, London, 1965.

62. J. Francis, T.J. Love, "Radiant Heat Transfer Analysis of Isothermal Diathermanous Coatings on a Conductor," AIAA Journal, April, 1966, Vol. 4, No. 4.

63. G. Gubareff, J. Janssen, R. Torborg, Thermal Radiation Properties Survey, Honeywell Research Center, Minneapolis, Minnesota.

64. B. Mikic and W.M. Rohsenow, "Thermal Contact Resistance", M.I.T. - EPL Report DSR 74542-41.

65. B. Mikic, "On the Mechanism of Dropwise Condensation", To be published in International Journal of Heat and Mass Transfer.

APPENDIX A - LITERATURE REVIEW

The problem of energy transfer through an absorbing-emitting media has received a great deal of attention recently due to its fundamental nature and practical importance. A large number of publications have dealt with radiative and coupled conductive and radiative transfer in absorbing-emitting media. The following sections contain a brief presentation of the methods used by various investigators.

A1 RADIATIVE EQUILIBRIUM

A state of radiative equilibrium exists within a medium far from the boundaries when the radiation heat flux is much larger than the convective or conductive fluxes or near the boundaries if the thermal conductivity is zero. Radiative equilibrium was introduced in astrophysics in connection with energy transfer in stars and galaxies and the transmission and reflection of light by planetary atmospheres. Reviews of astrophysics are given by Chandrasekhar [20] and Kourganoff [21] .

Several texts [5, 6, 22, 23] give an excellent description of radiative equilibrium for both gray and nongray media. A gray medium is one for which the absorption coefficient is independent of wavelength. Radiative equilibrium within gray media is dealt with first.

Usiskin and Sparrow [24] give detailed solutions for a nonisothermal uniformly generating gray medium between black walls, and they discuss the applicability of their results to nonblack walls. An exact integral formulation was used and the numerical results were calculated by the method of successive approximations. Heaslet and Warming [25] have shown that the emissive power profiles and heat fluxes within a gray medium surrounded by gray boundaries can be expressed in terms of functions that have been accurately tabulated by Chandrasekhar [20] . Specific attention was directed towards the evaluation of the temperature near the walls and the radiative heat flux. Viskanta and Grosh [26] have applied the method of undetermined parameters to obtain a solution for the temperature profiles and heat fluxes within a gray medium bounded by two infinite parallel gray plates. Lick [27] has applied an exponential kernal

approximation to derive an approximation solution for a gray medium. Deissler [28] and Probstein [12] used the concept of jump boundary conditions for temperature. In this method it was assumed that the Rosseland equation for the optically thich limit is valid in the interior but temperature jumps were used at the wall. The results of the analyses were accurate in predicting the magnitude of the temperature jump at the wall and the net radiative flux.

In addition, Probstein [12] has shown that the heat fluxes can be predicted accurately using superposition for combined radiation and conduction. Meghreblian [29] has developed an approximate-solution for radiative equilibrium in a gray medium. Cess and Sotak [30] used single iteration on an exponential kernal solution to solve the case of an absorbing-emitting medium with one specularly reflecting boundary and one black boundary. Several authors [31, 32, 33, 34] have developed modifications of the Rosseland or optically thick approximation which can be used accurately in gray media of moderate optical thickness. These solutions yield the correct values in the optically thin limit.

Several authors have dealt with radiative equilibrium in a nongray medium. Methods of calculating total radiation exchange have been presented by Hottel and Cohen [35] . A three gray-band approximation was used for the total emissivity. A finite difference method was used to predict the exchange between the walls of a container and the enclosed nonisothermal gas. The formulation is based on isothermal gas volumes and enclosure surface elements and leads to a set of simultaneous equations. Howell and Perlmutter [36] give a precise synthesis of the use of black wall solutions and use the Monte Carlo method for numerical solutions for a nongray medium. This method is valid for two and three dimensional cases. Edwards [1, 37] presents methods for calculating radiant heat transfer through isothermal nongray CO_2 - N_2 gas mixtures and through H_2O or CO_2 gas enclosed between nongray walls using band absorption methods. Simmons [2] used a strong-line model equivalent to one of the Curtis-Godson asymptotic relations for emission from a nonisothermal gas. Thomson [38] describes a model for calculating the spectral distribution of heat flux in a nonisothermal volume of high tem-

perature gas using a statistical band model and a modification of the Curtis-Godson approximation. Cess et al [39] using a method based on band absorptance, show that the commonly used gray gas approximation can lead to large errors when used for diatomic gases. Crosbie and Viskanta [40] analyze heat transfer in a nongray medium with a single absorbing band, between infinite parallel plates. Mean gray absorption coefficients are compared with nongray models, and the results indicate that the gray gas approximation can cause large errors.

Simmons [2] compared calculated spectral radiances with experimentally measured spectra in the 2.7 micron water vapour band on an optical path along with a known temperature gradient was imposed. The spectral radiance predictions were found to be accurate. Temperature profiles determined from experimental spectral radiance data were compared with measured temperature in rocket exhaust and the agreement was satisfactory. Krakow et al [3] compared spectral radiances calculated by the Curtis-Godson model with emission data from combustion products. The agreement was satisfactory. Herget et al [4] made experimental measurements of the spectral radiance and transmittance of rocket exhausts and calculated a temperature map of the exhaust. Edwards et al [41] report experimental measurements of absorption and emission of nonisothermal CO_2. The results are compared with a band model calculation and show quantitative agreement for total emissivity and absorptivity of the gas.

Combined convection and radiation in ammonia has been studied both experimentally and analytically by Gille and Goody [42] . It was shown that the temperature profile within the gas could be described by an integrodifferential equation for which the kernal was approximated by the first derivative of the gas emittance.

A2 RADIATION AND CONDUCTION

Several texts [5, 6, 22, 23, 43, 44] give an excellent description of coupled radiation and conduction heat transfer..

Heat transfer within porous insulation is not included in this synopsis because it involves scattering which is outside the scope of this in-

vestigation. The case of a plane layer of stagnant gray gas between a gray wall and a transparent wall was treated by Goulard [7]. Allowance was made for interaction between conduction and radiation, including the effect of the gray wall, but the emission from a gas layer was permitted to pass unattenuated to the boundaries in order to simplify the analysis. The problem of simultaneous radiation and conduction in an absorbing-emitting medium enclosed between two diffuse infinite parallel plates has been formulated by Viskanta and Grosh [8]. The nonlinear integrodifferential equation of energy conservation was converted to a nonlinear integral equation and the solutions for both black [8] and non-black [9] boundaries were obtained by the method of successive substitutions. Einstein [10] gives an analysis of and numerical results for the heat transfer to a uniformly absorbing gray gas between black rectangular plates with combined radiation conduction and convection. The flow region was divided into a number of zones and the two-dimensional integrodifferential equation of energy conservation was approximated by a system of algebraic equations. Probstein [12] indicated that the superposition of heat fluxes is accurate over a wide range of optical thicknesses. Lick [27] and Greif [46] present analyses of coupled radiation and conduction. Two models were used for the absorption coefficients; a gray gas model and a picket fence model. The results of several approximate methods are compared with the solutions obtained by numerical integration of the integrodifferential equation of energy conservation. Fowle et al [47] have analyzed heat transfer in multiple glaze windows for spacecraft. They give numerical results for the temperature profiles within the windows under varying heat fluxes. A method is presented by Gardon [48, 49] for computing time-dependent temperature distributions in glass sheets amid the complications of penetration of external radiation, internal emission, and multiple internal reflections.

A. Fowle et al [47] present experimental data for the temperature profiles across multiple glaze windows subject to varying heat fluxes. Due to the low temperature levels the heat transfer processes were dominated by conduction and the measured temperature profiles were essentially linear. Many investigators [5, 49, 50, 51, 52, 53] have

discussed the role of radiative conductivity for heat transfer through semitransparent media. This concept is useful if the medium is optically thick, as the radiative transfer can be modelled as a diffusion process, permitting the use of a radiative conductivity. However, if the medium is optically thin the use of a radiative conductivity can lead to large inaccuracies.

APPENDIX B - PROPERTIES OF GLASS

B1 ABSORPTION COEFFICIENT OF GLASS

i) INTRODUCTION

In order to calculate radiative heat fluxes and temperature profiles in glass it is necessary to know the infrared absorption properties of the glass. The use of published room temperature data in high temperature calculations can result in large errors.

An experiment was set up to provide data for the monochromatic absorption coefficient of water-white glass from 1.0 microns to 2.75 microns, between 2000°F and 2300°F. The resulting data agree in trend with temperature with that of previous investigators [54, 55, 56].

ii) DISCUSSION OF RESULTS

Figure B4 is a plot of the measured values of the monochromatic absorption coefficient at high temperatures. No data was taken below the devitrification temperature of the glass as it separated from the sapphire windows of the test section (see Fig. 87). Also, no data was taken below one-micron as the accuracy of the apparatus was limited by the limited energy of the source at short wavelengths.

The experimental reproducibility was found to be approximately ± 5 percent for the test section shown in Fig. B7. The water-white glass tested is a special form of optical glass which has a very low iron content. The data from this experiment agrees with that given by investigators [54, 55, 56] (see Fig. B2) for low-iron glasses at high temperatures. The monochromatic absorption coefficient increases monotonically with temperature between 2000°F and 2300°F, as can be seen in Fig. B4. Figure B5 compares with absorption coefficient of window glass with that of a low-iron "white glass". The white glass is more transparent than the window glass between .5 and 4 microns. The increase in absorptivity of the window glass near one micron is due to the iron content.

iii) APPARATUS

Figures B1 and B6 show the apparatus used in this experiment. A description of the main components follows.

a) Source

A tungsten-strip bulb was operated on a D.C. power source in order to avoid fluctuations in the source intensity. The beam from the source was interrupted at 13 hertz by a mechanical chopper, and then it was directed onto the test section by the optical system described below.

b) Optical System

Figure B6 shows the optical system which was used to focus the beam through the sample and into the monochromator entrance. Two spherical mirrors and three plane mirrors were used. Each mirror has a quarter-wave finish and was first-surface coated with aluminum.

The optical system focused an image of the tungsten strip source on the test section. The glass transmitted the image in a diverging beam which was refocussed on the monochromator slit by a spherical mirror.

c) Furnace

A tube furnace was built around an alumina core wound with KANTHAL AL* resistance wire which has a maximum operating temperature of 2450°F. The end sections of the furnace were wired separately in order to compensate for extra heat losses, and maintain a uniform temperature in the furnace. Three platinum-platinum/10% rhodium thermocouples were used to monitor the furnace temperature. One thermocouple was located at the test section and one on either side of the test section, three inches from it. A potentiometer was used to measure the voltage from the thermocouples, and the corresponding temperatures were read from standard thermocouple tables. The furnace was traversed perpendicular to the beam by means of a screw-feed mechanism. By traversing the furnace the measuring beam of light could alternately pass into the glass sample or the air reference path of the test section.

*Trademark of Kanthal Corporation.

d) Test Section

Figure B7 shows the test section which held the glass sample. The sample cell was a platinum foil lined alumina cylinder in which the glass sample was held by two synthetic sapphire windows. A hole was left in the top of the alumina cell in order to fill the cell with glass. The cell was then mounted eccentrically in a round firebrick plug. An alternate passage for the light beam was a rectangular hole cut through the test section. This alternate hole permitted measurement of the absorption of the air-path through the optical system. The test section was cemented with an alumina refractory cement.

e) Measurement of Monochromatic Intensity

A Perkin-Elmer model 83 single-beam prism monochromator was used. It was equipped with a calcium fluorite prism and a lead sulfide detector. The wavelength limits on the system were .66 microns to 2.72 microns. The light beam entering the monochromator had two components; a steady component due to the light emitted by the glass in the furnace, and a 13 hertz modulated component from the source, which was transmitted through the glass. Figure B8 shows the amplifier system which was built to separate the two components and measure only the 13 hertz modulated signal. The bandpass filter increased the signal to noise ratio by omitting all signals except those at 13 hertz. The output of the system was a 13 hertz A.C. signal with a peak-to-peak voltage varying from 50 mv. to 20 volts.

This signal was monitored on an oscilloscope and fed into an X-Y recorder which produced a plot of intensity versus drum number. This plot was converted to intensity versus wavelength through the use of the monochrometer calibration curve. Two plots were produced for each temperature. One curve is for the beam passing through the sample and the other curve is for the beam passing through the air-path only. Figures B9, B10, and B11 show typical data obtained from different portions of the spectrum.

iv) METHOD

A single-beam optical system was used, requiring two complete runs over the wavelength range for each temperature. The first run was made with the light beam passing through the sample cell of the test section (Fig. B7). For the second run the furnace was traversed perpendicular to the light beam so that the beam passed to the side of the sample through the rectangular hole in the test section.

Figure B6 shows the optical system used. Light from a tungsten-strip lamp was chopped at 13 hertz, focussed on the sample which was located in a tube furnace, and then was brought to a second focus on the entrance slit of the monochromator. A run was made with the empty test section (both windows, but not glass sample) up to 2300^{O}F in order to calibrate the test section (for the absorption of the windows). The cell was then assembled with a 1/4" thick disc of water-white glass between the sapphire windows. A piece of water-white glass was placed in the hole on the upper side of the test section. The test section was then placed inside the furnace and heated slowly to 2000^{O}F. The glass disc melted and the glass on the top of the test section melted, ran down into the sample cell and topped it up. The temperature was increased to 2300^{O}F for several hours until all the bubbles disappeared and the data were taken.

As previously mentioned, two complete runs were made at each temperature. Figures B9, B10, and B11 show that the relative intensity of the light passing through the glass sample was less than that passing through the air path. This is due to attenuation by absorption within the glass, absorption within the sapphire, and reflection losses at the sapphire-air interface. The apparent transmissivity of the cell is the ratio of the relative intensity of the beam through the sample compared to the beam through the air path.

This apparent sample transmissivity can be corrected for the absorption in the sapphire by using the data from the calibration test of the empty test cell. The reflection losses at the sapphire-air and sapphire-glass interface can be calculated from the Fresnel relation for the re-

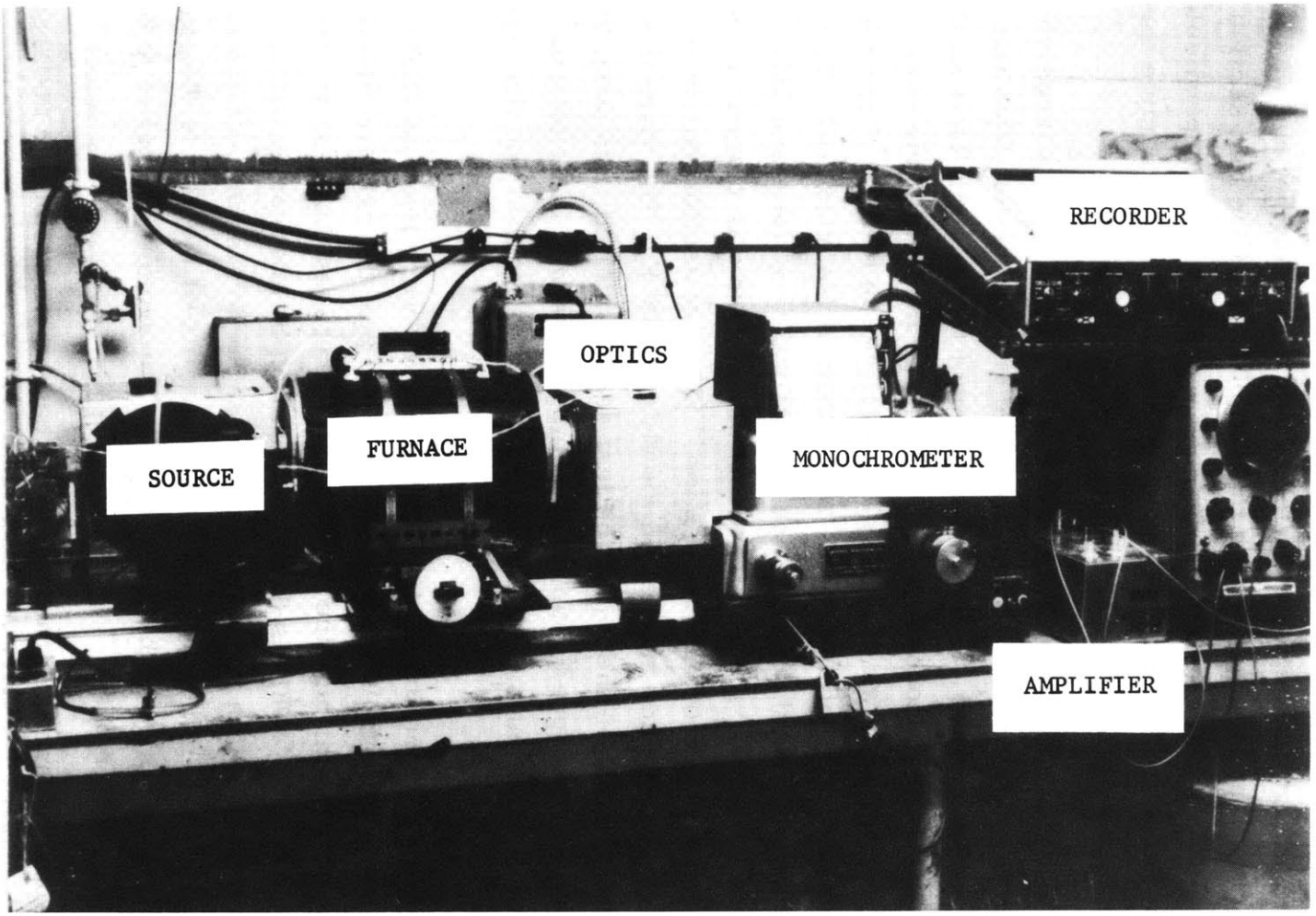

FIGURE B1 PHOTOGRAPH OF APPARATUS

DATA FROM REFERENCE [55]

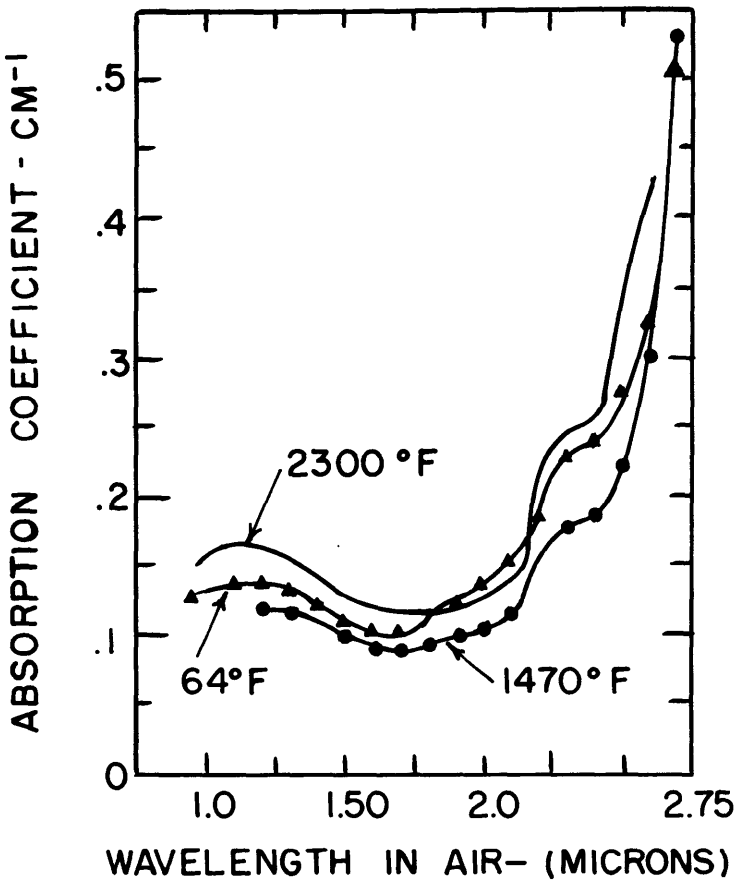

FIGURE B2 SPECTRAL ABSORPTION COEFFICIENT

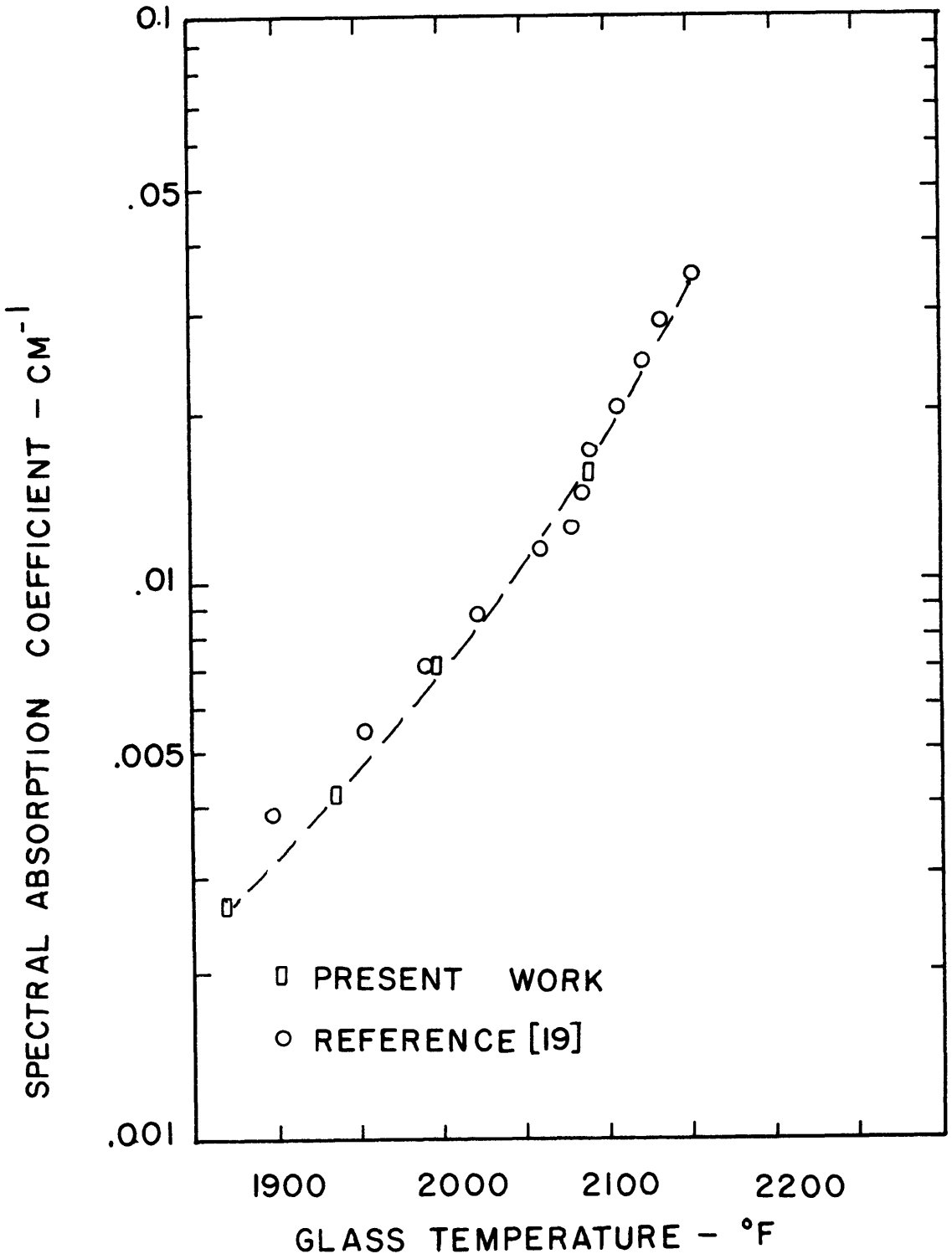

FIGURE B3 SPECTRAL ABSORPTION COEFFICIENT AT .6328 MICRONS VERSUS TEMPERATURE

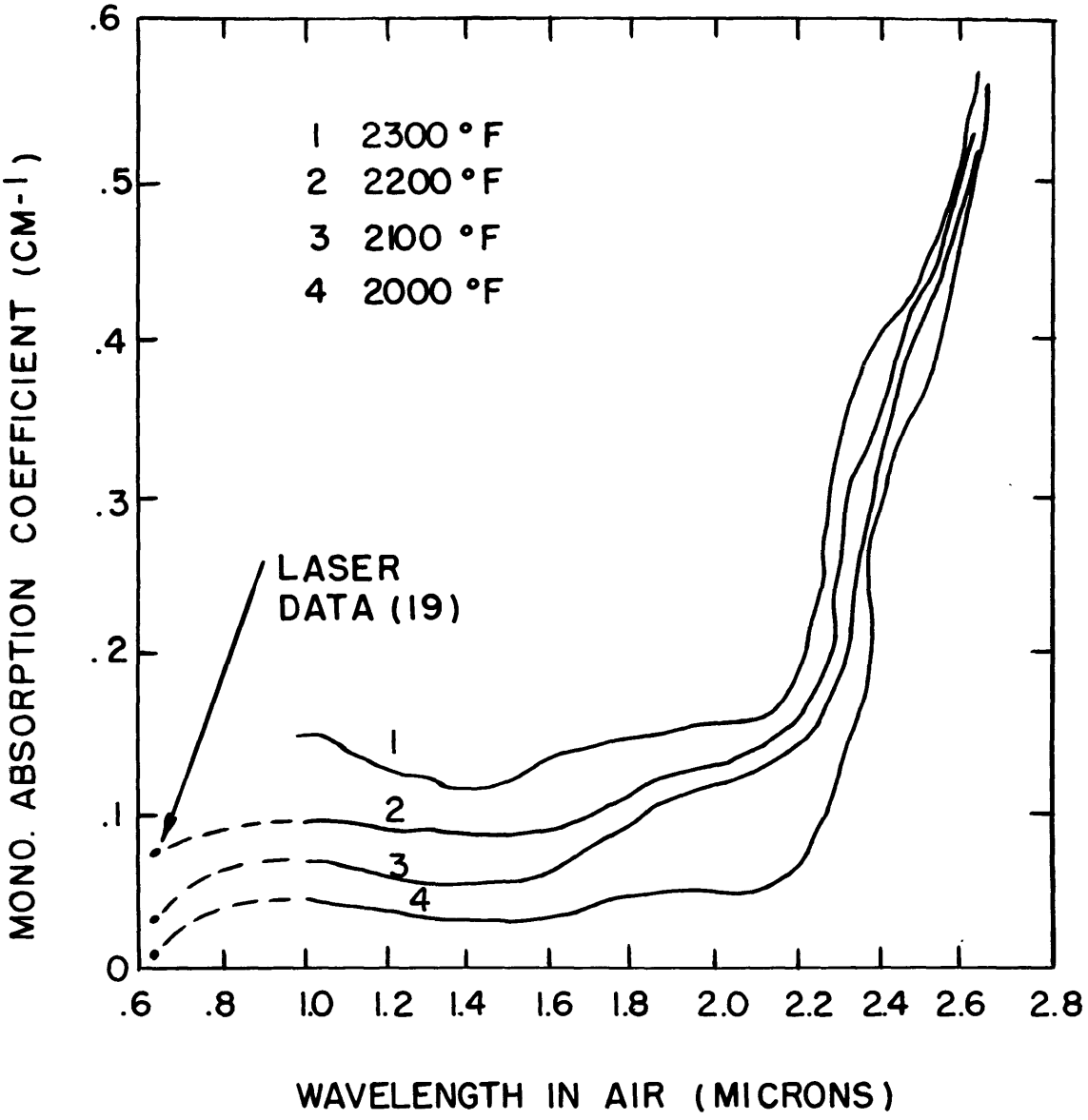

FIGURE B4 SPECTRAL ABSORPTION COEFFICIENT DATA

DATA FROM REFERENCE [55]

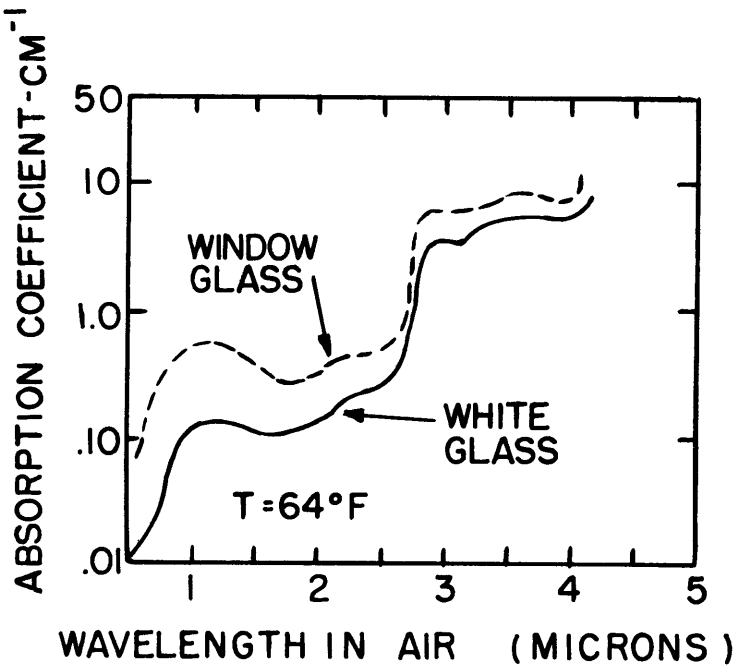

FIGURE B5 SPECTRAL ABSORPTION COEFFICIENT

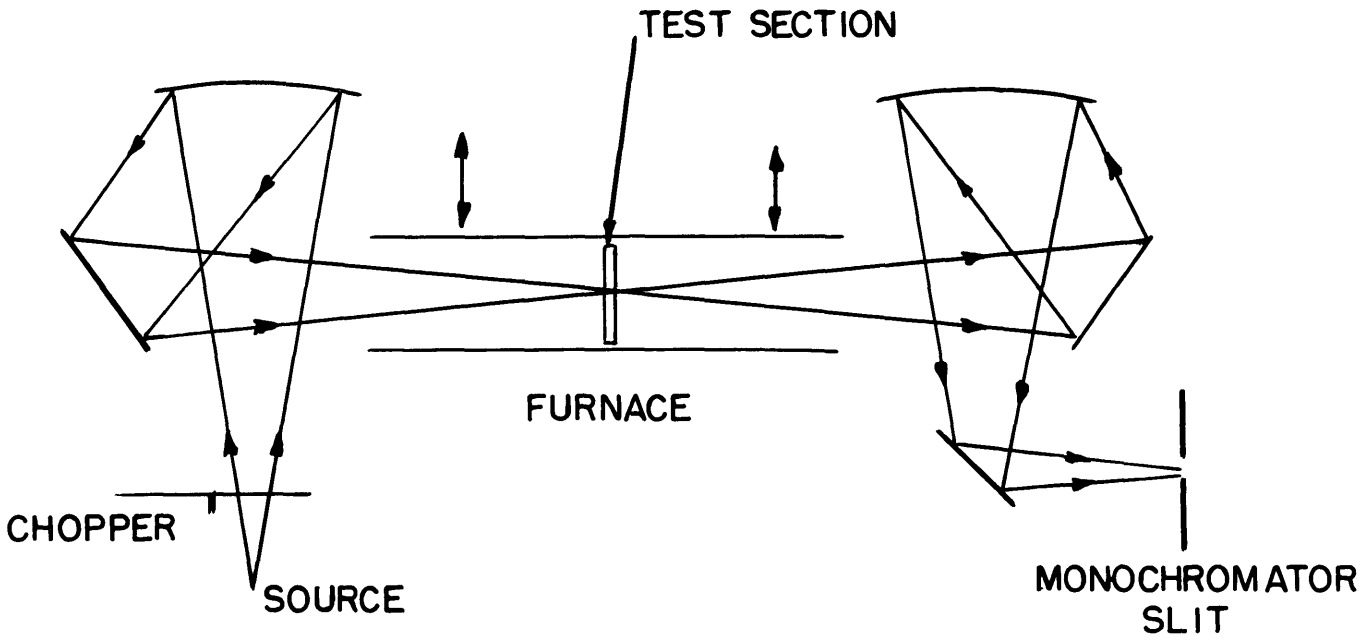

FIGURE B6 DIAGRAM OF OPTICS

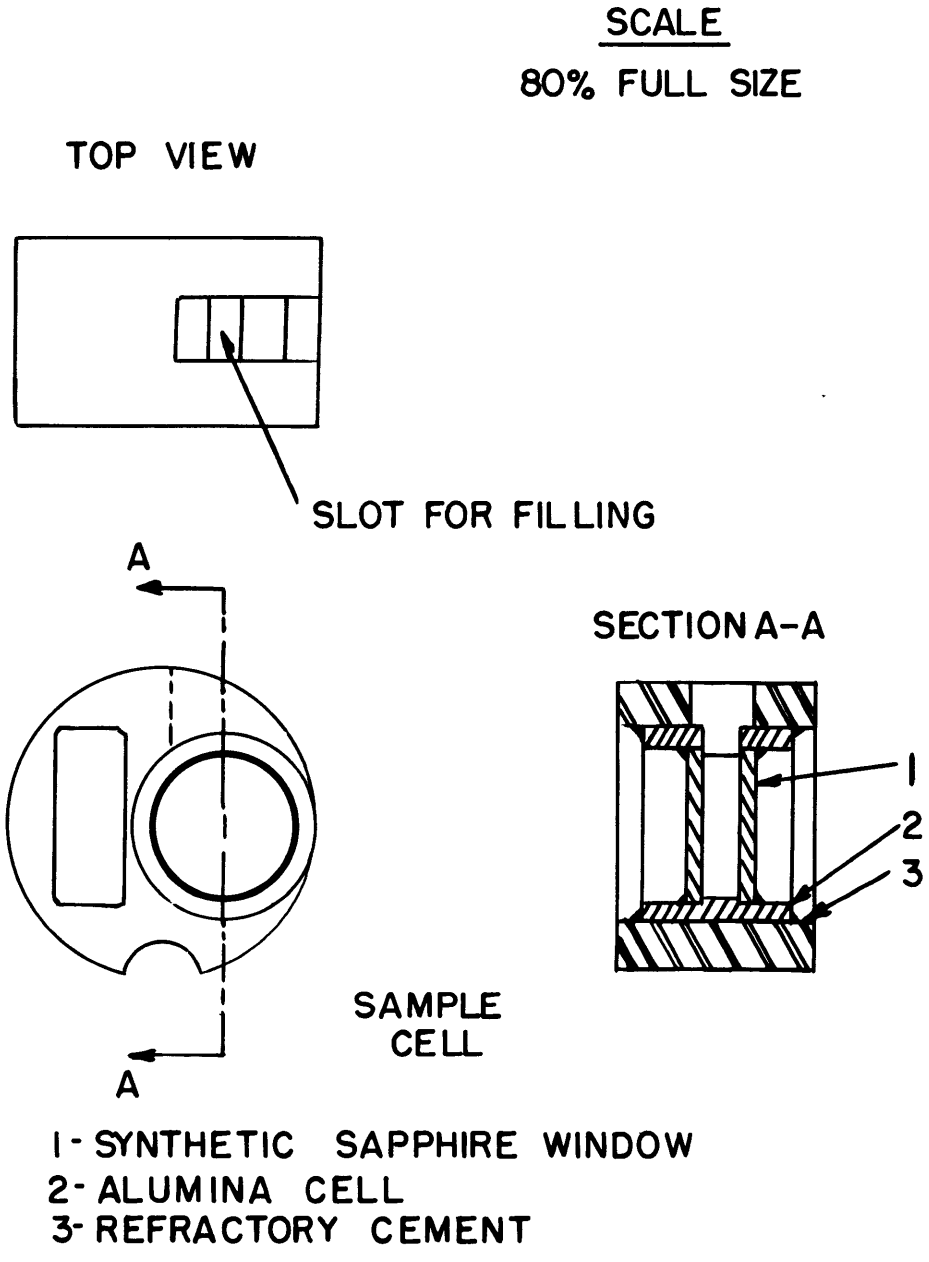

FIGURE B7 TEST SECTION

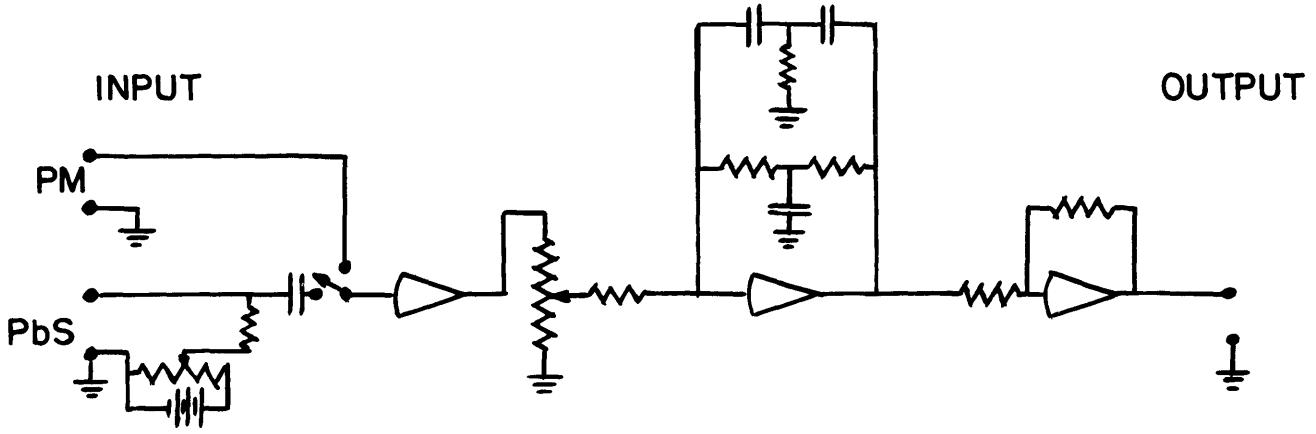

PM = PHOTOMULTIPLIER
PbS = LEAD SULFIDE CELL

FIGURE B8 AMPLIFIER SYSTEM

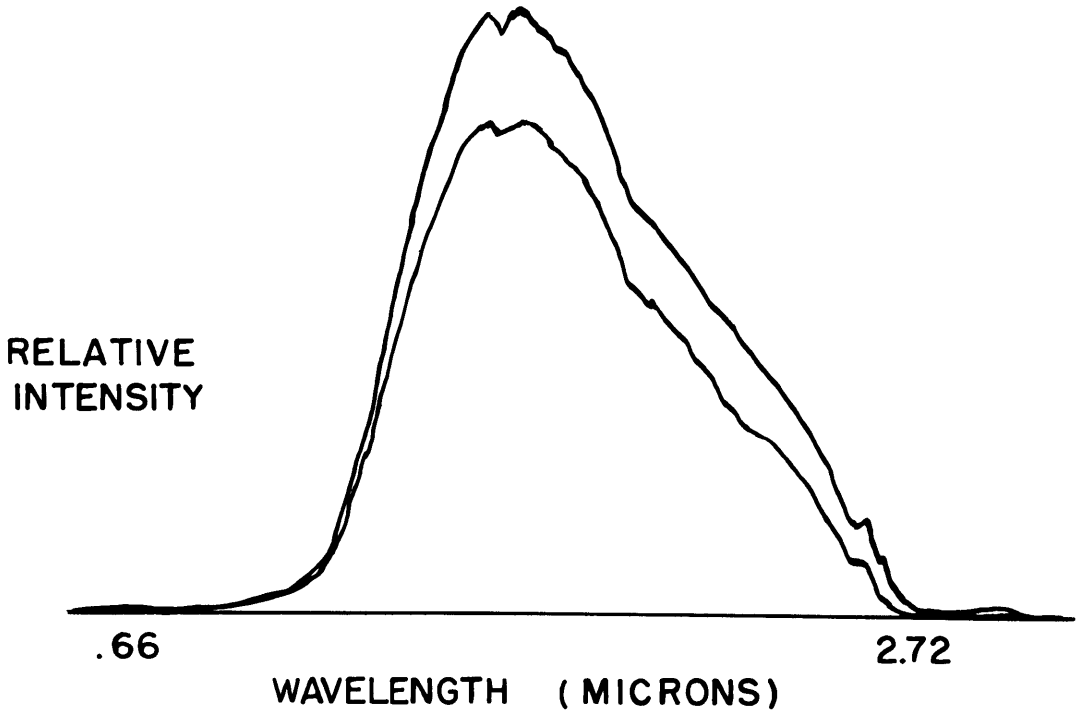

FIGURE B9 DATA

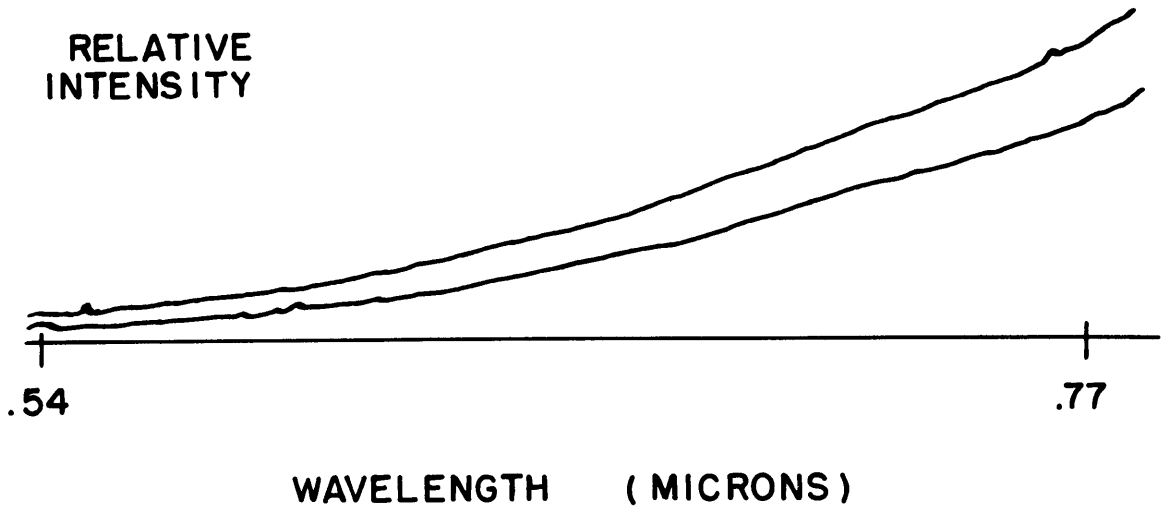

FIGURE B10 VISIBLE DATA

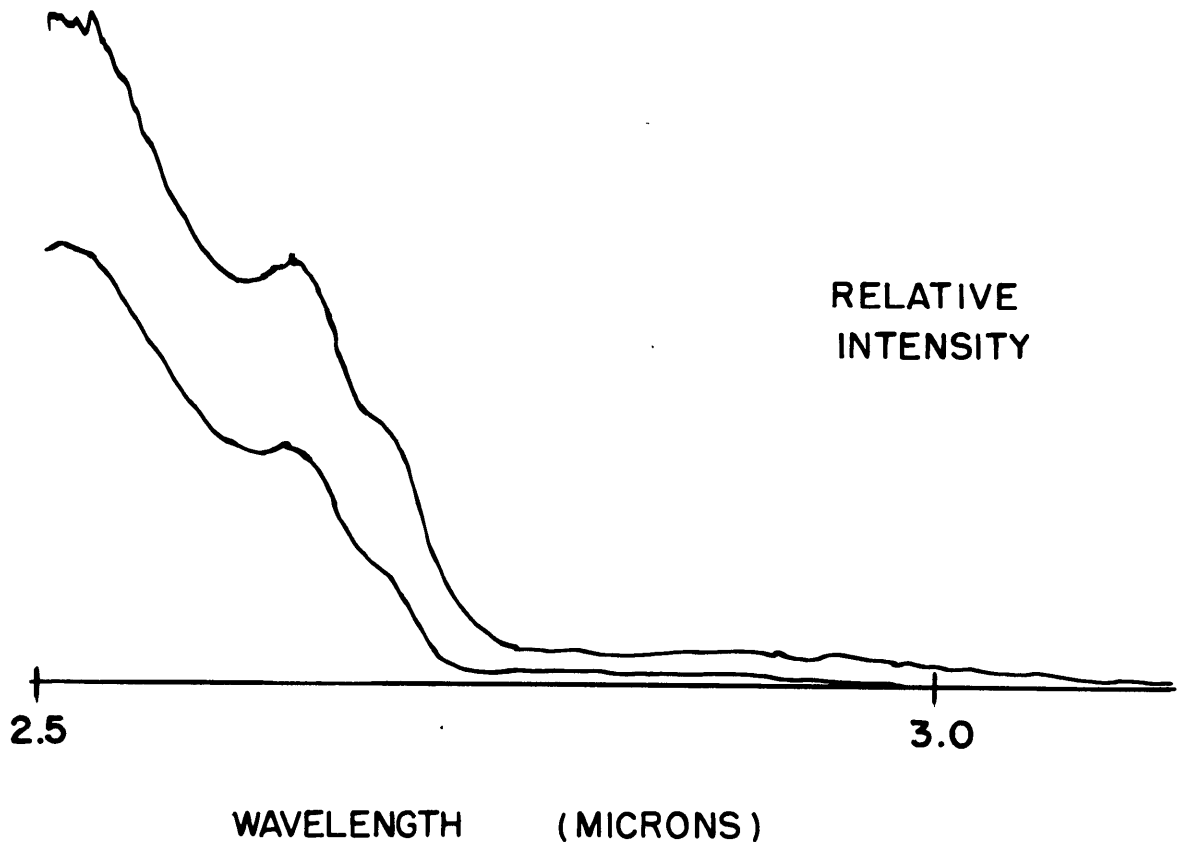

FIGURE B11 INFRARED DATA

flectivity of a normal ray at a dielectric-dielectric interface, assuming a smooth interface.

$$r = \left(\frac{n_2 - n_1}{n_2 + n_1}\right)^2$$

n_2 = index of refraction of medium 1

n_1 = index of refraction of medium 2

r = refection coefficient for a normal ray.

The monochromatic absorption coefficient is then calculated from

$$K = \frac{1}{L} \ln\left(\frac{1}{\tau}\right)$$

K - monochromatic absorption coefficient

L - path length of beam in sample

τ - corrected monochromatic transmissivity of the glass sample

In order to improve the accuracy of measuring the two relative intensities used to calculate the transmissivity, the curves were plotted directly onto 12" x 18" paper on a X-Y recorder and both the visible and infrared portions were plotted separately on expanded scales, as shown in Figs. B9, B10, and B11.

Data were taken from 2000°F to 2300°F during heating, cooling, and after repeated cycling. No hysteresis effects were evident. The .6328 micron data on Figures B3 and B4 are from the laser calibration in reference [19] and the calibration in Section 3.3.4 of this investigation.

B2 INDEX OF REFRACTION

The refractive index of a semi-transparent medium affects radiative transfer within the medium in two ways; it enters into the radiative transport equations, and it affects the boundary reflections through the Fresnel equations. The index of refraction is actually a complex quantity defined by:

$$\bar{n} = n - ik$$

where:

i - $\sqrt{-1}$

$\bar{n}$ - complex index of refraction

n - real index of refraction

k - extinction coefficient

The extinction coefficient is related to the absorption coefficient by the following equation:

$$k = \frac{n\lambda K}{4\pi}$$

where:

n - real index of refraction

λ - wavelength

K - absorption coefficient

Below five microns the extinction coefficient of glass is negligible compared to the refractive index due to the small values of its absorption coefficient. The index of refraction of glass was considered to be real for this analysis since the radiative transfer occurred only at shorter wavelengths where the glass does not absorb strongly.

The glass used in this analysis was a borosilicate crown optical glass manufactured by the Pittsburg Plate Glass Company under the name "Water-white". The index of refraction as supplied by the manufacturer was 1.523 at a wavelength of .5893 microns and at 70^{o}F. Dispersion data for the rate of change of the refractive index with wavelength was not available for this particular glass.

Dispersion data for a typical borosilicate crown optical glass [57] indicate that the change of the refractive index with wavelength is small

DATA FROM REFERENCE [58]

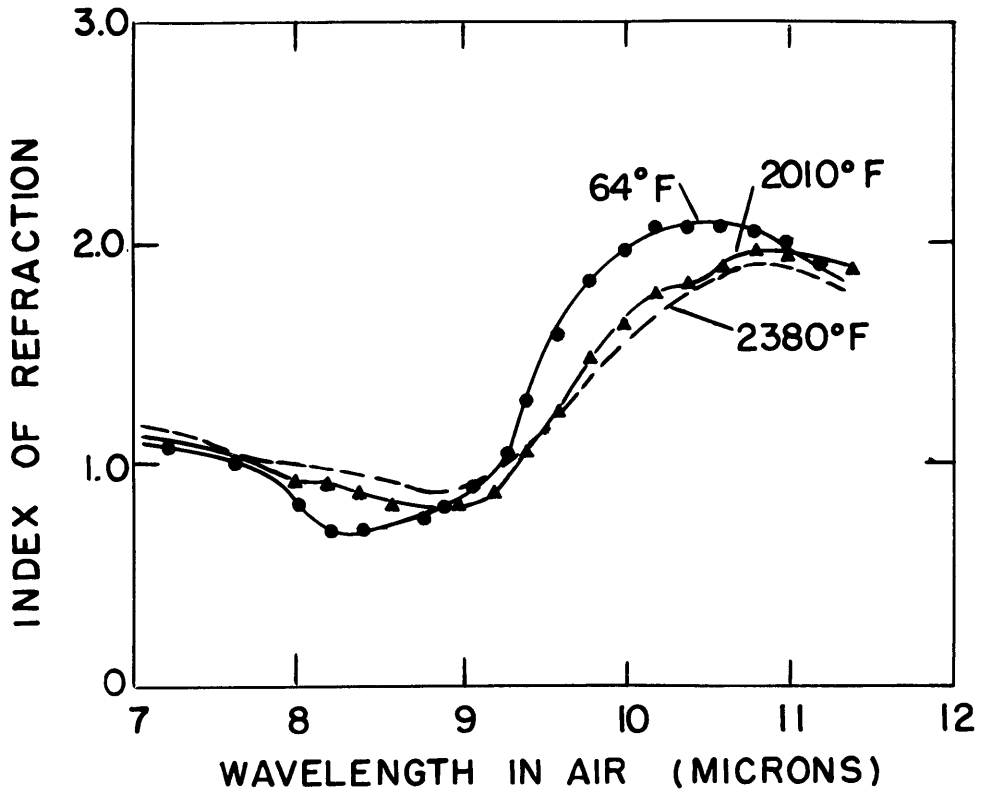

FIGURE B12-REFRACTIVE INDEX OF GLASS AT HIGH TEMPERATURES

in the visible position of the spectrum. The only data available for a similar glass in the infrared region is shown in Fig. B12. This data indicates that the refractive index changes from 1.523 at .5893 microns to approximately 1.2 at 7 microns. Figure B12 also indicates that away from the 10 micron region of strong absorption, temperature does not greatly affect the magnitude of the refractive index.

B3 - THERMAL CONDUCTIVITY OF GLASS

The thermal conductivity of glass has been evaluated at low temperatures by measuring the steady state heat flux through a slab of glass with a one-dimensional temperature gradient. Fouriers equation is then used to relate the thermal conductivity to the heat flux and temperature difference across the glass slab.

At elevated temperatures heat transfer within the glass occurs by conduction and radiation. The thermal conductivity cannot be simply related to the heat flux and temperature gradient. The radiative transfer within the glass depends upon the absorption properties of the glass and the emissivity of the glass boundaries. Due to the experimental difficulties involved in measuring the high temperature thermal conductivity of glass, very few data are available, and a wide range of values is reported for the same type of glass. Chen [59] gives values for the thermal conductivity of window glass at temperatures up to 1650°F. He used a heated glass slab, but corrected the measured thermal conductivity for radiative effects. Chen's data are shown on Fig. B13.

Several investigators [49, 50, 60] have reported values for the "effective thermal conductivity" of glass at elevated temperatures.

The effective thermal conductivity of a slab of glass is defined by:

$$\left(Q/A\right) = -K_{eff}\,\frac{\Delta T}{\Delta X}$$

$\left(Q/A\right)$ - measured heat flux

ΔT - temperature difference across slab

ΔX - thickness of slab

K_{eff} - effective thermal conductivity.

The actual thermal conductivity of glass cannot be measured directly at high temperatures using the same methods which are used for low temperature measurements.

Wray and Connolly [52] have measured the thermal conductivity of clear fused silica at temperatures up to 3200°F. A fine tungsten wire, embedded along the axis of a long silica rod, was heated electrically. The tungsten wire served as a heating element and also as a resistance thermometer. Their calculations indicate that only three percent of the total energy transfer within the silica was by radiation. Figure B13 shows the results from reference [52] and [59]. The thermal conductivity of fused silica and glass appear to increase quickly with temperature between 600°F and 1400°F. Then, an asymptote is reached and the thermal conductivity appears to be independent of the temperature. The glass reaches a lower asymptotic value than the fused silica.

B4 MISCELLANEOUS PROPERTIES

Chemical Composition of Waterwhite Glass (Calculated Values):

SiO_2	-	71.7%
CaO	-	13.8%
Na_2O	-	13.8%
Sb_2O_5	-	.75%

Viscosity of Borosilicate Glass:

1800°F	-	10,000 poise
2160°F	-	2,500 poise .

DATA FROM REFERENCE [42] & [21]

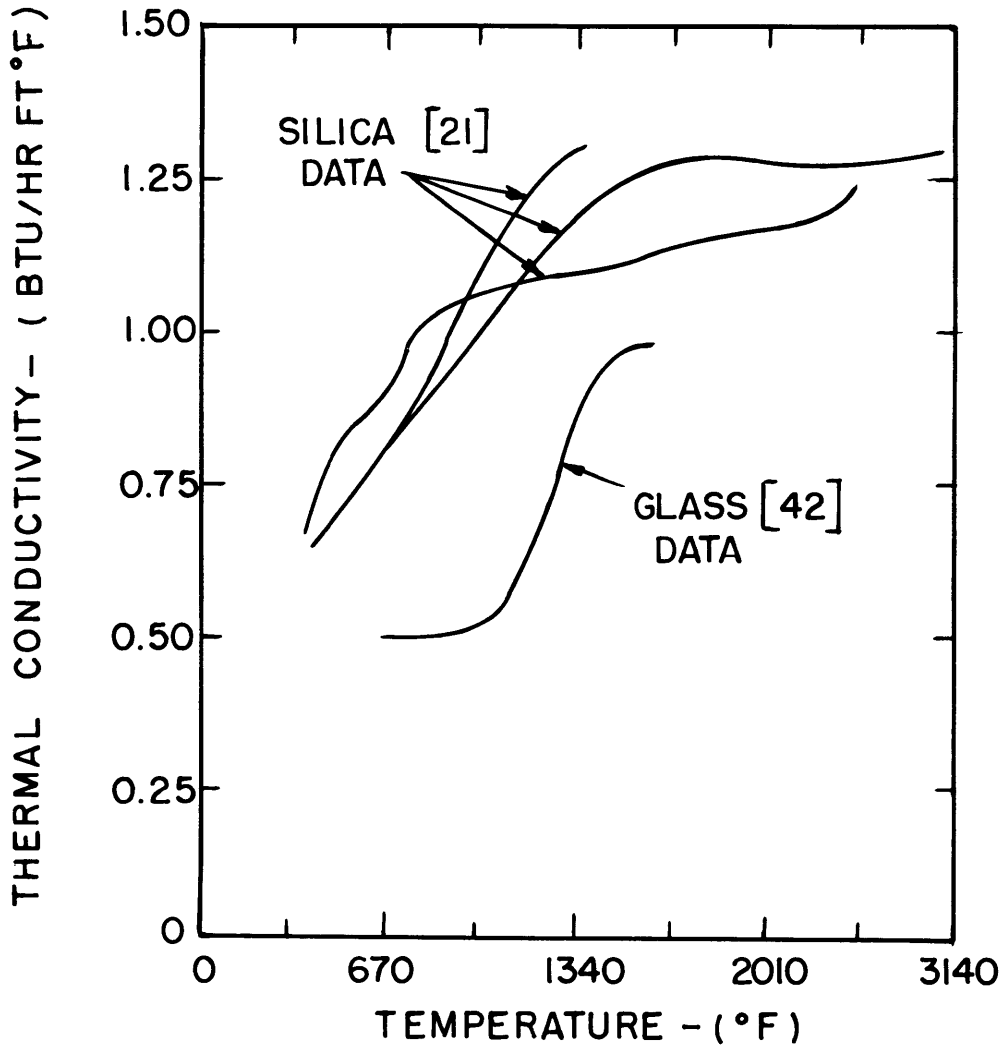

FIGURE B13 THERMAL CONDUCTIVITY OF GLASS

APPENDIX C - EMISSIVITY OF A PLATINUM-GLASS INTERFACE

C1 ELECTROMAGNETIC THEORY PREDICTIONS

In this section the platinum-glass interface is assumed to be perfectly smooth so that Fresnel's law of reflection [61] is valid. The analysis is similar to that of reference [62].

The radiant energy emitted by platinum in contact with glass is larger than the emission from platinum into a vacuum. The emissivity of a platinum-glass interface was evaluated by calculating the spectral absorptivity of the platinum surface for incoming radiation from the glass and equating this with the spectral emissivity of the metal using Kirchhoff's law. Consider a plane electromagnetic wave in glass incident on a plane platinum surface as shown below:

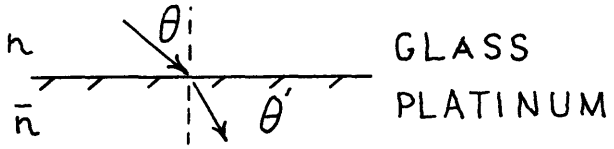

The index of refraction is actually a complex quantity:

$$\bar{n} = n - ik \qquad C1$$

$i - \sqrt{-1}$

$\bar{n}$ - complex index of refraction

k - extinction coefficient

Most dielectric materials, including glass at wavelengths below five microns, exhibit weak absorption properties and therefore have extremely small extinction coefficients. The index of refraction of glass is a real quantity as the imaginary component is negligible compared to the real. However, metals have a complex index of refraction due to their strong absorption properties.

Applying Snell's law to a dielectric-metal interface;

$$n_D \sin\theta = (n_m - ik_m) \sin\theta' \qquad C2$$

$i = \sqrt{-1}$

n_d - real index of refraction of glass

n_m - real index of refraction of the metal

k_m - extinction coefficient of the metal

θ - angle of incidence

θ' - complex angle of refraction

Fresnel's law can be simplified by applying the complex form of Snell's law and using trignometric identities:

$$R_\perp = \frac{\sin^2(\theta - \alpha) + \sinh^2\beta}{\sin^2(\theta + \alpha) + \sinh^2\beta} \qquad C3$$

$$R_{//} = R_\perp\left[\frac{\cos^2(\theta+\alpha) + \sinh^2\beta}{\cos^2(\theta-\alpha) + \sinh^2\beta}\right] \qquad C4$$

$$\rho(\theta',\theta) = \frac{1}{2}(R_\perp + R_{//}) \qquad C5$$

$$\epsilon(\theta) = 1 - \frac{1}{2}(R_\perp + R_{//}) \qquad C6$$

$R_\perp, R_{//}$ - reflectance for the two different modes of polarization

α - real part of the complex angle of refraction

β - imaginary part of the complex angle of refraction

θ - angle of incidence

ρ - monochromatic directional specular reflectivity

ϵ - monochromatic directional specular emissivity

Experimental data for the indices of refraction and extinction coefficients of platinum were taken from reference 17. Figures C1, C2, and C3 show the results for the emissivity of a platinum-air and a platinum-glass interface. The platinum-glass interface has a higher emissivity at all wavelengths than the platinum-air interface. Also, at short wavelengths the platinum-glass interface emissivity exhibits characteristics of a dielectric-dielectric interface, while at longer wavelengths the emissivity becomes more typical of a metal-dielectric interface, reaching its maximum value near the grazing angle. Room temperature optical constants were used to calculate the reflectivity of a platinum-glass interface at high temperature. The only justification for this is the fact that the same method applied to a platinum-air interface yields agreement with experimental data.

C2 EXPERIMENTAL DATA

This section presents experimental data [34, 39, 40] for the emissivity of platinum in air. The purity of the platinum and the surface preparation influence the data strongly. Platinum oxidizes above 1300°C, increasing the emissivity, as seen in Fig. C5. Curve 3 on Fig. C5 shows the normal spectral emissivity of platinum oxidized in air at 1420°K. This curve seems to be the upper bound for data on the normal spectral emissivity increases at short wavelengths.

Figure C4 is a plot of the total normal emissivity data for platinum in air, as a function of temperature. The emissivity appears to increase linearly with temperature, as predicted by the Hagen-Rubens relation.

No experimental data is available for the emissivity of a platinum-glass interface. Some data does exist for thin dielectric films but this data involves two interfaces rather than a simple dielectric-metal interface. The normal spectral emissivity calculated from the Fresnel relations in Appendix C1 is shown on Figure C5. The predicted emissivity agrees with the experimental values.

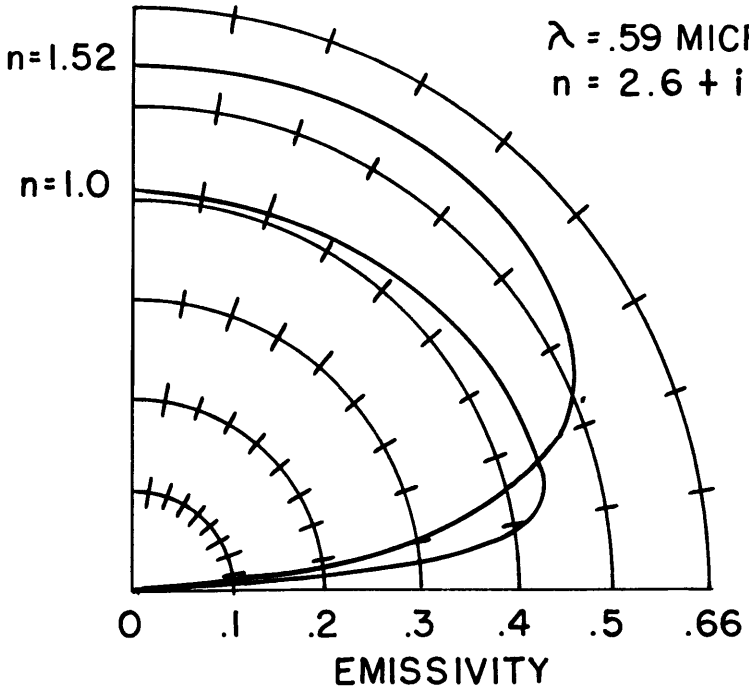

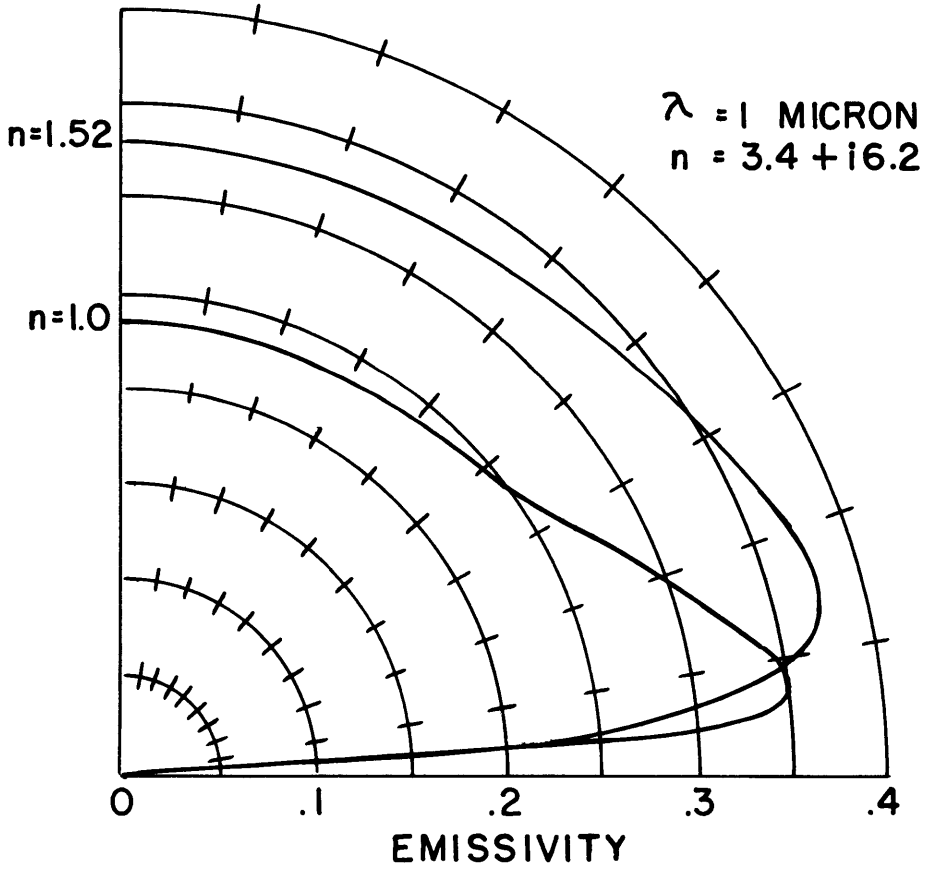

FIGURE C1 SPECTRAL DIRECTIONAL EMISSIVITY OF PLATINUM

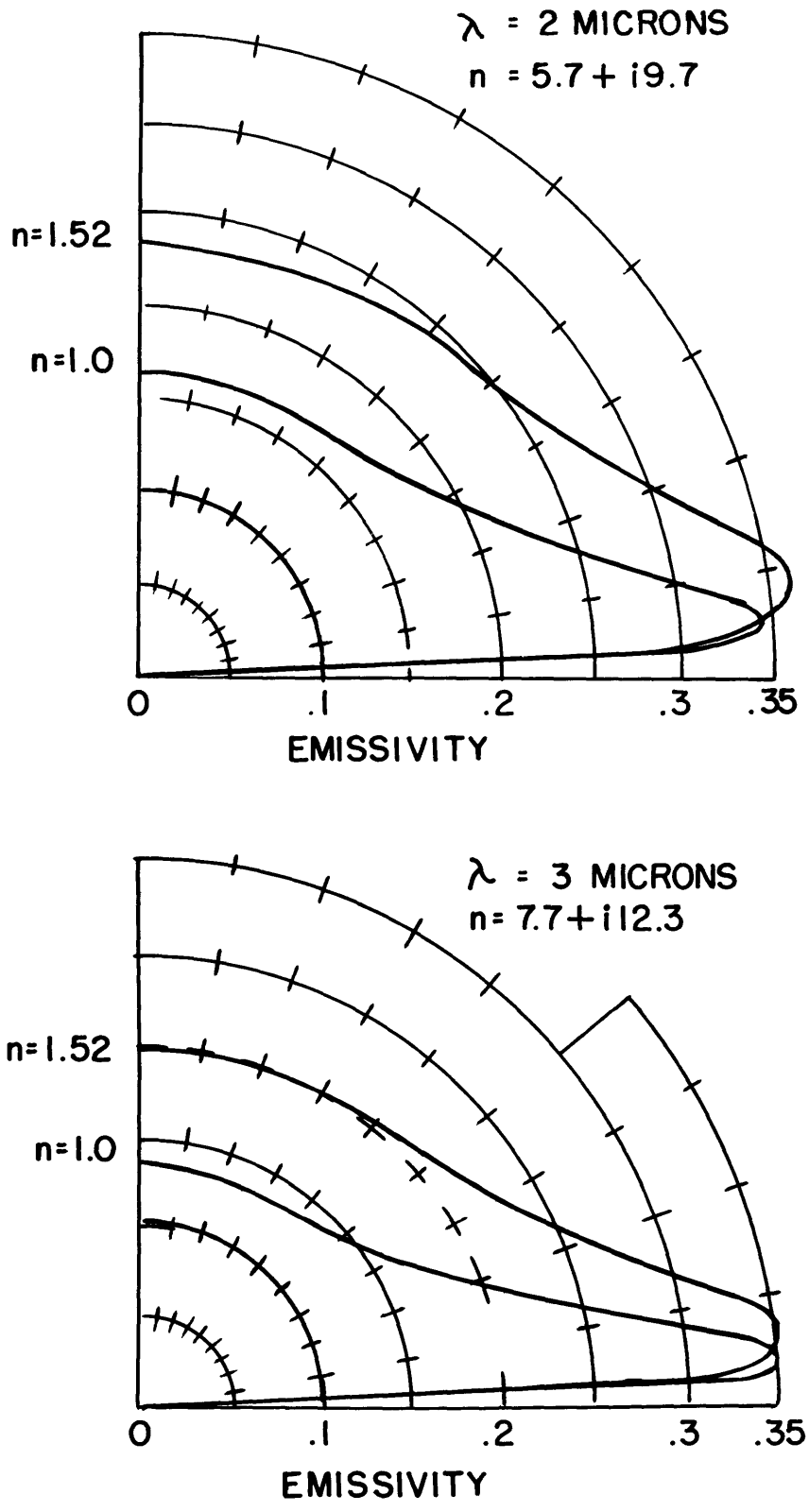

FIGURE C2 SPECTRAL DIRECTIONAL EMISSIVITY OF PLATINUM

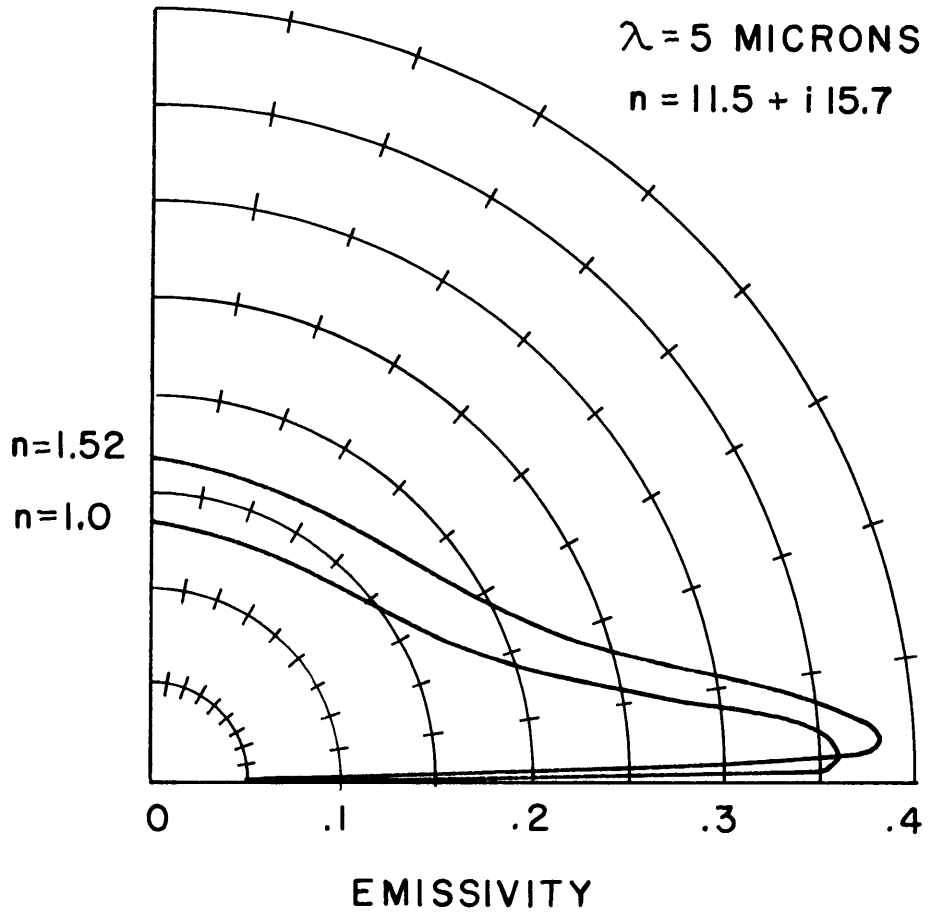

FIGURE C3 SPECTRAL DIRECTIONAL EMISSIVITY OF PLATINUM

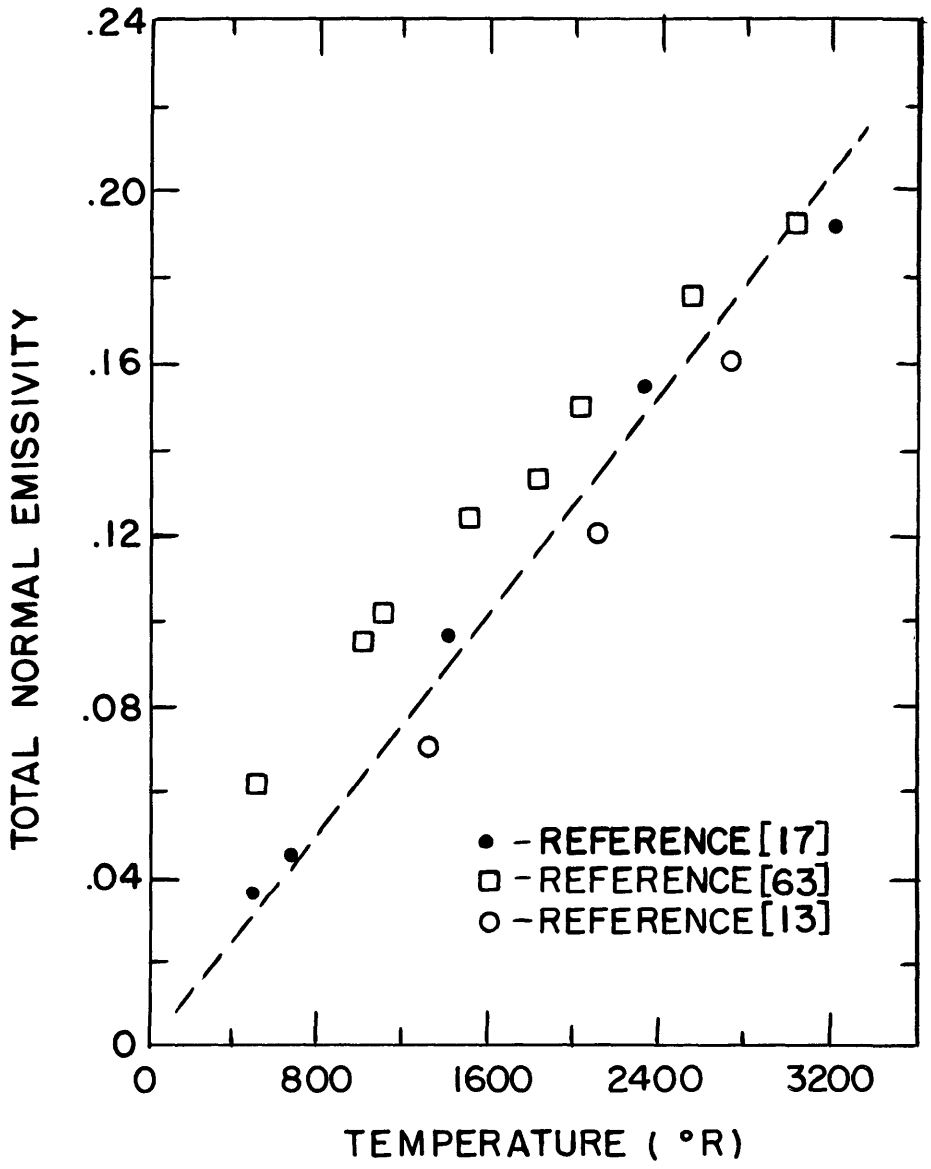

FIGURE C4 TOTAL NORMAL EMISSIVITY OF PLATINUM versus TEMPERATURE

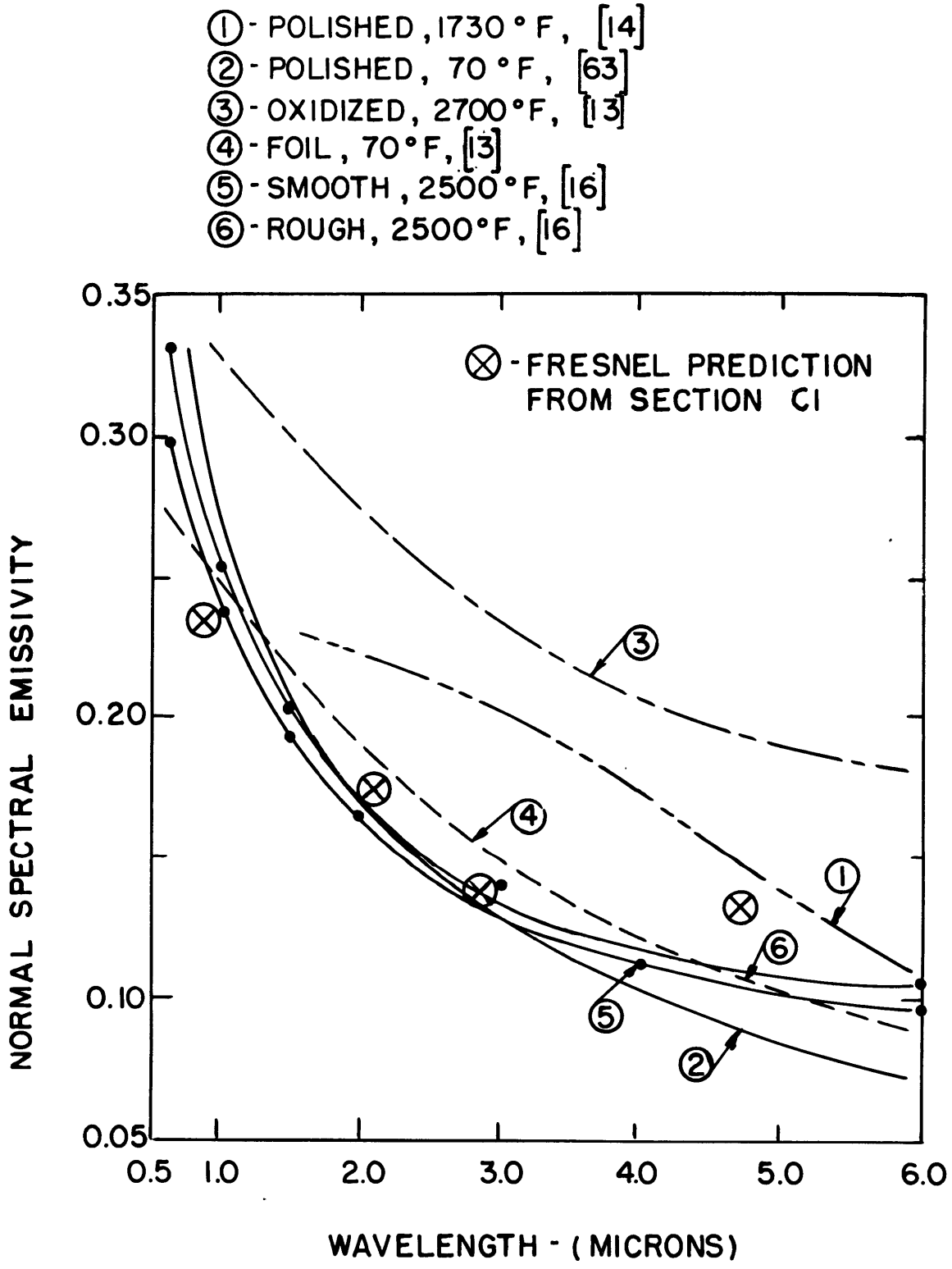

FIGURE C5 NORMAL SPECTRAL EMISSIVITY OF PLATINUM IN AIR

APPENDIX D - SPECULAR REFLECTION DERIVATIONS

This appendix contains derivations of the individual heat balance terms introduced in Section 2.6.1. Radiative and conductive heat transfer are considered in a slab of glass bounded by two parallel optically-smooth platinum boundaries. The platinum-glass interface is assumed to be a perfect specular reflector and Fresnel's equations are used to predict the directional reflectivity of the interface. As outlined in Section 2.6.1 the glass slab is divided into a number of thin slabs and a heat balance is performed on each slab. Two different types of radiative interchange between the medium and the boundaries exist; direct exchange and exchange by multiple internal reflections. Direct exchange occurs when radiant transfer takes place without reflecting from the wall, while multiple internal reflection interchange occurs solely as a result of reflections from the walls. The following sections contain derivations of each individual mode of heat transfer.

D1 MULTIPLE INTERNAL REFLECTIONS

In this section an expression is developed for the intensity at a plane within the medium, which is due to multiple internal reflections of a monochromatic beam of radiation of given polarization incident on the boundary at a given angle.

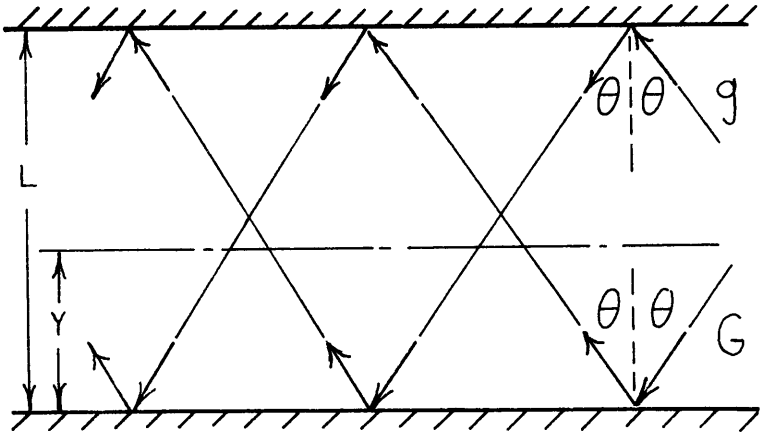

The above figure shows two monochromatic polarized beams with

intensities $G_{\lambda\theta 0\perp}$ and $g_{\lambda\theta 0\perp}$ arriving at the boundaries from within the medium, at an angle of incidence θ. The beams are partially reflected at the interface, attenuated within the medium and reflected at the other boundary. The incident intensities g and G are defined in the following sections.

A plane located at a distance y from one surface is traversed by the multiply reflected beams in both directions. Let $g_{\lambda\theta Y\perp}$ denote the sum of the intensities of all upward reflections of the original beam $g_{\lambda\theta 0\perp}$ at an angle θ.

$$\uparrow g_{\lambda\theta Y\perp} = g_{\lambda\theta 0\perp}\rho_\perp e^{\frac{-K_\lambda Y}{\cos\theta}}\left(\rho_\perp e^{\frac{-K_\lambda L}{\cos\theta}} + \rho_\perp^3 e^{\frac{-3K_\lambda L}{\cos\theta}} + \ldots\right) \qquad D1$$

Using the binomial series:

$$\uparrow g_{\lambda\theta Y\perp} = g_{\lambda\theta 0\perp}\rho_\perp^2 e^{\frac{-K_\lambda (L-Y)}{\cos\theta}}\left[\frac{1}{1-\rho_\perp^2 e^{\frac{-2K_\lambda L}{\cos\theta}}}\right] \qquad D2$$

Similarly, for the other beams:

$$\downarrow g_{\lambda\theta Y\perp} = g_{\lambda\theta 0\perp}\rho_\perp e^{\frac{-K_\lambda (L-Y)}{\cos\theta}}\left[\frac{1}{1-\rho_\perp^2 e^{\frac{-2K_\lambda L}{\cos\theta}}}\right] \qquad D3$$

$$\uparrow G_{\lambda\theta Y\perp} = G_{\lambda\theta 0\perp}\rho_\perp e^{\frac{-K_\lambda Y}{\cos\theta}}\left[\frac{1}{1-\rho_\perp^2 e^{\frac{-2K_\lambda L}{\cos\theta}}}\right] \qquad D4$$

$$G^{\downarrow}_{\lambda\theta Y\perp} = G_{\lambda\theta 0\perp}\rho_\perp^2 e^{-\frac{K_\lambda(2L-Y)}{\cos\alpha}}\left[\frac{1}{1-\rho_\perp^2 e^{-\frac{2K_\lambda L}{\cos\theta}}}\right] \qquad D5$$

summing these;

$$q_{\lambda\theta Y\perp} = \left[\frac{\rho_\perp}{1-\rho_\perp^2 e^{-\frac{2K_\lambda L}{\cos\theta}}}\right]\left[e^{-\frac{K_\lambda(L-Y)}{\cos\theta}} + \rho_\perp e^{-\frac{K_\lambda(L+Y)}{\cos\theta}}\right] q_{\lambda\theta 0\perp} \qquad D6$$

$$G_{\lambda\theta Y\perp} = \left[\frac{\rho_\perp}{1-\rho_\perp^2 e^{-\frac{2K_\lambda L}{\cos\theta}}}\right]\left[e^{-\frac{K_\lambda Y}{\cos\theta}} + \rho_\perp e^{-\frac{K_\lambda(2L-Y)}{\cos\theta}}\right] G_{\lambda\theta 0\perp} \qquad D7$$

If we set;

$$P_\perp = \frac{\rho_\perp}{1-\rho_\perp^2 e^{-\frac{2K_\lambda L}{\cos\theta}}} \; ; \; P_{//} = \frac{\rho_{//}}{1-\rho_{//}^2 e^{-\frac{2K_\lambda L}{\cos\theta}}} \qquad D8$$

the following expressions can be used to relate the intensity at y due to a beam of given polarization striking the boundary:

$$q_{\lambda\theta Y\perp} = P_\perp\left[e^{-\frac{K_\lambda(L-Y)}{\cos\theta}} + \rho_\perp e^{-\frac{K_\lambda(L+Y)}{\cos\theta}}\right] q_{\lambda\theta 0\perp} \qquad D9$$

$$q_{\lambda\theta Y//} = P_{//}\left[e^{-\frac{K_\lambda(L-Y)}{\cos\theta}} + \rho_{//} e^{-\frac{K_\lambda(L+Y)}{\cos\theta}}\right] q_{\lambda\theta 0//} \qquad D10$$

$$G_{\lambda\theta Y\perp} = P_{\perp}\left[e^{\frac{-K_{\lambda}Y}{\cos\theta}} + \rho_{\perp}e^{\frac{-K_{\lambda}(2L-Y)}{\cos\theta}}\right]G_{\lambda\theta 0\perp} \qquad D11$$

$$G_{\lambda\theta Y//} = P_{//}\left[e^{\frac{-K_{\lambda}Y}{\cos\theta}} + \rho_{//}e^{\frac{-K_{\lambda}(2L-Y)}{\cos\theta}}\right]G_{\lambda\theta 0//} \qquad D12$$

The above expressions are used in the following sections to evaluate the multiple internal reflections of radiant energy between the boundaries and the medium and between different elements of the medium.

D2 EMISSION FROM A LAYER

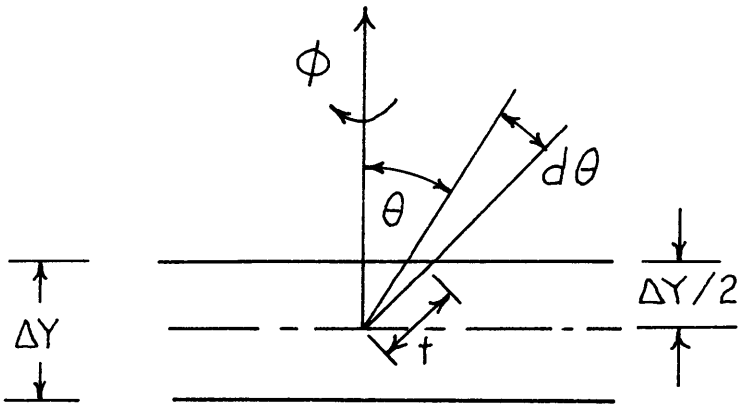

Consider the configuration shown in the above diagram. An infinite plate of radiating fluid located at the center of a volume element of thickness "ΔY" is radiating to the surroundings.

Kirchoff's law yields the following expression for the volumetric emission coefficient of a medium in thermodynamic equilibrium:

$$J_{\lambda} = \frac{K_{\lambda}}{\pi} e_{b\lambda} \qquad D13$$

The monochromatic emission from an elemental volume "dV" is calculated by integrating the above equation over the total solid angle

and by allowing for attenuation within the volume element considered. The resulting equation for the monochromatic emission is:

$$\left(\frac{dQ}{dV}\right)_\lambda = \int_0^{4\pi} \frac{K_\lambda e_{b\lambda} e^{-K_\lambda t}}{\pi} d\omega \qquad D14$$

Equation D14 is valid when $K\Delta Y$ is less than .2, as it assumes that emission occurs at the center of the layer, rather than over the entire thickness.

The following substitutions are made:

$$d\omega = \sin\theta d\theta d\phi, \quad t = \frac{\Delta Y}{2\cos\theta}, \quad d(\cos\theta) = -\sin\theta d\theta \qquad D15$$

The resulting expression is:

$$\left(\frac{dQ}{dV}\right)_\lambda = -\frac{2}{\pi} \int_0^{2\pi} \int_0^{\pi/2} K_\lambda e_{b\lambda} e^{-\frac{K_\lambda \Delta Y}{2\cos\theta}} d(\cos\theta) d\phi \qquad D16$$

The above equation must be integrated over all wavelengths in order to calculate the total emission. A weighted summation over all wavelengths is used to replace the integral. The result of this summation is shown below.

$$\left(\frac{dQ}{dV}\right) = -4n^2\sigma T^4 \Delta Y \sum_{i=1} K_i E_2\left(\frac{K_i \Delta Y}{2}\right) EB(n\lambda_i T, n\lambda_{i+1} T) \qquad D17$$

Where $EB(n\lambda_i T, n\lambda_{i+1} T)$ is the amount of black body energy occuring between $n\lambda_i T$ and $n\lambda_{i+1} T$.

Equation D-17 was used to calculate the net emission from a volume element.

D3 EMISSION FROM BOUNDARY TO A LAYER

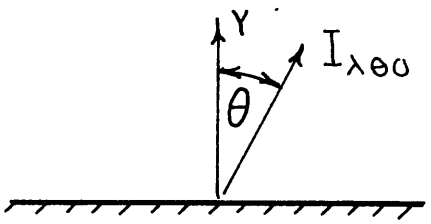

The platinum boundary is modelled by multiplying the intensity of the emitted radiation by the Fresnel transmissivity of the platinum-glass interface. The intensity of the radiation emitted from the lower platinum boundary is given by;

$$I_{\lambda\theta o} = \left|\frac{e_{b\lambda}}{\pi}\right|_2 n^2 \tau \qquad \text{D18}$$

τ' - Fresnel transmissivity of platinum-glass interface.

$$= 1 - \rho' = 1 - \tfrac{1}{2}\left(\rho_\perp + \rho_{||}\right). \qquad \text{D19}$$

The emitted boundary radiation is of random polarization, giving an average polarization equal to that of a uniformly polarized beam. The polarized components of the intensity of the emitted radiation are given by:

$$I_{\lambda\theta o\perp} = I_{\lambda\theta o||} = \frac{I_{\lambda\theta o}}{2} \qquad \text{D20}$$

These beams reach the level y with an intensity of:

$$I_{\lambda\theta Y\perp} = I_{\lambda\theta Y||} = \tfrac{1}{2} I_{\lambda\theta 0}\, e^{-\frac{K_\lambda Y}{\cos\theta}} \qquad \text{D21}$$

The plane at y is also traversed by multiple reflections of the energy emitted by the lower boundary. The following equation gives the intensity of the beam emitted at the lower plate just prior to its first reflection at the upper plate:

$$I_{\lambda\theta L\perp} = I_{\lambda\theta L||} = \tfrac{1}{2} I_{\lambda\theta 0}\, e^{-\frac{K_\lambda L}{\cos\theta}} \qquad \text{D22}$$

The intensity due to emission at the boundary then takes the place of $G_{\lambda\theta o\perp}$ and $G_{\lambda\theta o//}$ in the multiple internal reflection analysis of section D5. The intensities at level y due to all multiple internal reflections of monochromatic radiation emitted by the lower boundary are similar to equations D11 and D12 and are given by:

$$I_{\lambda\theta Y\perp} = P_{\perp}\left[e^{-\frac{K_\lambda(L-Y)}{\cos\theta}} + \rho_{\perp} e^{-\frac{K_\lambda(L-Y)}{\cos\theta}}\right] I_{\lambda\theta L\perp} \qquad D23$$

$$I_{\lambda\theta Y//} = P_{//}\left[e^{-\frac{K_\lambda(L-Y)}{\cos\theta}} + \rho_{//} e^{-\frac{K_\lambda(L+Y)}{\cos\theta}}\right] I_{\lambda\theta L//} \qquad D24$$

The total spectral intensity of all the radiation from the lower boundary at level y is given by:

$$I_{\lambda\theta YT} = I^{*}_{\lambda\theta Y\perp} + I^{*}_{\lambda\theta Y//} + I_{\lambda\theta Y\perp} + I_{\lambda\theta Y//} \qquad D25$$

The rate of absorption in a slab of thickness "Δy" is:

$$\delta I_{\lambda\theta YT} = \frac{K_\lambda \Delta Y}{\cos\theta} I_{\lambda\theta YT} \qquad D26$$

The rate of accumulation of energy per unit volume withing the slice due to the rate of spectral flux absorption is calculated by integrating over all angles.

$$Q_{\Delta Y} = \frac{2\pi}{\Delta Y}\int_0^{\pi/2} \delta I_{\lambda\theta YT} \cos\theta \sin\theta \, d\theta \qquad D27$$

The above equation must be integrated over all wavelengths in order to calculate the total energy absorption rate. This integral is replaced by a finite sum over wavelength.

$$Q_{AY} = \frac{2\pi}{\Delta Y} \sum_{j=1}^{n} \int_{0}^{\pi/2} \delta I_{\lambda\theta YT} \cos\theta \sin\theta \, d\theta \qquad D28$$

The above equation gives the net heat radiated from the lower boundary into a slab at the distance y from the lower boundary. A similar analysis leads to expressions for the heat radiated from the upper boundary to the same slab now (L-y) away from the upper boundary.

D4 PRIMARY INTERCHANGE BETWEEN LAYERS

DIAGRAM :

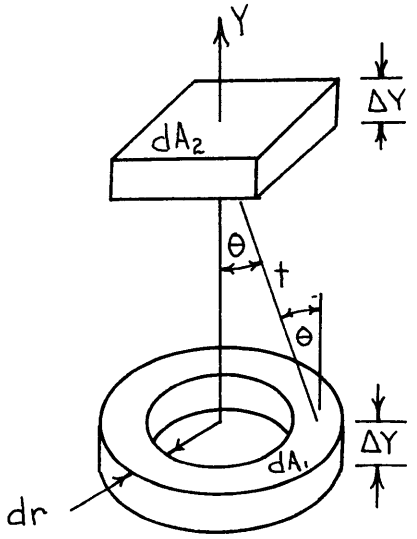

dA_1 - fluid volume radiating to fluid layer dA_2

dA_2 - fluid volume receiving radiation from dA_1

Consider the configuration shown in the above diagram. A fluid volume of thickness ΔY is radiating energy which is absorbed by a similar fluid volume a distance Y away.

The monochromatic radiant energy leaving surface "dA_1" is given by the following equation :

$$d\phi_\lambda = \frac{K_\lambda}{\pi} e_{b\lambda} \Delta Y \, dA_1 \, d\omega \qquad D29$$

The following substitutions are made:

$$d\omega = \frac{dA_2 \cos\theta}{t^2} \quad , \quad dA_1 = 2\pi r dr, \quad r = Y\frac{\sin\theta}{\cos\theta}$$

$$dr = Y\sec^2\theta d\theta \quad , \quad t = \frac{Y}{\cos\theta}$$

The resulting equation is:

$$dQ_\lambda = 2K_\lambda \Delta Y e_{b\lambda} d(\cos\theta)\, dA_2 \qquad D30$$

Due to attenuation in the interval between the two fluid volumes considered the monochromatic energy flux at "dA_2" is:

$$\left(\frac{dQ_\lambda}{dA_2}\right) = -2K_\lambda \Delta Y e_{b\lambda} e^{\frac{-K_\lambda Y}{\cos\theta}} d(\cos\theta) \qquad D31$$

The energy absorbed in the volume "$\Delta Y dA_2$" is given by the flux times the path length times the absorption coefficient.

$$\left(\frac{dQ}{dV}\right)_\lambda = 2\Delta Y^2 K_\lambda^2 e_{b\lambda} e^{\frac{-K_\lambda Y}{\cos\theta}} \frac{d(\cos\theta)}{\cos\theta} \qquad D32$$

Integrating over the interval $0-2\pi$ to calculate the net monochromatic energy received at dA_2:

$$\left(\frac{dQ}{dV}\right)_\lambda = -2\Delta Y e_{b\lambda} \int_1^0 \frac{K_\lambda^2 e^{\frac{-K_\lambda Y}{\cos\theta}} d\cos\theta}{\cos\theta}$$

$$= 2\Delta Y^2 e_{b\lambda} K_\lambda^2 E_1(K_\lambda Y) \qquad D33$$

The above equation must be summed over all wavelengths in order to calculate the total radiant energy interchange.

$$\left(\frac{dQ}{dV}\right) = 2\Delta Y^2 n^2 \sigma T^4 \sum_{i=1}^{n} K_i^2 E_1(K_i Y)\, EB(n\lambda_i T, n\lambda_{i+1} T) \qquad D34$$

The above equation was used to calculate the primary heat exchange between fluid elements. Radiant transfer by reflection from the boundaries is considered to the next section.

D5 REABSORPTION OF MULTIPLY REFLECTED INTERNALLY EMITTED RADIATION

Figure 9 shows the geometry used for this analysis. A slab of material of thickness ΔY at level Y between the boundaries emits radiation with the following spectral intensity :

$$\delta I_{\lambda\theta} = \frac{j_{\lambda\theta}(Y)\,\Delta Y}{\cos\theta} \qquad D35$$

Because the average polarization of emitted light is equal to that of a uniformly polarized beam the intensities for the two modes of polarization are:

$$\delta I_{\lambda\theta\perp} = \delta I_{\lambda\theta//} = \frac{1}{2}\delta I_{\lambda\theta} \qquad D36$$

Due to attenuation by absorption the intensity at the lower wall is :

$$\delta I_{\lambda\theta o\perp} = \delta I_{\lambda\theta o//} = \frac{j_\lambda(Y)}{2}\,\Delta Y\, e^{\frac{-K_\lambda Y}{\cos\theta}} \qquad D37$$

Similarly, the intensity at the upper wall due to emission in the layer at Y is given by:

$$\delta i_{\lambda\theta L\perp} = \delta i_{\lambda\theta L//} = \frac{j_\lambda Y}{2}\,\Delta Y\, e^{\frac{-K_\lambda L - Y}{\cos\theta}} \qquad D38$$

The intensities in D37 and D38 can be substituted into the multiple internal reflection relations in section D1 to get the following expressions for the intensities at y due to reflections of the energy emitted at Y.

$$\delta I_{\lambda\theta Y\perp} = P_\perp \left[e^{-\frac{K_\lambda (L-Y)}{\cos\theta}} + \rho_\perp e^{-\frac{K_\lambda (L+Y)}{\cos\theta}} \right] \delta I_{\lambda\theta o\perp} \qquad \text{D39}$$

$$\delta I_{\lambda\theta Y//} = P_{//} \left[e^{-\frac{K_\lambda (L-Y)}{\cos\theta}} + \rho_{//} e^{-\frac{K_\lambda (L+Y)}{\cos\theta}} \right] \delta I_{\lambda\theta o//} \qquad \text{D40}$$

$$\delta i_{\lambda\theta Y\perp} = P_\perp \left[e^{-\frac{K_\lambda Y}{\cos\theta}} + \rho_\perp e^{-\frac{K_\lambda (2L-Y)}{\cos\theta}} \right] \delta i_{\lambda\theta L\perp} \qquad \text{D41}$$

$$\delta i_{\lambda\theta Y//} = P_{//} \left[e^{-\frac{K_\lambda Y}{\cos\theta}} + \rho_{//} e^{-\frac{K_\lambda (2L-Y)}{\cos\theta}} \right] \delta i_{\lambda\theta L//} \qquad \text{D42}$$

The net monochromatic intensity at y due to the reflections of the energy emitted at Y is :

$$\delta I^*_{\lambda\theta Y} = \delta I_{\lambda\theta Y\perp} + \delta I_{\lambda\theta Y//} + \delta i_{\lambda\theta Y\perp} + \delta i_{\lambda\theta Y//} \qquad \text{D43}$$

The amount of this radiation absorbed in a slice of thickness Y located at y is given by:

$$\delta W_{\lambda Y} = 2\pi \int_0^{\pi/2} K_\lambda \, \delta I^*_{\lambda\theta Y} \, \frac{\Delta Y}{\cos\theta} \, \sin\theta \, d\theta \qquad \text{D44}$$

The above equation was used to calculate the monochromatic radiative heat flux to an element at y due to multiple internal reflections of the energy emitted at Y. This equation was then integrated over all wavelengths in the same manner as equation D27.

D6 CONDUCTION HEAT TRANSFER

(a) Within the Fluid

DIAGRAM:

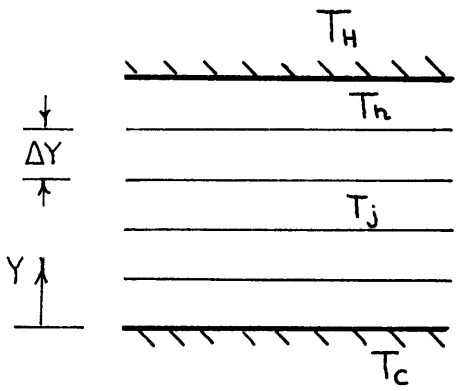

Consider the configuration shown in the above diagram. The fluid has been divided up into small volumes of thickness. By considering the temperature at the center of each volume, the following one-dimensional central difference equation can be written for the conduction equation:

$$q_{net} = \frac{K_T}{\Delta Y^2}\left(T_{j+1} + T_{j-1} - 2T_j\right) \qquad D45$$

The above equation was used to calculate the net heat flow into a given volume.

(b) Conduction at the Wall

DIAGRAM:

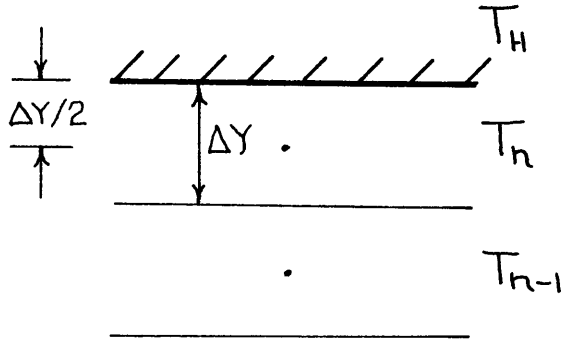

Consider the configuration shown above. The wall is transferring heat to the fluid by conduction. The central difference technique is applied to the node nearest the wall. The resulting equation is:

$$q_{net} = \frac{K_T}{\Delta Y^2}\left(4T_w + 2T_{n-1} - 6T_n\right) \qquad D45$$

The above equation was used to calculate the net heat flux into a given volume, adjacent to the wall.

D7 NET RADIATIVE FLUX

The net radiative flux was calculated by performing a radiative flux balance on a layer next to the lower wall. The contributions from the upper wall, lower wall, and other fluid elements were summed to get the net radiative flux at that level. Both direct flux and multiple internal reflections were considered in the calculation.

APPENDIX E: TEMPERATURE DISTURBANCE CAUSED BY SAPPHIRE WINDOWS

The sapphire windows in the ends of the platinum tray will cause a distortion of the temperature profiles within the molten glass, due to the heat radiated through the windows to the surroundings. In this section simple calculations are made to bound the magnitude of the temperature distortion caused by the windows.

The radiative transfer cannot be accurately modelled as optically thick or optically thin due to the non-gray absorption properties of glass. For the temperature levels and characteristic lengths in this project most of the radiation occurs at intermediate values of the optical thickness.

An upper bound on the effect of the window can be obtained by considering the glass as optically thin, and neglecting conduction effects. A heat balance on a infinitesimal spherical volume gives:

$$\delta\omega\,\sigma T_o^4 + \left(1 - \delta\omega\right)\sigma T_w^4 = \sigma T_y^4 \qquad \text{E1}$$

$\delta\omega$ - solid angle from volume to window(s)

T_o - temperature outside of window

T_w - temperature of platinum walls

T_y - temperature of volume

σ - Stefan - Boltzman constant

The results of the above calculations are shown in Figure E1. The optically thin solution indicates that the effect of the windows decreases quickly as the distance from the window increases. This model gives an upper bound on the effects of the window as it neglects molecular conduction and absorption and emission within the glass.

A lower bound on the effect of the windows was obtained by using the modified Rosseland equation for optically thick radiation.

$$q_R = \left(K + \frac{4\sigma T^3}{3K_R}\right)\frac{dT}{dY} = K_{eff}\frac{dT}{dY} \qquad E2$$

$$\frac{1}{K_R} = \int_0^\infty \frac{1}{K_\lambda}\frac{de_{b\lambda}}{de_b}\,d\lambda \qquad E3$$

k - thermal conductivity

q_R - radiative heat flux

σ - Stefan Boltzman constant

T - absolute temperature

y - distance coordinate

k_{eff} - effective thermal conductivity

The optically thick radiation model is a diffusion process and a two dimensional conduction heat transfer solution was applied, using the effective thermal conductivity rather than the usual thermal conductivity. The effective conductivity was evaluated at the mean temperature of the glass and held constant.

The following two-dimensional conduction model [64] was used

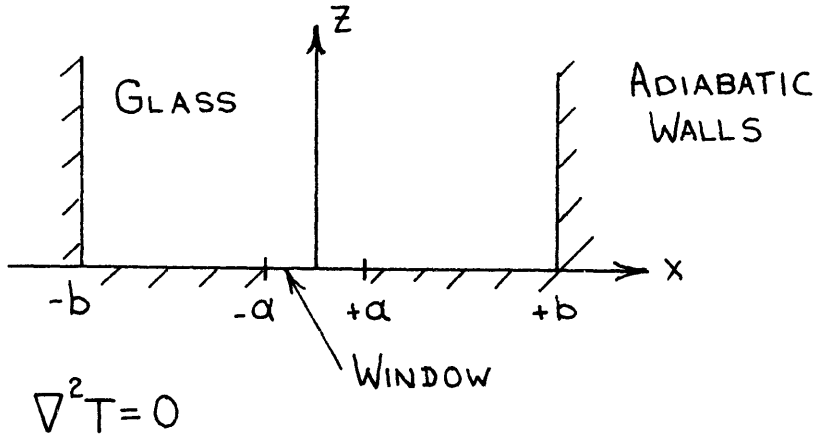

Boundary Conditions :

$$-K_{eff}\frac{\partial T}{\partial z} = \frac{Q}{2a} \qquad \text{at } z=0,\ -a<x<a$$

$$-K_{eff}\frac{\partial T}{\partial z} = 0 \qquad \text{at } z=0,\ a<x<-a$$

$$-K_{eff}\frac{\partial T}{\partial z} = \frac{Q}{2b} \qquad z \rightarrow \infty$$

$$-K_{eff}\frac{\partial T}{\partial z} = 0 \qquad x = \pm b$$

Mikic [41] gives the following solution for the above equation and boundary conditions:

$$\Delta T = \frac{Q\,b}{K_{eff}\,a\,\pi^2}\sum_{n=1}^{\infty}\frac{1}{n^2}\exp\left(\frac{-n\pi z}{b}\right)\sin\left(\frac{n\pi a}{b}\right)\cos\left(\frac{n\pi x}{b}\right) \qquad \text{E4}$$

For x = 0, along the centerline of the window,

$$\Delta T = \frac{Q\,b}{\pi^2 K_{eff} a}\sum_{n=1}^{\infty}\frac{\sin\left(n\pi a/b\right)}{n^2\exp\left(-n\pi z/b\right)} \qquad \text{E5}$$

Q - total heat loss from outside of window

- $\epsilon\sigma A T^4$

ϵ - hemispherical emissivity of sapphire-air interface = .96

ΔT - temperature disturbance caused by the window

A - area of window

σ - Stefan-Boltzman constant

The calculations were done for a window temperature of 2560^{o}R a window width of .25 inches and a platinum tray 9 inches square. The results for the optically thick solution are shown in Figure E2. The results are pessimistic as a solid angle of 4π was used to calculate the heat losses from the outside of the sapphire window.

Figure E-2 indicates that the upper bound would cause a temperature disturbance which would affect the experimental results strongly. The temperature disturbance indicated by the lower bound would have a small effect on the experimental results.

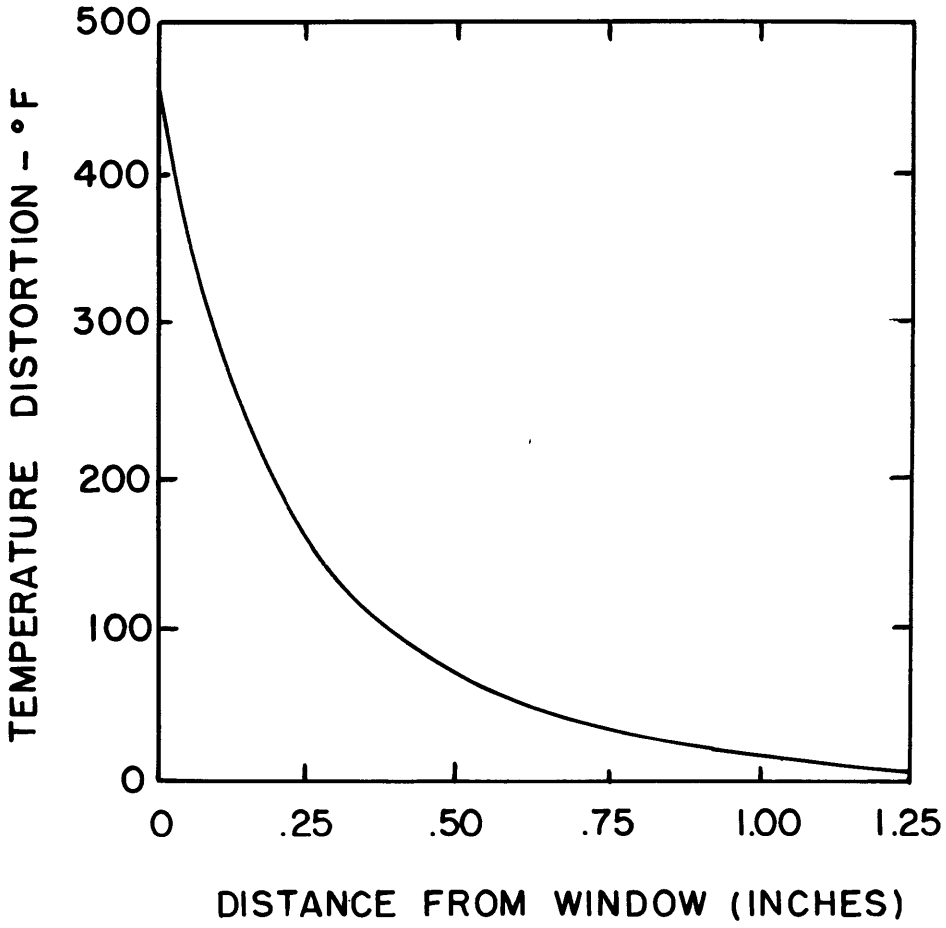

FIGURE E1 TEMPERATURE DISTURBANCE FOR OPTICALLY THIN SOLUTION

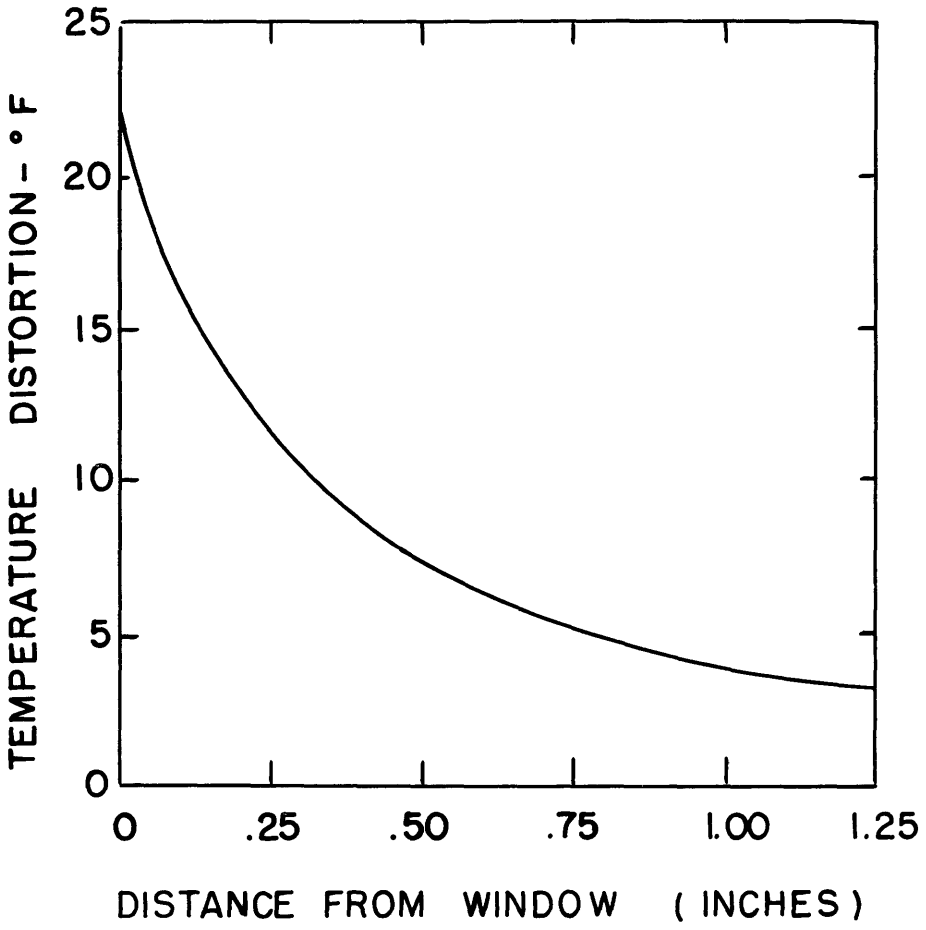

FIGURE E2 TEMPERATURE DISTURBANCE FOR OPTICALLY THICK SOLUTION

APPENDIX F - COMPUTER PROGRAM DOCUMENTATION

F1 DIFFUSE PROGRAM DOCUMENTATION

This appendix contains a description of the computer programs used to perform the numerical computations. Program listings, flow charts, data card descriptions and symbol explanations are included. The programs were run on an IBM 360 Model 65 at the MIT Computation Center, using FORTRAN IV, level G.

MAIN PROGRAM NOMEMCLATURE

AK(I) - monochromatic absorption coefficient (ft^{-1})
- (I) denotes wavelength band

WV(I) - minimum wavelength in band I - (microns)

TK - thermal conductivity (Btu/hr $ft^{o}F$)

T1, T2 - temperature of boundaries (^{o}Rankine)

E1(I) - monochromatic emissivity of boundary 1

E2(I) - monochromatic emissivity of boundary 2

BL - spacing between plates (ft)

RI - real part of the refractive index

B1(I) - dimensionless radiosity of wall 1

B2(I) - dimensionless radiosity of wall 2

NL - number of spatial divisions between the plates

NO - number of wavelength bands used

T(I) - local temperature (degrees Rankine)

TT(J) - dimensionless local temperature (T(J)/T1)

SIG - Stefan-Boltzman constant

H - thickness of spatial increments (ft)

TO - optical distance between plates

HY - optical thickness of spatial increment

EB(A,B) - emissive power of a black body at T_1, occurring between $A = n_1 \lambda_1 T_1$ and $B = n_2 \lambda_2 T_1$. This was calculated by a separate subroutine.

MAIN DIFFUSE PROGRAM

This program solves for the temperature profile and heat flux across a one-dimensional glass slab which is contained between two diffuse boundaries.

The program iterates on equations 2.34 and 2.35 until the convergence criterion given by 2.36 is satisfied. The preceding flow chart outlines the basic steps used and also indicates the required subroutines EB, EX, and WA.

PROGRAM INPUT

TK - thermal conductivity (Btu/hr ft^{o}F)

T1 - temperature of boundary 1 (^{o}R)

T2 - temperature of boundary 2 (^{o}R)

BL - spacing between boundaries (ft)

RI - refractive index

T(J) - initial guess at temperature profile (^{o}R)

WV(I) - wavelength bands (microns)

AK(I) - monochromatic absorption coefficient of glass (ft^{-1})

E1(I) - monochromatic emissivity of boundary 1

E2(I) - monochromatic emissivity of boundary 2

NL - number of layers between plates

NO - number of wavelength bands used

DATA CARDS FOR DIFFUSE PROGRAM

a) First Card: (Format 8 F 10.0)

The parameters appearing on the first card are:
thermal conductivity (Btu/hrft ^{o}F), hot wall temperature (^{o}Rankine), cold water temperature (^{o}Rankine), cold wall emissivity, hot wall emissivity, plate separation (ft), index of refraction and the number of spatial increments.
NOTE: If both wall emissivities equal unity the program calculates assuming black boundaries.

b) Second Card: (Format 1F 10.0, 2 I 2)

The parameters appearing on the second card are:
tolerance on the relative error in an iteration; maximum number of iterations, and the number of initial iterations that are averaged to avoid oscillations.
NOTE: Typical value of tolerance = .0001

c) Third Card: (Format 10 F 8.0)

This card contains the initial temperatures used to start the iteration. The number of temperatures is one less than the number of increments.

d) Fourth Card: (Format 8 F 10.0)

This card contains the cutoff wavelengths (in microns) for the band calculations. The number of wavelengths is equal to the number of bands plus one.

e) Fifth Card: (Format 10 F 8.0)

This card contains the absorption coefficient (ft^{-1}) for each band considered. The values must be greater than zero.

f) Sixth Card: (Format 10 F 8.0)

This card contains the monochromatic hemispherical emissivity of the hot wall for each band considered.

g) Seventh Card: (Format 10 F 8.0)

This card contains the monochromatic hemispherical emissivity of the cold wall for each band considered.

h) Cards 8 - 93: (Format 2 F 10.0)

These cards contain tabulated values of the black body emissive power distribution, and must be read in each time.

FUNCTION EB(A,B) this function subroutine calculates the percent of black body energy occurring between $A = n_1 \lambda_1 T_1$ and $B = n_2 \lambda_2 T_1$ The value is found by interpolation in a table of values which was read into the computer.

FUNCTION EX(N,T) - This subroutine calculates the value of the N^{th} exponential integral with an argument of T:

$$E_N(T) = \int_0^1 \mu^{N-2} e^{-\frac{T}{\mu}} d\mu$$

The value of $E_N(T)$ was calculated by two polynomials with the following errors:

$$0 \leq x \leq 1 \qquad \epsilon(x) < 2 \times 10^{-7}$$

$$1 \leq x \leq \infty \qquad \epsilon(x) < 5 \times 10^{-5}$$

SUBROUTING WA(E1, E2, RI, T1, T2, AK, WV, B1, B2, N0, N00, TT, H, BL)

This subroutine was used to calculate the dimensionless wall radiosities defined by equations 2.26 and 2.27. The radiosities were calculated for each wavelength band and for each iteration.

F2 SPECULAR PROGRAM DOCUMENTATION

PROGRAM FRESNEL

This program calculates the reflection coefficients for parallel and perpendicular polarized rays striking a platinum surface bounded by glass. The coefficients are calculated as a function of angle and wavelength.

PROGRAM INPUT

ANG(I) - angles at which the reflection coefficients are to be evaluated

RIM(I) - refractive index of platinum

RID(I) - refractive index of glass

EX(I) - extinction coefficient of platinum

The reflection coefficients were punched on cards to be used for inupt to another program.

SUBROUTINE SPEC

This program generates the exchange matrix terms defined in Appendix C. The output consists of one two dimensional matrix and one three dimensional matrix. The two dimensional matrix is used for heat transfer from the boundary to a layer, for each wavelength band. The three dimensional matrix is for heat transfer between fluid layers, for each wavelength band.

PROGRAM INPUT

ANA - number of angular increments used for Gaussian quadrature

ANW - number of wavelength bands

ALA - distance between boundaries

ANI - number of layers

ANG(I) - angles used for Gaussian quadrature

WT(I) - weighing factors for Gaussian quadrature

AK(I) - absorption coefficients for layers

RS(I, J) - Fresnel reflection coefficient for a beam of perpendicular polarization in wavelength band I, for angle J

RP(I, J) - Fresnel reflection coefficient for a beam of parallel polarization in wavelength band I, for angle J.

AH2(I,K) - Matrix for boundary to layer K exchange in wavelength band I

QQ(K, L, I) - Matrix for layer K to layer L exchange in wavelength band I

DATA CARDS FOR FRESNEL PROGRAM

a) First Card: (Format 2 F 10.0)

The parameters appearing on the first card are:
the number of wavelength bands and the number of angles at which the Fresnel reflection coefficients are to be calculated.

b) Second Card: (Format 8 F 10.0)

This card contains the angles (in radians) at which the Fresnel reflection coefficients are to be evaluated.

c) Third Card: (Format 3 F 10.0)

The parameters appearing on this card are the real component of the refractive index of the metal, the extinction coefficient of the metal, and the refractive index of the dielectric.

MAIN SPECULAR PROGRAM

This program solves for the temperature profile and heat flux across a one dimensional glass slab which is contained between two parallel specularly reflecting boundaries. The matrix equations 2.38 and 2.39 were solved according to the iterative method outlined in Section 2.6.1. Figure F2 shows a flow chart for the program indicating that two smaller programs (FRESNEL and SUBROUTINE SPEC) are used to input data to the main program.

PROGRAM INPUT

AINI - number of increments of angle

AIMAX - maximum number of iterations

TOL - convergence criterion

TR(J) - local temperature (^{O}R)

WV(I) - wavelength of band (MICRONS)

AK(I) - absorption coefficient (ft^{-1})

TH - hot wall temperature (^{O}R)

TC - cold wall temperature (^{O}R)

CON - thermal conductivity (Btu/hr ft^{O}F)

AN - index of refraction

AL - plate separation (ft)

ANO - number of layers between the boundaries

R1 - reflectivity of wall 1

R2 - reflectivity of wall 2

DY - slab thickness

DATA CARDS FOR SPECULAR PROGRAM

a) Initial Cards: (Format 3 F 10.0)

These cards, which are always read in first, contain tables of the black body emissive power as a function of wavelength.

b) First Card: (Format 8 F 10.0)

The following parameters appear on this card: number of spatial increments, thermal conductivity (Btu/hr^{O}Fft), plate separation (ft), refractive index, hot wall temperature (^{O}Rankine), cold wall temperature (^{O}Rankine), hot wall reflectivity, and cold wall reflectivity. When the last two parameters are zero the calculations are performed for black walls.

c) Second Card: (Format 8 F 10.0)

This card contains the number of angles used for numerical integration over angle, the number of wavelength bands considered, the maximum number of iterations, and the number of different data sets to be run.

d) Third Card: (Format 10 F 8.0)

This card contains the initial temperatures (^{O}Rankine) used to start

the iteration. One temperature is required for each slab.

e) Fourth Card: (Format 10 F 8.0)

This card contains the wavelengths (microns) defining each wavelength band. The number of wavelengths is equal to the number of bands plus one.

f) Fifth Card: (Format 10 F 8.0)

This card contains the spectral absorption coefficient (ft^{-1}) used in each band. The values must be greater than zero.

NOTE: The next three cards are used only if the last two fields on the first card are greater than zero, indicating that the boundaries are specular, not black.

g) Sixth Card: (Format 8 F 10.0)

This card contains the individual angles (in radians) for numerical integration over angles.

h) Seventh Card: (Format 8 F 10.0)

This card contains the Gaussian quadrature weighing coefficients for each individual angle on card six.

i) Eigth Card: (Format 4 F 10.0)

The Fresnel reflection coefficients for each individual angle on card six are contained on this card.

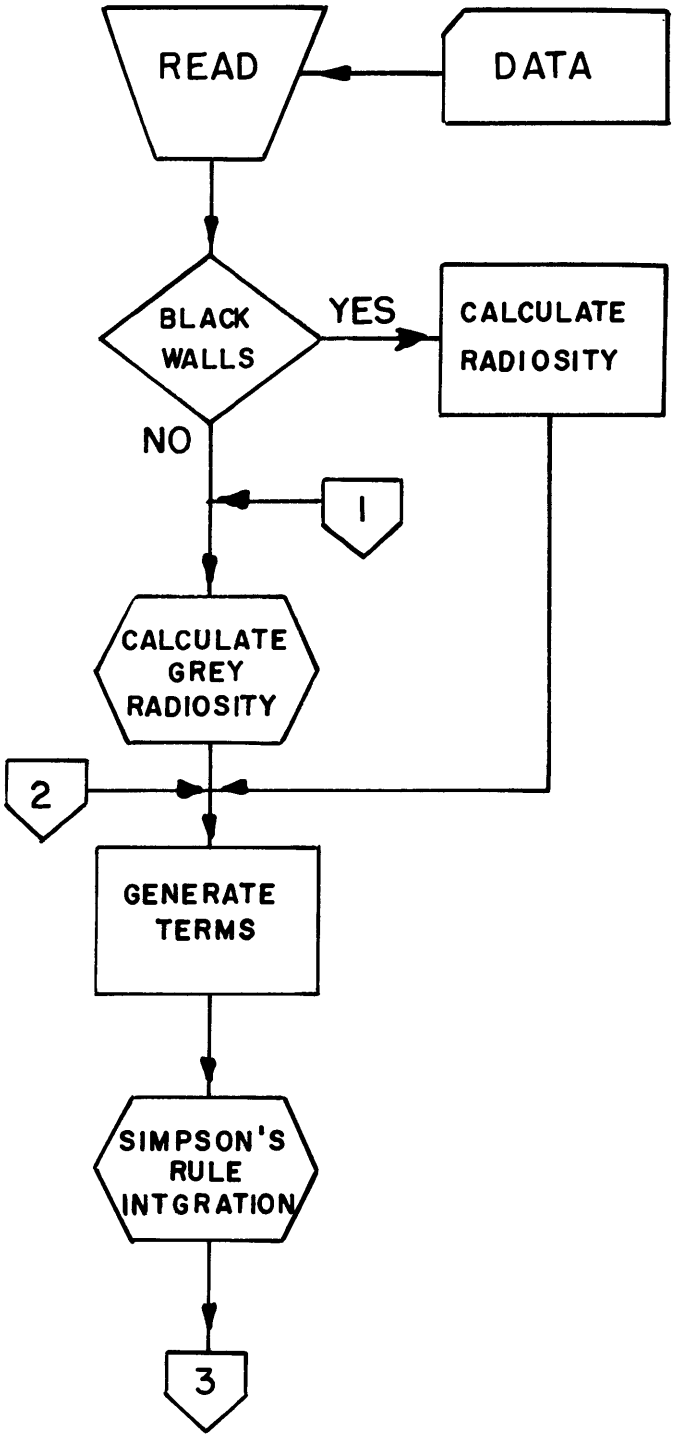

FIGURE F1 FLOW CHART FOR DIFFUSE SURFACE PROGRAM

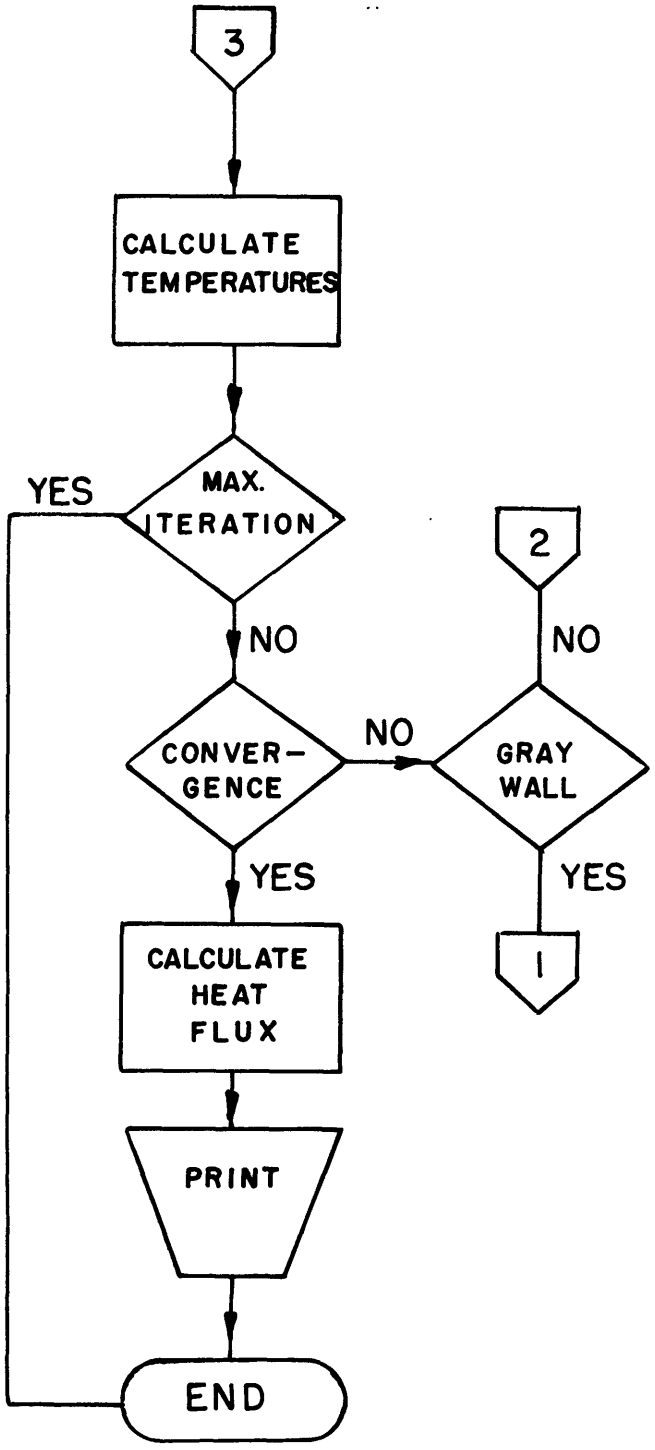

FIGURE F1 FLOW CHART - continued

PAGE 1

```
      FUNCTION EX(N,T)
C     THIS SUBROUTINE CALCULATES THE EXPONENTIAL INTEGRALS
C     OF ORDER 2,3,4 FROM A SERIES
C     EX=0. FOR ARGUMENTS  5.0
      A1=2.334733
      A2=0.250621
      B1=3.330657
      B2=1.681534
      AA0=-.57721566
       AA1=.99999193
      AA2=-.24991055
      AA3=.05519968
      AA4=-.00976004
      AA5=.00107857
      IF(T.NE.0.)GO TO 97
      EX=1./(N-1)
      GO TO 99
   97 CONTINUE
      IF(T-50.)13,14,14
   14 EX=0.
      GO TO 99
   13 IF(T.LE.1.)GO TO 12
      AA=T**2+A1*T+A2
      AB=T**2+B1*T+B2
      E1=AA/(AB*T*EXP(T))
       GO TO 27
   12 E1=-ALOG(T)+AA0+AA1*T+AA2*T**2+AA3*T**3+AA4*T**4
     1 +AA5*T**5
   27 GO TO (20,21,22,23),N
   20 EX=E1
      GO TO 99
   21 EX= -T*E1+1./EXP(T)
      GO TO 99
   22 EX=.5*((T**2)*E1+(1-T)/EXP(T))
      GO TO 99
   23 EX=(1./6.)*(-(T**3)*E1 +(2.-T+T**2)/EXP(T))
   99 CONTINUE
      RETURN
      END
```

PAGE 1

```
      FUNCTION EB(A,B)
C     THIS SUBROUTINE CALCULATES THE ( OF B.B. RADIATION
C     IN A WAVELENGTH BAND BY INTERPOLATION IN A TABLE
C     B GREATER THAN A
      COMMON TNL(93),EBLL(93),AR1(10,50),AR2(10,50)
      COMMON AR3(10,50),R1,R2
      COMMON TO1,TO2,I,G,T,GMU
      DIMENSION G(50,50),T(50,50),GMU(50)
      DIMENSION EA(2)
      R=1.0E+5
      AKY=A
      DO 11 I=1,2
      IF(1000.-AKY)31,30,30
   30 EA(I)=0.
      GO TO 11
   31 IF(R-AKY) 7,22,8
    7 EA(I)=1.
      GO TO 11
   22 EA(I)=.9992
      GO TO 11
    8 DO 1 J=1,93
      IF(TNL(J)-AKY)1,2,3
    2 EA(I)=EBLL(J)
      GO TO 11
    3 EA(I)=EBLL(J-1)+((EBLL(J)-EBLL(J-1))
     1 *(AKY-TNL(J-1))/(TNL(J)-TNL(J-1)))
      GO TO 11
    1 CONTINUE
   11 AKY=B
      EB=ABS(EA(2)-EA(1))
      RETURN
      END
```

```
PAGE   1

      SUBROUTINE WA(E1,E2,RI,T1,T2,AK,WV,B1,B2,NO,NOO,TT,H,BL)
      DIMENSION AT(51),TH(51),AK(10),WV(10),TV1(51),TV2(51)
      DIMENSION ZX(51),ZZ(51),B1B(10),B2B(10)
      DIMENSION B1(10),B2(10),TT(51),E1(10),E2(10)
C     CALCULATES DIMENSIONLESS WALL RADIOSITY
      DO1 J=1,NOO
    1 AT(J+1)=TT(J)*T1
      AT(1)=T1
      NDIM=NOO+2
      AT(NDIM)=T2
      DO 2 J=1,NOO
    2 TH(J+1)=TT(J)
      TH(1)=1.
      TH(NDIM)=T2/T1
      DO 30 I=1,NO
      TO=BL*AK(I)
      DO 20 J=1,NDIM
      TF=AK(I)*H*(J-1)
      A=RI*WV(I)*AT(J)
      B=RI*WV(I+1)*AT(J)
      TV1(J)=EX(2,TF)*(TH(J)**4)*EB(A,B)*RI**2
      TB=TO-TF
   20 TV2(J)=EX(2,TB)*(TH(J)**4)*EB(A,B)*RI**2
      HY=AK(I)*H
      CALL QSF(HY,TV1,ZX,NDIM)
      B1B(I)=ZX(NDIM)
      CALLQSF(HY,TV2,ZZ,NDIM)
      B2B(I)=ZZ(NDIM)
      AB=-(1.-E2(I))/(2.*(1.-E1(I))*(1.-E2(I))*(EX(3,TO))**2
     1  -.5)
      C=RI*WV(I)*T1
      D=RI*WV(I+1)*T1
      E=RI*WV(I)*T2
      F=RI*WV(I+1)*T2
      D1=EB(C,D)
      D1=EB(C,D)*RI**2
      D2=EB(E,F)*RI**2
      B2(I)=AB*(E1(I)*D1*EX(3,TO)+(E2(I)*D2*(T2/T1)**4)
     1 /(2.*(1.-E2(I)))+2.*(1.-E1(I))*B1B(I)*EX(3,TO)+B2B(I))
   30 B1(I)=E1(I)*D1+2.*(1.-E1(I))*(B2(I)*EX(3,TO)+B1B(I))
      RETURN
      END
```

```
PAGE   1

C      PROGRAM INPUT
C      AK(I),I=1,5   ABSORPTION COEFFICIENT OF BAND I
C      WV(I) ,I=1,6   CUT OFF WAVELENGTHS
C      TK  THERMAL CONDUCTIVITY
C      T1,T2   TEMPERATURE OF BOUNDARIES
C      EP1,EP2   EMISSIVITY OF BOUNDARIES (DIFFUSE,GRAY)
C      BL   SPACING BETWEEN PARALLEL BOUNDARIES
C      RI   REFRACTIVE INDEX(REAL)
C      B1(I)   DIMENSIONLESS RADIOSITY AT BOUNDARY 1
C      B2(I)   DIMENSIONLESS RADIOSITY AT BOUNDARY 2
C      NL  NUMBER OF SLABS BETWEEN PLATES
C      NO-- NUMBER OF WAVELENGTH BANDS
C      CN--RAD./COND. PARAMETER
C      T1-- HOT WALL TEMPERATURE
C      T(J)--DENOTES ABSOLUTE TEMPERATURES
C      NOO=NO. OF SPATIAL INTEGRALS
C      SIG   STEFAN BOLTZMAN RADIATION CONSTANT
C
       DIMENSION AK(10),WV(10),G(10,51),B1(10),B2(10)
       DIMENSION T(51),TT(51)
       DIMENSION TV(51),BINT3(10,51),Z(51)
       DIMENSION BB(51),GI(51),E1(10),E2(10)
       COMMON TNL(93),EBLL(93)
   101 FORMAT(8F10.0)
   102 FORMAT(10X,20HSTILL GOING ON ITER I3)
   103 FORMAT(2(5X,F10.6))
   104 FORMAT(10F8.0)
   105 FORMAT(1F10.4)
   106 FORMAT(2F10.0)
   107 FORMAT(10F10.5//)
   108 FORMAT(5X,14HEND OF PROGRAM)
   109 FORMAT(10F8.3)
   110 FORMAT(8F10.4/)
   111 FORMAT(30X,10HINPUT DATA//)
   112 FORMAT(5X,2E14.6,4F10.3)
   113 FORMAT(20X,E14.6)
   114 FORMAT(30X,20HTEMPERATURE SOLUTION/ )
   115 FORMAT(5X,24HNET HEAT FLUX ACROSS GAP2XF8.0
      1 ,2X,10HBTU/HR FT2//)
   116 FORMAT(10F8.6)
   117 FORMAT(2I2)
   118 FORMAT(3X,7HCONDUCT,4X,2HT1,8X,2HT2,4X,
      1 10HEMISSIVITY,10HEMISSIVITY
      1   ,10HSPACING FT,1X,9HREF INDEX,1X,9HNO. STEPS//)
   119 FORMAT(5X,24HCON HEAT FLUX ACROSS GAP2XF8.0,2X,
      1 10HBTU/HR FT2//)
   120 FORMAT(5X,24HRAD HEAT FLUX ACROSS GAP2XF8.0,2X,
      1 10HBTU/HR FT2//)
   121 FORMAT(20X,25HINITIAL TEMPERATURE GUESS//)
```

```
PAGE   2

  122 FORMAT(20X,16HWAVELENGTH BANDS//)
  123 FORMAT(20X,23HABSORPTION COEFFICIENTS//)
  124 FORMAT(20X,20HWALL EMISSIVITY(1+2)//)
  125 FORMAT(5X,9HTOLERANCE,F10.8,12HCONV. FACTOR,F10.3,
     1 5HFIRST,F10.3/)
      IM=5
      IX=6
      IFA=0
      SIG=1.714E-9
      WRITE(IX,111)
      READ(IM,101)TK,T1,T2,EP1,EP2,BL,RI,SN
      READ(IM,101)TOLER,CONV,DEMO
      NL=IFIX(SN)
      NOO=NL-1
      WRITE(IX,118)
      WRITE(IX,110)TK,T1,T2,EP1,EP2,BL,RI,SN
      WRITE(IX,125)TOLER,CONV,DEMO
      READ(IM,104)(T(J),J=1,NOO)
      WRITE(IX,121)
      WRITE(IX,104)(T(J),J=1,NOO)
      READ(IM,104)(WV(I),I=1,10)
      WRITE(IX,122)
      WRITE(IX,107)(WV(I),I=1,10)
      READ(IM,104)(AK(I),I=1,10)
      READ(IM,104)(E1(I),I=1,10)
      READ(IM,104)(E2(I),I=1,10)
      WRITE(IX,124)
      WRITE(IX,107)(E1(I),I=1,10)
      WRITE(IX,107)(E2(I),I=1,10)
      READ(IM,117)ISTO,IFB
      WRITE(IX,123)
      WRITE(IX,107)(AK(I),I=1,10)
      READ(IM,106)(TNL(J),EBLL(J),J=1,93)
      CN=TK/(4.*SIG*T1**3)
      H=BL/NL
      IFL=1
      NDIM=NL+1
      DO 89 J=1,10
      IF(AK(J).NE.0)GO TO 89
      NO=J-1
      GO TO 88
   89 CONTINUE
   88 CONTINUE
      IF(EP1.EQ.1..AND.EP2.EQ.1.)IFL=4
      IF(IFL.NE.4)GO TO 85
C     RADIOSITY OF BLACK WALLS IS CALC. NEXT
      DO 91 I=1,NO
      A=RI*T1*WV(I)
      B=RI*T1*WV(I+1)
```

```
      B1(I)=EB(A,B)*RI**2
      C=RI*T2*WV(I)
      D=RI*T2*WV(I+1)
      B2(I)=EB(C,D)*(RI**2)*(T2/T1)**4
   91 CONTINUE
      WRITE(IX,103)(B1(I),B2(I),I=1,NO)
   85 DO 92 J=1,NOO
   92 TT(J)=T(J)/T1
   98 CONTINUE
C
C     MAIN ITERATION BEGINS
C
      DO 60 I=1,NO
      IF(I.GT.1.OR.IFL.EQ.4)GO TO 81
      CALL WA(E1,E2,RI,T1,T2,AK,WV,B1,B2,NO,NOO,TT,H,BL)
   81 CONTINUE
      TL=AK(I)*BL
      HY=H*AK(I)
      DO 60 J=1,NOO
      Y=J*H
      TA=AK(I)*Y
      TR=TA/TL
      TB=TL-TA
      G1=-EX(4,TA)+TR*EX(4,TL)+(1.-TR)/3.
      G2=(1.-TR)*EX(4,TL)-EX(4,TB)+TR/3.
      G(I,J)=(B1(I)*G1+B2(I)*G2)/(2.*CN*AK(I))
      GI(J)=1.+TR*(T2/T1-1)
      KK=J+1
      DO 80 K=1,NDIM
      Y=H*(K-1)
      TF=AK(I)*Y
      TIR=ABS(TA-TF)
      TBR=TL-TF
      ZG=T1
      IF(K.GT.1.AND.K.LT.NDIM)ZG=T(K-1)
      IF(K.EQ.NDIM)ZG=T2
      R=RI*ZG*WV(I)
      S=RI*ZG*WV(I+1)
      EE=EB(R,S)
   80 TV(K)=(-EX(3,TIR)+EX(3,TF)+TR*(EX(3,TBR)-
     1 EX(3,TF)))*EE$(ZG/T1)**4
      CALL QSF(HY,TV,Z,NDIM)
      BINT3(I,J)=Z(NDIM)
   60 CONTINUE
C
C     NOW TEMPS ARE CALC
C
      IFA=IFA+1
      DO 90 J=1,NOO
```

```
PAGE   4

      BB(J)=TT(J)
      AB=0.
      DO 20 I=1,NO
      TT(J)=AB+G(I,J)+(RI**2)*BINT3(I,J)/(2.*CN*AK(I))
   20 AB=TT(J)
      TT(J)=TT(J)+GI(J)
   90 CONTINUE
      WRITE(IX,102)IFA
      WRITE(IX,114)
      WRITE(IX,107)(TT(J),J=1,NOO)
      IF(IFA.GT.ISTO)GO TO 99
      DO 61 J=1,NOO
      ER=ABS((TT(J)-BB(J))/BB(J))
      IF(ER.GE.TOLER)GO TO  96
   61 CONTINUE
      GO TO 97
   96 IF(IFA.GT.IFB)GO TO 98
      COVV=CONV
      IF(IFA.EQ.1)COVV=DEMO*CONV
      DO 94 J=1,NOO
   94 TT(J)=BB(J)+(TT(J)-BB(J))/(2.*COVV)
      DO 93 J=1,NOO
   93 T(J)=TT(J)*T1
      GO TO 98
   99 CONTINUE
C
C     HEAT FLUX IS CALC NEXT
C
   97 QCON=TK*(T2-T1)/BL
      WRITE(IX,104)(T(J),J=1,NOO)
      WRITE(IX,119)QCON
      DO 65 J=1,NOO
 65   TT(J+1)=T(J)
      TT(1)=T1
      TT(NDIM)=T2
      DO 62 I=1,NO
      C=RI*T2*WV(I)
      D=RI*T2*WV(I+1)
      HY=H*AK(I)
      TO=BL*AK(I)
      QW1=(B1(I)*SIG*T1**4)*((1.-E2(I))*EX(3,TO)+EX(
     1 4, TO)/TO-1./(3.*TO))
      QW2=(B2(I)*SIG*T1**4)*(-EX(4,TO)/TO-.5+1./
     1 (3.*TO))+.5*E2(I)*SIG*(T2**4)*EB(C,D)*RI**2
      BB(I)=2.*(QW1+QW2)
      DO 63  J=1,NDIM
      Y=H*(J-1)
      TA=AK(I)*Y
      TB=TO-TA
```

```
PAGE    5

      R=RI*TT(J)*WV(I)
      S=RI*TT(J)*WV(I+1)
      EE=EB(R,S)
   63 TV(J)=((1.-E2(I))*EX(2,TB)+EX(3,TB)/TO-EX(3,TA)
     1 /TO)*(RI**2)*SIG*EE*TT(J)**4
     1EE*TT(J)**4
      CALL QSF(HY,TV,Z,NDIM)
   62 GI(I)=Z(NDIM)
C
C     RAD AND COND FLUXES SUMMED
C
      AB=0.
      DO 64 J=1,NO
      QR=AB+BB(J)+GI(J)*2
   64 AB=QR
      WRITE(IX,120)QR
      QTOT=QCON+QR
      WRITE(IX,115)QTOT
      WRITE(IX,108)
      CALL EXIT
      END
```

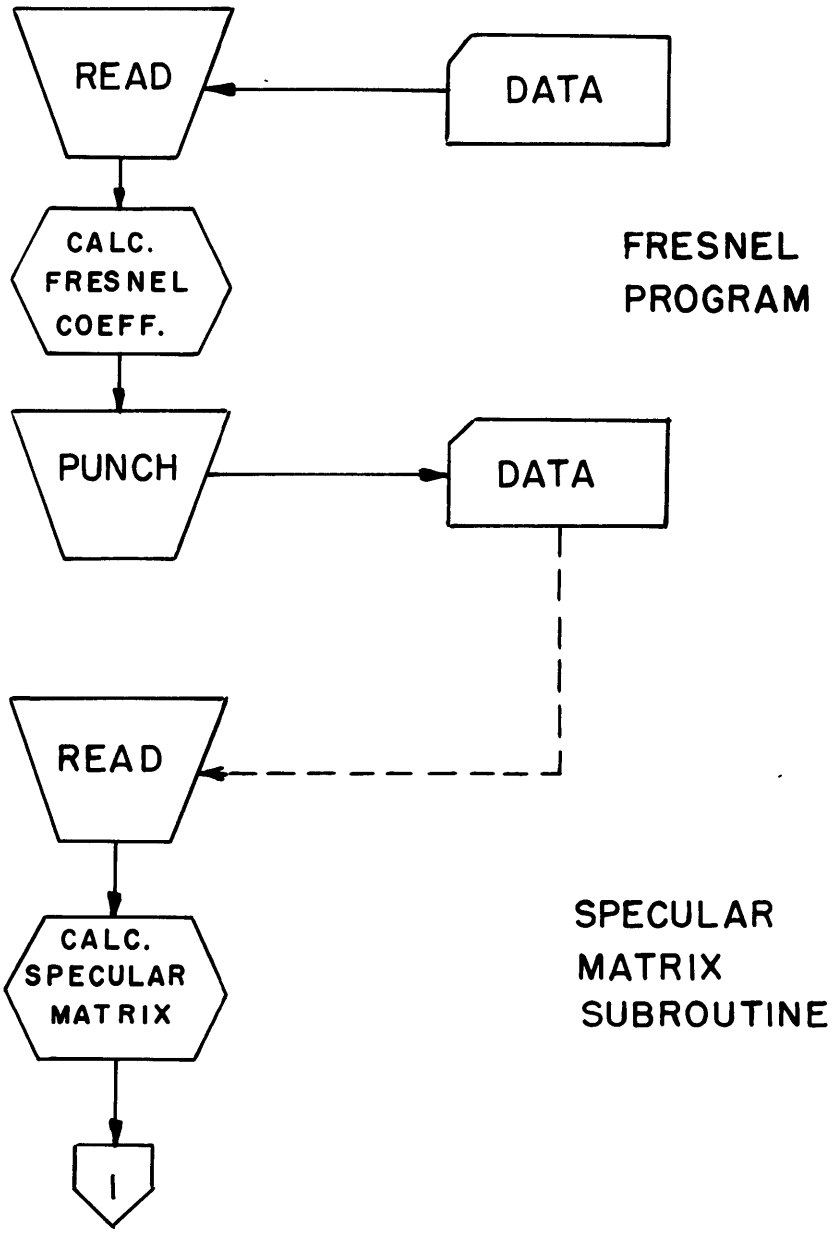

FIGURE F2 FLOW CHART FOR SPECULAR SURFACE PROGRAM

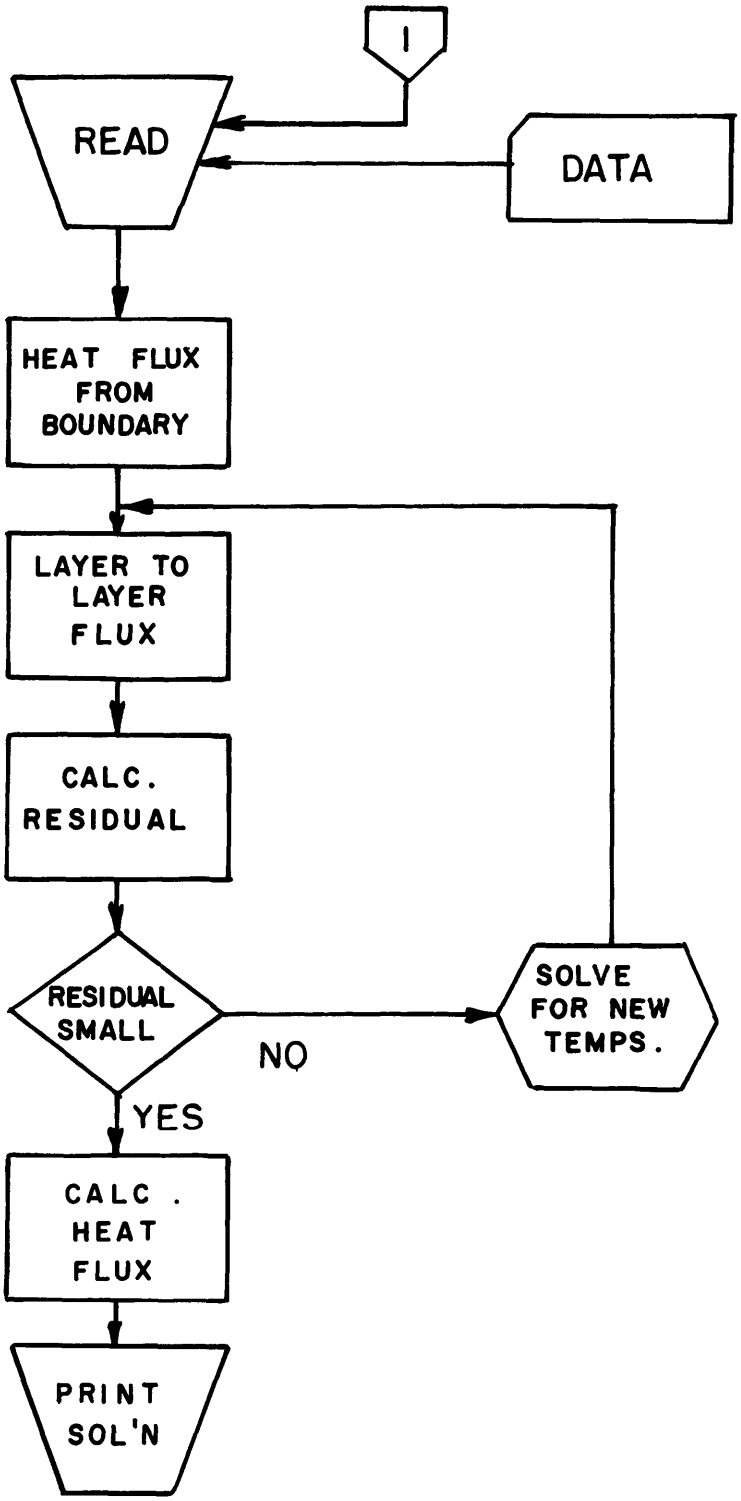

FIGURE F2 FLOW CHART - continued

PAGE 1

```
C       PROGRAM FOR FRESNEL CALC. OF PLATINUM-GLASS EMISSIVITY
C       REFRACTIVE INDEX OF PLATINUM
C       RID-REFRACTIVE INDEX OF GLASS
C       EX-EXTINCTION COEFF OF PLAT
C       J-DENOTES WAVELENGTH BAND NO.
C       J-DENOTES ANGLE
C       RP-PARALLEL POLAR.
C       RS-PERPENDICULAR POLAR.
        DIMENSION RIM(10),EX(10),RID(10),EP(10,20)
        DIMENSION RS(10,50),RP(10,50)
        DIMENSION ANG(20)
        COMPLEX AR,AS,ST,CT,TA,TZ,BR
  100 FORMAT(3F10.0)
  101 FORMAT(5X,17HOPTICAL CONSTANTS,5X,3F10.5//)
  102 FORMAT(1X,19F6.4)
  103 FORMAT(8F10.0)
  104 FORMAT(4F10.8)
      IM=5
      IX=6
      IL=7
      READ(IM,100)ANW,ANA
      NW=ANW
      NA=ANA
      READ(IM,103)(ANG(I),I=1,NA)
      READ(IM,100)((RIM(I),EX(I),RID(I)),I=1,NW)
      DO 1 I=1,NW
      DO 1 J=1,NA
      TH=(3.14159/2.)*(.5+ANG(J))
      CST=RID(I)*SIN(TH)/(RIM(I)**2+EX(I)**2)
      AR=(0.,1.)*CST*EX(I)
      AS=(1.,0.)*CST*RIM(I)
      ST=AR+AS
      BR=1.-ST**2
      CT=CSQRT(BR)
      TA=CT+(0.,1.)*ST
      TZ=(0.,-1)*CLOG(TA)
      ALP=TZ
      BD=CABS(TZ)**2-ALP**2
      BET=SQRT(BD)
      T1=TH-ALP
      T2=TH+ALP
      RS(I,J)=(SIN(T1)**2+SINH(BET)**2)/(SIN(T2)**2
     1 +SINH(BET)**2)
      F=(COS(T2)**2+SINH(BET)**2)/(COS(T1)**2+SINH(BET)**2)
      RP(I,J)=F*RS(I,J)
    1 CONTINUE
      DO 2 I=1,NW
      WRITE(IX,101)(RIM(I),EX(I),RID(I))
    2 WRITE(IX,104)((RS(I,J),RP(I,J)),J=1,NA)
```

PAGE 2

```
      WRITE(IL,104)(((RS(I,J),RP(I,J)),I=1,NW),J=1,NA)
      CALL EXIT
      END
```

```
PAGE   1

      SUBROUTINE SPEC(ANI,NW,ALA,NI,QQ,AK,ANG,WT,NA)
C     PROGRAM FOR SPECULAR MATRICES
C     NA- NO. OF ANGLES
C     NW- NO. OF WAVELENGTHS
C     NI- NO OF SPATIAL INCREMENTS
C     RS-PER--PERPENDICULAR POLAR.
C     RP,PAR--PARALLEL POLAR.
      COMMON TNL(93),EBLL(93),RS(10,50),AH2(10,50)
      COMMON RP(10,50),R1,R2
      COMMON TO1,TO2,II,S,T,GMU
      DIMENSION PAR(10,20),PER(10,20),AH1(10,20)
      DIMENSION QQ(50,50,10),A1(10,50,20),A2(10,50,20)
      DIMENSION ANG(20),WT(20),AK(10)
      DIMENSION GMU(50),S(50,50),T(50,50)
      NI=ANI
      API=3.14159
C     M.I.R. COEFF. CALC. NEXT
      DO 1 I=1,NW
      DO 1 J=1,NA
      TH=(API/2.)*(.5+ANG(J))
      A=-2.*AK(I)*ALA/COS(TH)
      IF(A.LT.-20.)A=-20.
      ER=EXP(A)
      PER(I,J)=RS(I,J)/(1.-(RS(I,J)**2)*ER)
    1 PAR(I,J)=RP(I,J)/(1.-(RP(I,J)**2)*ER)
C     RAD. FROM BDY. BY M.I.R. AND DIRECT
      DO 5 I=1,NW
      DO 5 K=1,NI
      T(K,I)=0.
      IF(K.NE.1)GO TO 8
      GMU(I)=0.
      S(1,I)=0.
    8 CONTINUE
      REA=K
      Y=(REA-.5)*ALA/ANI
      AC=0.
      DO 2 J=1,NA
      TH=(API/2.)*(.5+ANG(J))
      A=-AK(I)*(ALA-Y)/COS(TH)
      B=-AK(I)*(ALA+Y)/COS(TH)
      C=-AK(I)*Y/COS(TH)
      D=-AK(I)*ALA/COS(TH)
      IF(A.LT.-20.)A=-20.
      IF(B.LT.-20.)B=-20.
      IF(C.LT.-20.)C=-20.
      IF(D.LT.-20.)D=-20.
      A1(I,J,K)=(PER(I,J)*(EXP(A)+RS(I,J)*EXP(B))+PAR(I,J)
     1 *(EXP(A)+RP(I,J)*EXP(B)))*.5*EXP(D)
      IF(K.NE.1)GO TO 6
```

```
      DEM=(-1.+1./RS(I,J))*PER(I,J) +(-1.+1./RP(I,J))*PAR(I,J)
      DAM=(1.-RS(I,J))*PER(I,J)+(1.-RP(I,J))*PAR(I,J)
      GMU(I)=GMU(I)+.5*API*WT(J)*DEM*EXP(D)*SIN(TH)*COS(TH)
     1*(1.-.5*(RS(I,J)+RP(I,J)))**2
      S(1,I)=S(1,I)+GMU(I)*(1./(1.-.5*(RS(I,J)
     1+RP(I,J)))-DAM/DEM)*EXP(D)
    6 CONTINUE
      AMZ=(PER(I,J)*(1.+RS(I,J))+PAR(I,J)*(1.+RP(I,J)))
     1 *EXP(A+D)
      BMZ=(PER(I,J)*RS(I,J)+PAR(I,J)*RP(I,J))*EXP(B+D)
      T(K,I)=T(K,I)+.5*API*AK(I)*(ALA/ANI)*WT(J)
     1 *(AMZ+BMZ)*SIN(TH)*(1.-.5*(RS(I,J)+RP(I,J)))
      AI2=(A1(I,J,K)+EXP(C))*(1.-.5*(RP(I,J)+RS(I,J)))
     1          *SIN(TH)*WT(J)*AK(I)
      AH2(I,K)=AC+AI2*(API/2.)
    2 AC=AH2(I,K)
    5 CONTINUE
C     RAD. FROM OTHER ELEMENTS BY M.I.R.
      DO 3 I=1,NW
      DO 3 K=1,NI
      DO 3 L=1,NI
      DB=0.
      REA=L
      Y=(REA-.5)*ALA/ANI
      DO 4 J=1,NA
      TH=(API/2.)*(.5+ANG(J))
      A=-AK(I)*Y/COS(TH)
      IF(A.LT.-20.)A=-20.
      DD=DB+ (A1(I,J,K)*EXP( -A))
     1 *TAN(TH)*WT(J)*((AK(I)*ALA/ANI)**2)*API
    4 DB=DD
      IF(K.NE.L)GO TO 7
      BR=4.*ALA/ANI
      GO TO 9
    7 BR=2.*(ALA/ANI)**2
    9 CONTINUE
      QQ(K,L,I)=DD/BR
    3 CONTINUE
      RETURN
      END
```

```
PAGE   1

C      THIS PROGRAM CALCULATES HEAT FLUX AND
C      TEMPERATURE PROFILES FOR RADIATION AND CONDUCTION
C      BETWEEN TWO INFINITE PARALLEL PLATES SEPARATED
C      BY AN ABSORBING EMITTING MEDIUM
C      BOUNDARIES ARE SPECULAR REFLECTORS
C      TEMPERATURES ARE IN DEGREES RANKINE
C      LENGTHS ARE IN FEET
C      NO.- NO. OF SLABS BETWEEN PLATES
C      SIG-STEFAN-BOLTZMAN CONSTANT
C      CON-THERMAL CONDUCTIVITY
C      AN-INDEX OF REFRACTION
C      DY-SLAB THICKNESS
C      AK(I)-ABSORPTION COEFF.  FT.-1
C      INI-NO. OF INCR. IN ANGLE
C       NN- NO. OF WAVELENGTH INTERVALS
C      AL-PLATE SEPARATION
C      WV(I)-WAVELENGTH
       COMMON TNL(93),EBLL(93),AR1(10,50),AR2(10,50)
       COMMON AR3(10,50),R1,R2
       COMMON TO1,TO2,II,S,T,GMU
       DIMENSION A(50,50),B(50,50),C(50),TR(50)
       DIMENSION AK(10),R(50),E(50),RO(50)
       DIMENSION G(50,50),WV(10),VEC1(50),VEC2(50)
       DIMENSION VIN1(50),VIN2(50)
       DIMENSION Q(50),RES(50)
       DIMENSION T(50,50)
       DIMENSION GMU(50),S(50,50)
       DIMENSION QQ(50,50,10)
       DIMENSION ANG(20),WT(20)
       IM=5
       IX=6
  100  FORMAT(8F10.0)
  104  FORMAT(2F10.0)
  107  FORMAT(10F10.5//)
  108  FORMAT(5X,12HIFLAG EQ ONE,//)
  119  FORMAT(35X,24HINITIAL DATA FOR PROBLEM//)
  120  FORMAT(5X,20HTHERMAL CONDUCTIVITY,2X,F6.3,
     1 2X,12HBTU/HR-FT-F,//)
  121  FORMAT(5X,16HPLATE SEPARATION,2X,F6.3,2X,2HFT,//)
  122  FORMAT(5X,8HHOT WALL,2X,F8.1,2X,9HCOLD WALL,2X,F8.1,//)
  123  FORMAT(20X,23HABSORPTION COEFFICIENTS//)
  124  FORMAT(5X,15HCOLD WALL REFL,,2X,F6.4,2X,
     1 14HHOT WALL REFL,2X,F6.4//)
  126  FORMAT(5X,19HINDEX OF REFRACTION,2X,F4.2,//)
  127  FORMAT(4E14.8)
  150  FORMAT(10F8.0)
  199  FORMAT(4F10.0)
  200  FORMAT(2X,10(E10.3,1X)//)
  201  FORMAT(10X,11HRAD HT FLUX,1E14.7)
```

```
PAGE   2

  232 FORMAT(5X,23HCOEFFICIENT MATRIX FOR
     1 ,21HRADIATION FROM PLATES//)
  233 FORMAT(5X,26HINITIAL TEMPERATURE VECTOR//)
  240 FORMAT(5X,22HRESIDUAL VECTOR AFTER,2X,I4,
     1 2X,10HITERATIONS//)
  243 FORMAT(5X,22HNEW TEMPERATURE VECTOR//)
  800 FORMAT(2X,10F8.2,/)
      READ(IM,104)(TNL(J),EBLL(J),J=1,93)
      IBLA=0.
      DATU=0.
 1001 CONTINUE
      READ(IM,100)ANO,CON,AL,AN,TH,TC,R1,R2
      IF(R1.EQ.0..AND.R2.EQ.0.)IBLA=1
      NO=ANO
      READ(IM,100)AINI,ANN,AIMAX,DMAX
      NA=AINI
      NN=ANN
      READ(IM,150)(TR(J),J=1,NO)
      READ(IM,150)(WV(I),I=1,10)
      READ(IM,150)(AK(I),I=1,10)
      IF(IBLA.EQ.1)GO TO 1002
      READ(IM,100)(ANG(I),I=1,NA)
      READ(IM,100)(WT(I),I=1,NA)
      READ(IM,199)(((AR1(I,J),AR3(I,J)),I=1,NN),J=1,NA)
 1002 CONTINUE
      WRITE(IX,119)
      WRITE(IX,122)TH,TC
      WRITE(IX,120)CON
      WRITE(IX,121)AL
      WRITE(IX,126)AN
      WRITE(IX,123)
      WRITE(IX,107)(AK(I),I=1,10)
      WRITE(IX,107)(WV(I),I=1,10)
      WRITE(IX,124)R1,R2
      WRITE(IX,233)
      WRITE(IX,200)(TR(J),J=1,NO)
      DY=AL/ANO
      INI=AINI
      IMAX=AIMAX
      ITER=0
      API=3.1415927
      SIG=1.714E-9
      ERB=(AN**2)*SIG*TC**4
C
C     GENERATE COEFF. MTX OF LIN TEMP VECTOR
C
      DO 2 I=1,NO
      DO 2 J=1,NO
    2 A(I,J)=0.
```

```
PAGE   3

      INA=NO-1
      DO 3 J=2,INA
      A(J,J)=-2.*CON/DY
      A(J,J-1)=CON/DY
    3 A(J,J+1)=CON/DY
      A(1,1)=-6.*CON/DY
      A(1,2)=2.*CON/DY
      A(NO,INA)=2.*CON/DY
      A(NO,NO)=-6.*CON/DY
      IF(IBLA.EQ.1)GO TO 36
      CALL SPEC( ANO,NN,AL,NO,QQ,AK,ANG,WT,NA)
   36 CONTINUE
C
C     PRIMARY HEAT FLUX FROM BOUNDARIES
C
      DO 8 J=1,NO
      M=NO+1-J
      REA=J
      YH=(REA-.5)*DY
      YC=AL-YH
      CS=0.
      HS=0.
      DO 81 N=1,NN
      AA=AN*WV(N)*TC
      AB=AN*WV(N+1)*TC
      AC=AN*WV(N)*TH
      AD=AN*WV(N+1)*TH
      AZ=AK(N)*YH
      AX=AK(N)*YC
      IF(IBLA.EQ.1)GO TO 35
      CS=CS+AR2(N,M)*EB(AA,AB)
      HS=HS+AR2(N,J)*EB(AC,AD)
      GO TO 81
   35 CS=CS+AK(N)*EX(2,AX)*EB(AA,AB)
      HS=HS+AK(N)*EX(2,AZ)*EB(AC,AD)
   81 CONTINUE
      IF(J.NE.1)GO TO 8
      CT=CS
      HT=HS
    8 C(J)=2.*DY*SIG*(AN**2)*(CS*TC**4+HS*TH**4)
      WRITE(IX,232)
      WRITE(IX,200)(C(J),J=1,NO)
       DO 27 J=1,NO
   27 E(J)=SIG*(TR(J)**4)*AN**2
C
C     MAIN ITERATION
C
  203 CONTINUE
C
```

```
PAGE   4

C      DIAGONAL OF RAD. COEFF. MTX
C
       ITER=ITER+1
       DO 45 J=1,NO
       M=NO+1-J
       AZ=0.
       DO 5 N=1,NN
       D=AN*WV(N)*TR(J)
       F=AN*WV(N+1)*TR(J)
       AR=AK(N)*DY/2.
       IF(IBLA.EQ.1)GO TO 49
       AZ=AZ+(QQ(J,J,N)+QQ(M,M,N)-AK(N)*EX(2,AR))*EB(D,F)
       GO TO 5
   49  AZ=AZ-AK(N)*EX(2,AR)*EB(D,F)
    5  CONTINUE
   45  B(J,J)=4.*DY*AZ
C
C      OFF DIAG. TERMS IN RAD. COEFF. MTX
C
       DO 6 N=1,NO
       DO 6 J=1,NO
       M=NO+1-J
       L=NO+1-N
       ARB=0.
       IF(N.EQ.J)GO TO 6
       Y=IABS(N-J)*DY
       DO 46 K=1,NN
       D=AN*WV(K)*TR(J)
       F=AN*WV(K+1)*TR(J)
       APZ=AK(K)*Y
       IF(IBLA.EQ.1)GO TO 47
       ARB=ARB+(QQ(N,J,K)+QQ(L,M,K))*EB(D,F)
   47  ARB=ARB+(AK(K)**2)*EX(1,APZ)*EB(D,F)
   46  CONTINUE
       B(N,J)=2.*(DY**2)*ARB
    6  CONTINUE
C
C      RESIDUAL VECTOR CALC. NEXT
C
       DO 77 I=1,NO
       AB=0.
       DO 777 J=1,NO
  777  AB=AB+A(I,J)*TR(J)
   77  R(I)=AB
       R(1)=R(1)+4.*TH*CON/DY
       R(NO)=R(NO)+4.*TC*CON/DY
       DO 78 I=1,NO
       CA=0.
       DO 778 J=1,NO
```

```
  778 CA=CA+B(I,J)*E(J)
   78 RO(I)=CA
      DO 28 J=1,NO
   28 RES(J)=-(R(J)+RO(J)+C(J))
      WRITE(IX,240)ITER
      WRITE(IX,200)(RES(J),J=1,NO)
      DO 48 J=1,NO
      R11=ABS(RES(J))
      IF(R11.GT.50.)GO TO 998
   48 CONTINUE
      GO TO 999
  998 CONTINUE
C
C     SOLVE FOR TEMP. CORR. DLE(J)
C
      DO 79 I=1,NO
      DO 79 J=1,NO
   79 G(I,J)=B(I,J)+(TR(J)/(4.*E(J)))*A(I,J)
      CALL ARRAY(2,NO,NO,50,50,T,G)
      CALL SIMQ(T,RES,NO,KS)
      ZZ=1.
      DO 99 I=1,NO
      E(I)=E(I)+RES(I)/ZZ
      IF(E(I).LT.ERB)E(I)=ERB
   99 TR(I)=(E(I)/(SIG*(AN**2)))**.25
      WRITE(IX,243)
      WRITE(IX,800)(TR(J),J=1,NO)
      IF(ITER.GT.IMAX)GO TO 999
      GO TO 203
  999 CONTINUE
C     CONDUCTION HEAT FLUX IS CALC. NEXT
      DO 7 J=2,INA
    7 Q(J)=-CON*(-TR(J-1)+TR(J+1))/(2.*DY)
      Q(1)=-CON*(-TH+(TR(1)+TR(2))/2.)/DY
      Q(NO)= CON*((-TR(NO)+TR(INA))/2.+TC)/DY
      WRITE(IX,125)
  125 FORMAT(5X,21HLOCAL CONDUCTION FLUX//)
      WRITE(IX,200)(Q(J),J=1,NO)
      QCO1=CON*(9.*TR(NO)-8.*TC-TR(INA))/(3.*DY)
      QCO2=-CON*(9.*TR(1)-8.*TH-TR(2))/(3.*DY)
      WRITE(IX,200)QCO1,QCO2
      IF(IBLA.EQ.1)GO TO 996
C     RAD. HEAT FLUX CALC. BY HEAT BAL. ON LOWER
C     WALL ELEMENT
C     MEDIUM TO WALL EXCHANGE
      RAB=0.
      DO 10 I=1,NN
      DO 10 J=1,NO
      W=AN*WV(I)*TR(J)
```

```
PAGE   6

      X=AN*WV(I+1)*TR(J)
   10 RAB=RAB+T(J,I)*E(J)*EB(W,X)
C     TOP PLATE TO LOWER
C     LOWER TO MEDIUM
      CHS=0.
      CCS=0.
      DO 11 I=1,NN
      W=AN*WV(I)*TC
      X=AN*WV(I+1)*TC
      Y=AN*WV(I)*TH
      Z=AN*WV(I+1)*TH
      CCS=CCS+GMU(I)*EB(W,X)*SIG*(AN**2)*TC**4
   11 CHS=CHS+S(1,I)*EB(Y,Z)*SIG*(AN**2)*TH**4
      QRAD=RAB+CCS-CHS
      WRITE(IX,201)QRAD
      WRITE(IX,201)RAB
      WRITE(IX,201)CCS
      WRITE(IX,201)CHS
      GO TO 1000
C     CONDUCTION FLUX
  996 INA=NO-1
      QCON=CON*(9.*TR(NO)-8.*TC-TR(INA))/(3.*DY)
C     HEAT FROM HOT WALL
      BR=0.
      DO 995 I=1,NN
      D=AN*WV(I)*TH
      F=AN*WV(I+1)*TH
      ALB=AK(I)*AL
  995 BR=BR+EB(D,F)*EX(3,ALB)
      QHOT=2.*(AN**2)*SIG*(TH**4)*BR
C     EMISSION FROM WALL
      QCOLD=(AN**2)*SIG*TC**4
C     HEAT FROM FLUID
      QFL=0.
      DO 627 J=1,NO
      DO 627 I=1,NN
      RE=J
      Y=AL-(RE-.5)*DY
      AM=AK(I)*Y
      X=AN*WV(I)*TR(J)
      Z=AN*WV(I+1)*TR(J)
      QFL= QFL+E(J)*AK(I)*EX(2,AM)*EB(X,Z)*DY*2.
  627 CONTINUE
      QNET=QHOT-QCOLD+QFL
      WRITE(IX,201)QNET
      WRITE(IX,201)QCON
 1000 CONTINUE
      DATU=DATU+1.
      IF(DATU.LT.DMAX)GO TO 1001
```

PAGE 7

```
      CALL EXIT
      END
```

APPENDIX G - EXPERIMENTAL DATA

The tables on the following pages contain the raw experimental data for five calibration tests and four temperature profile tests.

A test thermocouple from the roll of platinum - platinum/10% rhodium thermocouple wire used for the tray thermocouples was tested against a calibrated thermocouple at the following temperature levels:

$2100^{o}F$ - add $3.5^{o}F$ to reading

$2300^{o}F$ - add $4.5^{o}F$ to reading

During the tests some of the thermocouples ceased to operate as the leads parted at the high temperature levels attained by the apparatus. The broken thermocouples are omitted from the tabular data.

Figure G1 shows the calibration curve for the variable polarizer in terms of attenuator setting versus reference signal voltage.

The distance from the laser beam to the bottom plate is given by adding .25 inches to the mirror position number in tables G2 and G3.

Tests C1, C2, C3, C4, and C5 refer to calibration tests while T1, T2, T3 and T4 refer to the data shown in Figures 24, 23, 22, and 21.

Thermocouple number 21 was located near the heating elements in order to monitor their temperature level.

The thermal conductivity of the Momofrax A ceramic was measured by the Dynatech Corporation with the following results:

Temperature	K_T - $(BTU/hr^{o}Fft^{2}/in)$
1470	44.6
1830	42.5
2020	41.5
2200	40.7

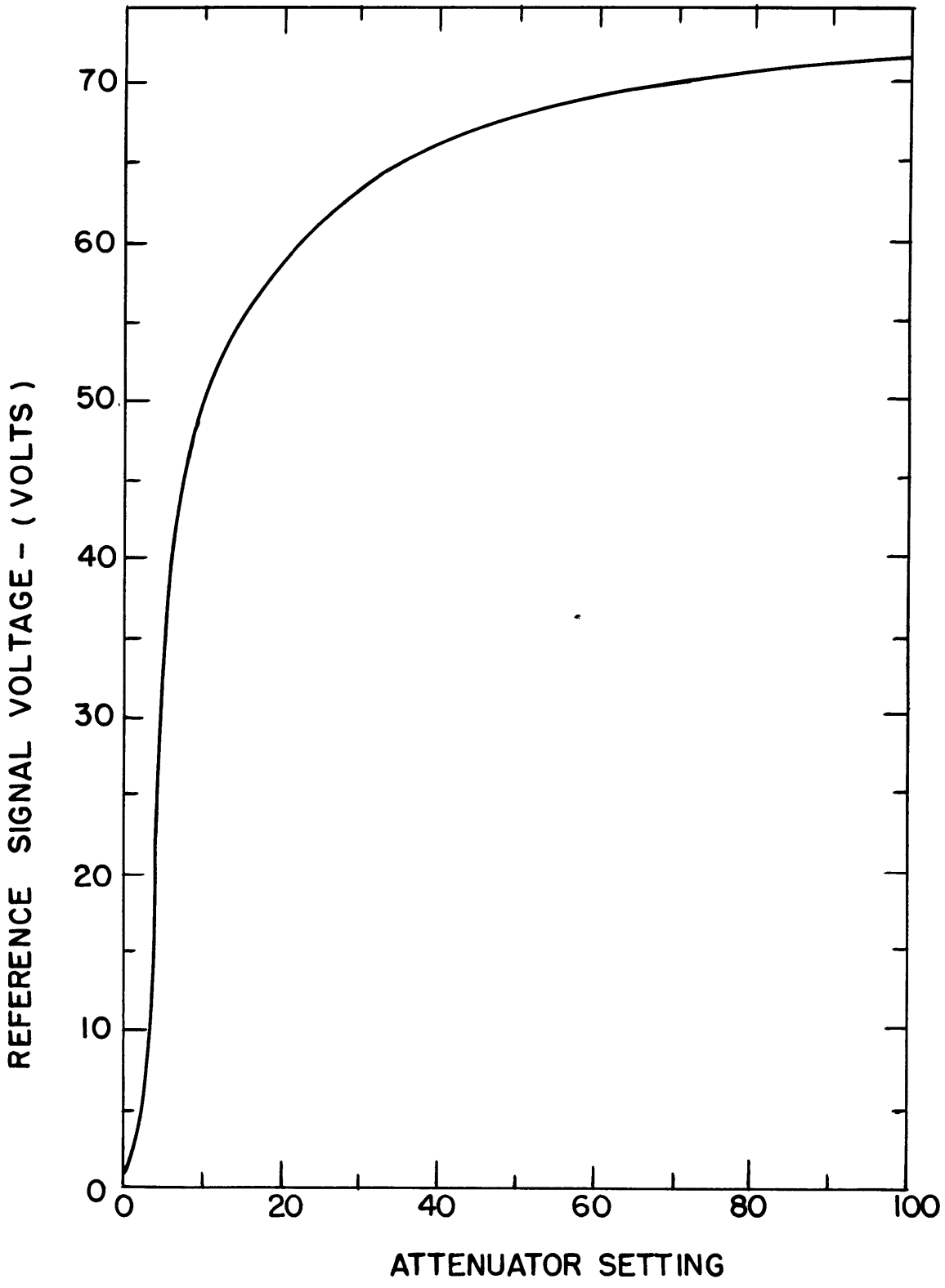

FIGURE G1 REFERENCE SIGNAL VOLTAGE versus ATTENUATOR SETTING

TEST NUMBER	THERMOCOUPLE NUMBER													
	1	2	3	4	6	8	11	12	13	14	15	16	17	21
C1	1890	1893	1880	1878	1872	1877	1867	1877	1871	1914	1873	1869	1865	2247
C2	1831	1838	1834	1829	1826	1823	1820	1829	1824	1860	1819	1822	1825	2193
C3	1936	1941	1947	1938	1932	1928	1921	1936	1929	1975	1928	1920	1919	2312
C4	2009	2013	1998	1990	1986	1980	1987	1989	1980	2038	1984	1987	1982	2403
C5	2117	2126	2119	2128	2119	2114	2109	2118	2107	2175	2108	2110	2114	2512
T1	1935	1940	1950	1948	1896	1919	1790	1846	1842	2123	1765	1772	1775	2256
T2	1985	1979	1980	1954	1963	1948	1901	1861	1850	2132	1876	1882	1865	2360
T3	2009	2013	1993	2008	1983	1978	1863	1907	1886	2246	1818	1812	1830	2403
T4	2160	2174	2177	2171	2150	2143	1898	1815	1801	2585	1890	1892	1898	2520

TABLE G1 - THERMOCOUPLE READINGS (^{o}F)

TEST NUMBER	MIRROR POSITION	ATTENUATOR NULL	TEST NUMBER	MIRROR POSITION	ATTENUATOR NULL
C1	.9	620	C4	.9	479
	.8	623		.8	483
	.7			.7	477
	.6	620		.6	479
	.5	619		.5	472
	.4	615		.4	474
	.3	616		.3	470
	.2	614		.2	468
C2	.9	667	C5	.9	265
	.8	660		.8	269
	.7	658		.7	263
	.6	662		.6	267
	.5	653		.5	262
	.4	649		.4	263
	.3	652		.3	259
	.2	646		.2	261
C3	.9	563			
	.8	560			
	.7	568			
	.6	558			
	.5	562			
	.4	557			
	.3	564			
	.2	549			

TABLE G2 - CALIBRATION DATA

TEST NUMBER	MIRROR POSITION	ATTENUATOR NULL	TEST NUMBER	MIRROR POSITION	ATTENUATOR NULL
T1	.9	651	T3	.9	628
	.8	648		.8	617
	.7	647		.7	610
	.6			.6	
	.5	642		.5	589
	.4			.4	
	.3	632		.3	577
	.2	629		.2	568
	.1	612		.1	561
T2	.9	596	T4	.9	477
	.8	591		.8	446
	.7	580		.7	422
	.6	576		.6	412
	.5	570		.5	391
	.4			.4	366
	.3	568		.3	351
	.2	563		.2	326
	.1	550		.1	286

TABLE G3 - TEST DATA

APPENDIX H - ERROR ANALYSIS

H1 WALL TEMPERATURE ERROR

In the experiments the temperature of the platinum foil boundaries was measured by platinum-platinum/10% rhodium thermocouples located at the ceramic-platinum foil interface as indicated below:

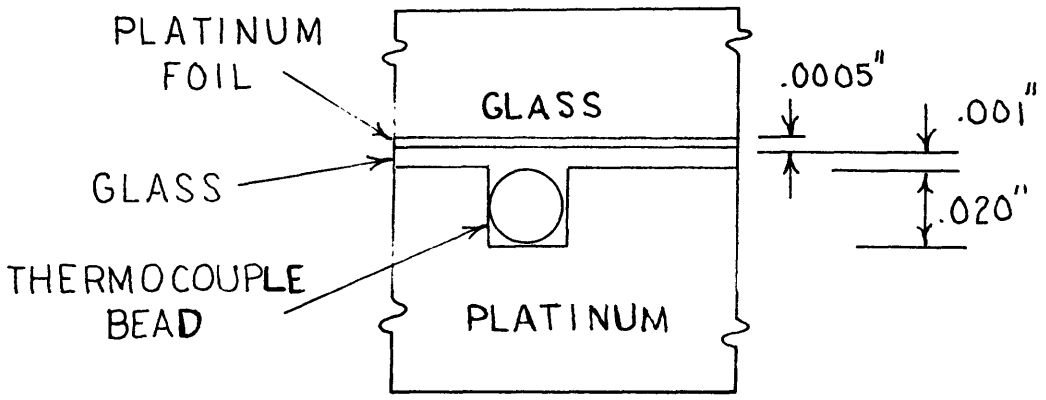

The thermal contact conductance of the ceramic-platinum foil interface was increased due to the presence of a thin layer of glass which leaked into the interface during the experiments. The thermal conductance of this interface was calculated to be approximately 13,000 Btu/hrft^{2o}F. Even at the highest heat fluxes of the experiment this resistance would cause a temperature drop less than 1.5^{o}F.

The presence of small air bubbles (.002" diameter) at the platinum-glass interface caused another resistance to heat flow. This interface conductance was evaluated with a relation for the microscopic constriction resistance for a single drop in dropwise condensation on a metal surface [65].

$$h = \frac{4 n k_T r}{\frac{32}{3\pi^2}\left(1-\beta^{.5}\right)^{1.5}}$$

n - number of bubbles on a unit surface area

k_T - thermal conductivity of surface

r - radius of bubble

β - fraction of surface covered by bubbles

This conductance was calculated to be in excess of 50,000 Btu/hrft^2^{o}F and produced a negligible temperature drop at the heat fluxes run in the experiments.

Due to the above considerations the accuracy of the wall temperature measurements was considered to be $\pm 3^oF$.

H2 GLASS TEMPERATURE ERROR

The accuracy of the laser temperature measurement technique is influenced by the operation and calibration of the complete optical system, which was designed to minimize measurement errors. The laser head was water cooled in order to avoid changes in its thermal environment. All mirrors were first surface optical quality and were shielded from emission from the furnace when they were not in use. A split beam nulling system was used in order to compensate for any small changes in the source intensity. The entire optical system was contained in a light-proof box to protect it from stray light. A very stable high voltage power supply was used to operate the photomultiplier tube in order to avoid changes in gain. From considerations and also the reproducibility of the calibration data it was estimated that the glass temperature error was $\pm 3^oF$.

H3 ERROR IN HEAT FLUX

The heat flux through the glass slab was calculated by measuring the gradient across the bottom of the ceramic tray and applying Fourier's equation. The accuracy of the heat flux is influenced by the following parameters; temperature gradient, measurements, thermal conductivity of the ceramic, and the thickness of the ceramic plate. The error in the thermocouple reading at the top of the ceramic plate was estimated as $\pm 3^oF$ in Appendix G1, while the error in the lower therocouple was es-

timated to be ± $1^{o}F$, as it was cemented into a slot in the ceramic. The thermal conductivity of the ceramic was measured by the Dynatech Corporation, Cambridge, Mass. to an accuracy of ± 5%. Therefore the error in the heat flux measurements was estimated to be less than ± 6%.

BIOGRAPHICAL SKETCH

Born in Brockville, Ontario, Canada on March 28, 1944, Dennis Eryou shortly thereafter moved to Flin Flon, Manitoba, where he completed both elementary and secondary schooling. Upon completion of high school he entered the Engineering School at the University of Manitoba from which he graduated in May of 1966; at that time he was the recepient of the gold medal in Mechanical Engineering, indicative of the highest standing in his class. In May of 1967, he received his Master of Engineering Degree from Carleton University, Ottawa, Ontario.

After completing his studies at M.I.T., he is leaving for Eindhoven, The Netherlands where he will be employed by the Philips Company.